OXIDATION AND SORPTION KINETICS OF ARSENIC ON A POORLY CRYSTALLINE MANGANESE OXIDE

by

Brandon J. Lafferty

A dissertation submitted to the Faculty of the University of Delaware in partial fulfillment of the requirements for the degree of Doctor of Philosophy in Plant and Soil Sciences

Summer 2010

OXIDATION AND SORPTION KINETICS OF ARSENIC ON A POORLY CRYSTALLINE MANGANESE OXIDE

by

Brandon J. Lafferty

Approved: _____
Blake C. Meyers, Ph.D.
Chair of the Department of Plant and Soil Sciences

Approved: _____
Robin W. Morgan, Ph.D.
Dean of the College of Agriculture and Natural Resources

Approved: _____
Debra Hess Norris, M.S.
Vice Provost for Graduate and Professional Education

I certify that I have read this dissertation and that in my opinion it meets the academic and professional standard required by the University as a dissertation for the degree of Doctor of Philosophy.

Signed: _____

Donald L. Sparks, Ph.D.
Professor in charge of dissertation

I certify that I have read this dissertation and that in my opinion it meets the academic and professional standard required by the University as a dissertation for the degree of Doctor of Philosophy.

Signed: _____

Jeffry J. Fuhrmann, Ph.D.
Member of dissertation committee

I certify that I have read this dissertation and that in my opinion it meets the academic and professional standard required by the University as a dissertation for the degree of Doctor of Philosophy.

Signed: _____

Thomas E. Hanson, Ph.D.
Member of dissertation committee

I certify that I have read this dissertation and that in my opinion it meets the academic and professional standard required by the University as a dissertation for the degree of Doctor of Philosophy.

Signed: _____

James T. Sims, Ph.D.
Member of dissertation committee

ACKNOWLEDGMENTS

I thank my advisor, Dr. Donald Sparks, for all of his support and guidance during my stay at the University of Delaware. I greatly appreciate the support I received from a Donald L. and Joy G. Sparks Graduate Fellowship in Soil Science. I also appreciate Drs. Sims, Hanson and Fuhrman for their insights and advice as I was conducting this research. The assistance and camaraderie of the Environmental Soil Chemistry Group has been one of the most rewarding aspects of my Ph.D. studies. I will miss our days in the farmhouse and will always smile when I remember our road trip to Pittsburgh and our many group picnics. Special acknowledgement is due to Jerry Hendricks and Caroline Golt for their assistance with this research.

I am deeply thankful for the continuous love and encouragement of my family as I pursued this degree. My parents, Toni and Jim Lafferty, and my parents-in-law, Jodi and Van Wilkinson, supported me in countless ways, for which I am eternally grateful. Most importantly, I am sincerely grateful to my wife, Kelli, for her love and friendship during our time in Delaware. She and our children, Jackson and Mollie, have brought immeasurable joy and peace to me during our time in Delaware.

TABLE OF CONTENTS

LIST OF TABLES vii
LIST OF FIGURES viii
ABSTRACT xi
INTRODUCTION 1
Manganese Oxides 1
Arsenic 4
As^{III} Oxidation by Phyllomanganates 8
Research Objectives 11
References 13
Arsenite Oxidation by a Poorly-Crystalline Manganese Oxide: Stirred-Flow Experiments 19
Abstract 19
Introduction 20
Materials and Methods 23
δ-MnO_2 Synthesis and Characterization 23
Stirred-Flow Experiments 24
Results and Discussion 28
As^{III} Oxidation by δ-MnO_2 28
Arsenic Sorption 32
Role of Mn Speciation in δ-MnO_2 Reactivity 37
References 46
Arsenite Oxidation by a Poorly-Crystalline Manganese Oxide: Results from X-ray Absorption Spectroscopy and X-ray Diffraction 50
Abstract 50
Introduction 52
Materials and Methods 55
δ-MnO_2 Synthesis and Characterization 55
Stirred-Flow Experiments 55
Solid-Phase Characterization 58
Results and Discussion 60
δ-MnO_2 Structure 60
Mn Sorption on δ-MnO_2 During As^{III} Oxidation 64
Mn^{III} Formation During As^{III} Oxidation 68
As Speciation and Binding Mechanisms During As^{III} Oxidation 71
References 80

Desorption of Arsenic and Manganese from a Poorly Crystalline Manganese Oxide 85
Abstract 85
Introduction 86
Materials and Methods 88
Stirred Flow Method 88
As, Mn, Ca, and P Analysis 89
Sorption and Desorption Calculations 89
Results and Discussion 93
δ-MnO_2 Structure 93
As^{III} Oxidation and Sorption 94
Mn Desorption 95
As^{III} Desorption 100
As^{V} Desorption 101
Implications for As Mobility 104
References 106
Conclusions 110
Future Research 113

LIST OF TABLES

Table 2.1. Percentages of Mn^{II}, Mn^{III}, and Mn^{IV} in the solid phase after reacting δ-MnO_2 with As^{III} for 0.5, 4, 10, 24, and 48 hours. Percentages are calculated from linear combination fits of standard compounds ($MnSO_4$, Mn_2O_3, and δ-MnO_2). 69

Table 2.2. Structural parameters derived from least-squares fits to raw k^3-weighted Mn-EXAFS spectra of unreacted δ-MnO_2 and δ-MnO_2 reacted with As^{III} for 0.5, 4, 10, 24, and 48 hours. 72

Table 2.3. Structural parameters derived from least-square fits to raw k^3-weighted As-EXAFS spectra for sorption standards and As^{III} oxidation samples taken at 0.5, 4, 10, 24, and 48 hours of reaction..... 74

Table 3.1. Amounts (nmol) and percentages of As^{V}, As^{III}, and Mn^{II} desorbed by PO_4, Ca^{2+}, and background electrolyte (10 mM NaCl, 5mM MOPS) after 4, 10, and 24 hours of As^{III} oxidation by δ-MnO_2. 99

LIST OF FIGURES

Figure 1. Schematic representations of: A. hollandite, a 2x2 tectomanganate, B. lithiophorite, a phyllomanganate with alternating layers of MnO_6 octahedra (blue) and (Al / Li) $(OH)_6$ octahedra (green), C. Na birnessite with unstructured hydrated Na^+ in interlayers (red) to balance the negative charge of Mn octahedral layers (blue), and D. top view of one Mn octahedral sheet in hexagonal birnessite with vacancy sites. 3

Figure 1.1. Point of zero charge of δ-MnO_2 measured by the prolonged salt titration method. 25

Figure 1.2. Transmission electron micrographs of unreacted δ-MnO_2 (A and B), and δ-MnO_2 reacted with As^{III} for 48 hours (C and D). 26

Figure 1.3. (A.) The amount (nmol) of As sorbed as well as amounts (nmol) of As^{III}, As^{V}, and Mn^{II} in the effluent of a stirred-flow experiment reacting 1 g/L δ-MnO_2 with 100 μM As^{III} flowing at 1 mL/min for 48 hours. (B.) The proportion (%) of As as As^{III}, As^{V}, and As sorbed to δ-MnO_2 during the first 15 hours of the same stirred-flow experiment. 29

Figure 1.4. Percentage of As sorbed by δ-MnO_2 over time in four stirred-flow experiments. Three stirred-flow experiments were conducted by reacting 1 g/L of pristine δ-MnO_2 with 100 μM As^{III}, 100 μM As^{V}, or 100 μM As^{V} and 100 μM Mn^{II} simultaneously, while the other experiment was conducted by reacting 1 g/L of Mn^{II}-saturated δ-MnO_2 with 100 μM As^{III}. 35

Figure 1.5. As^{V}, As^{III}, and Mn^{II} concentrations in the effluent of a stirred-flow reaction in which a 1 g/L suspension of Mn^{II}-saturated δ-MnO_2 was reacted with 100 μM As^{III} flowing at 1 mL/min for 48 hours. δ-MnO_2 was saturated by reaction with 50 μM Mn^{II}, and no Mn was added to the stirred-flow reactor during the time period shown. 38

Figure 1.6. Change in Mn^{II} concentration over time in the effluent of six stirred-flow reactions. Stirred-flow experiments were conducted by reacting 1 g/L of pristine δ-MnO_2 with: 50 μM Mn^{II}, or 100 μM Mn^{II}, or 100 μM As^{III}, or 100 μM Mn^{II} and 50 μM As^{V} simultaneously, or 100 μM Mn^{II} and 100 μM As^{V} simultaneously. Also, one stirred-flow reaction was conducted by reacting 100 μM As^{III} with 1 g/L of Mn^{II}-saturated δ-MnO_2. 42

Figure 1.7. Batch reaction of As^{III} with manganite (γ-$Mn^{III}OOH$) in the presence of 10 mM NaCl and 5 mM MOPS (pH = 7.2). 43

Figure 2.1. Vertical lines represent the duration of five stirred-flow reactions measuring As^{III} oxidation by δ-MnO_2 (1 g/L δ-MnO_2 and 100 μM As^{III}). Each reaction was stopped at the time indicated at the top of the graph (0.5, 4, 10, 24, or 48 hours), at which point all remaining δ-MnO_2 was collected for analysis. Data show the amount (nmol) of As sorbed by δ-MnO_2, as well as amounts (nmol) of As^{III}, As^{V}, and Mn^{II} in the effluent from the stirred-flow experiment. 57

Figure 2.2. Manganese K-edge EXAFS (A.), Fourier transformed EXAFS (B.), and XANES (C.) of unreacted δ-MnO_2 and δ-MnO_2 (1 mg/L) reacted with As^{III} (100 μM) in a stirred-flow reactor for 0.5, 4, 10, 24, and 48 hours. XAS data is presented as solid lines and fits are presented as dashed lines (fit data provided in Table 2.2). Arrow in panel A indicates the shoulder at ~ 6.5 $Å^{-1}$ which is present beyond 0.5 hours. 62

Figure 2.3. Synchrotron XRD patterns of unreacted δ-MnO_2 and δ-MnO_2 (1 mg/L) reacted with As^{III} (100 μM) in a stirred-flow reactor for 0.5, 4, 10, 24, and 48 hours. Arrow indicates the position of the 'dip' at 45º that increases with reaction time. 63

Figure 2.4. The amplitude of first Mn-O, first Mn-Mn, and Mn-Mn multiple scattering shell from Fourier transformed Mn-EXAFS data. 67

Figure 2.5. Arsenic K-edge derivative XANES (A.), As K-edge EXAFS (B.), and Fourier transformed EXAFS (C.) of unreacted δ-MnO_2 and δ-MnO_2 (1 mg/L) reacted with As^{III} (100 μM) in a stirred-flow reactor for 0.5, 4, 10, 24, and 48 hours. XAS data is presented as solid lines and fits are presented as dashed lines (fit data provided in Table 2.3). 73

Figure 2.6. Proposed reaction mechanism for As^{III} oxidation by δ-MnO_2 over 48 hours in a stirred-flow reactor. Throughout the reaction, As^{III} is oxidized by Mn^{IV} at δ-MnO_2 edge sites, producing Mn^{II} and As^{V}. (A.) Unreacted δ-MnO_2 octahedral layers consist of primarily Mn^{4+}, and have reaction sites at layer edges (edge sites) and vacancy sites. (B.) During the first 4 hours of As^{III} oxidation, Mn^{II} sorbs at δ-MnO_2 vacancy sites, and As^{V} sorbs at edge sites in bidentate-binuclear and monodentate-mononuclear complexes. Also, a portion of sorbed Mn^{II} reacts with Mn^{IV} at vacancy sites to form Mn^{III}. (C.) Between 4 and ~ 6 hours of reaction, vacancy sites become filled with $Mn^{II/III}$, Mn^{II} begins to sorb at δ-MnO_2 edge sites, and As^{V} sorption continues in the same sorption complexes. (D.) Beyond ~ 6 hours of reaction, Mn^{II} at edge sites (and probably vacancy sites) reacts with Mn^{III} in δ-MnO_2 octahedral layers to form Mn^{III}. The resulting Mn^{III} changes the bonding environment of As^{V}, which begins to sorb in bidentate-mononuclear complexes and the As-Mn distance in As^{V} bidentate-binuclear complexes increases slightly. 77

Figure 3.1. Raw data from one replicate of As^{III} oxidation by δ-MnO_2 followed by desorption by $CaCl_2$. As^{III} oxidation was carried out for the first 24 hours, and desorption by $CaCl_2$ was carried out from 24 to 48 hours. 90

Figure 3.2. Amount of As^{III}, As^{V}, and Mn^{II} in solution as well as amount of As sorbed, all during As^{III} oxidation by δ-MnO_2 (A.) and desorption by $CaCl_2$ (B.). Also plotted is the calculated dilution curve of predicted As in stirred-flow effluent under ideal conditions (i.e. no sorption) in each case. 92

Figure 3.3. The amount (nmol) of As^{III}, As^{V}, and Mn^{II} in stirred flow reactor effluent as well as the amount (nmol) of As sorbed during As^{III} oxidation by δ-MnO_2, prior to desorption by Ca^{2+}, PO_4, or background electrolyte. Vertical dashed lines indicate times at which desorption was initiated. 96

Figure 3.4. Amount (nmol) of Mn^{II} (left) and As^{V} (right) desorbed by Ca^{2+}, PO_4, and background electrolyte (10 mM NaCl, 5 mM MOPS) after 4, 10, and 24 hours of As^{III} oxidation by δ-MnO_2. The initial data points on each graph (time = 0 hours) correspond to the beginning of desorption (initial As^{III} oxidation data not shown). Data shown are first ~10 hours of 24 hour desorption experiments. 98

ABSTRACT

Manganese oxides (Mn-oxides) are some of the most reactive minerals in the environment, and are known to readily oxidize toxic arsenite (As^{III}) to less toxic arsenate (As^{V}). However, As^{III} oxidation by Mn-oxides can be quite complex, involving many simultaneous reactions. Also, when As^{III} is oxidized by Mn-oxides, a reduction in the oxidation rate is often observed, which has been attributed to Mn-oxide surface passivation. Although As^{III} oxidation by Mn-oxides has been studied, fundamental understanding of the mechanisms of As^{III} oxidation, and subsequent Mn-oxide passivation by poorly crystalline, layered Mn-oxides (i.e. phyllomanganates), is lacking. In stirred-flow experiments, As^{III} oxidation by δ-MnO_2 (a poorly crystalline phyllomanganate) is initially rapid but slows appreciably as the mineral surface became passivated. Mn^{II} is the only reduced product of As^{III} oxidation by δ-MnO_2 during the initial period of the reaction, indicating that As^{III} oxidation does not proceed through a Mn^{III} intermediate. Also, X-ray absorption spectroscopy (XAS) and X-ray diffraction (XRD) show that Mn^{II} sorption is the primary cause of δ-MnO_2 passivation during the early periods of As^{III} oxidation. There is also evidence that formation of Mn^{III} observed in previous studies is a result of conproportionation of Mn^{II} sorbed onto Mn^{IV} reaction sites of δ-MnO_2. It is possible that Mn^{III} formed through $Mn^{II\ /\ IV}$ conproportionation also plays a role in δ-MnO_2 passivation. Only As^{V} is observed bound to δ-MnO_2 during As^{III} oxidation, and it is present in several adsorption complexes that change as the Mn^{III} content in δ-MnO_2 increases. Although As^{V} is directly bound to the δ-MnO_2 surface, a significant fraction is quite mobile. These findings show that As^{III} oxidation by poorly crystalline δ-MnO_2 involves

several simultaneous reactions and emphasizes the importance of Mn oxidation state in the reactivity of Mn-oxides. Also demonstrated is the value of studying reaction mechanisms over a range of time scales.

INTRODUCTION

Manganese Oxides

Manganese-oxide minerals (Mn-oxides) are nearly ubiquitous in soils and sediments. They commonly occur as fine-grained particles or coatings in terrestrial and aquatic environments, usually exhibiting high reactivity due to their large surface area and negative charge (Post, 1999). Due to their unusually high reactivity, Mn-oxides tend to greatly influence many chemical processes in the environment (Jenne, 1968; Post, 1999). For example, Mn-oxides can readily sorb and oxidize many metals and metalloids under typical environmental conditions (Fendorf and Zasoski, 1992; Foster et al., 2003; Hess and Blanchar, 1976; Manceau et al., 2002; McKenzie, 1972; Murray, 1975a; Murray, 1975b; Murray and Dillard, 1979; Oscarson et al., 1983; Posselt et al., 1968).

In the environment, Mn exists in three oxidation states: +2, +3, and +4 (i.e. II, III, and IV). The presence of multiple Mn oxidation states, in part, leads to the occurrence of a wide variety of Mn-oxide minerals in the environment (Post, 1999). The basic building block for Mn-oxides is the MnO_6 octahedron. In Mn-oxides with tunnel structures (i.e. tectomanganates) Mn octahedra share both edges and corners (Figure 1a), while in Mn-oxides with layered structures (i.e. phyllomanganates), Mn octahedra are arranged in sheets by sharing edges (Figure 1b, c, and d) (Dixon and White, 2002). Phyllomanganates and tectomanganates are the two dominant groups of Mn-oxides in the environment (Post, 1999). The most commonly identified Mn-oxide

minerals in soils are lithiophorite, hollandite, and birnessite (Figure 1), however, many Mn-oxides observed in nature are poorly-crystalline and are not able to be identified (Post, 1999).

Interestingly, some bacteria and fungi are able to precipitate Mn-oxides on the surfaces of their cells (Tebo et al., 1997; Tebo et al., 2004). These Mn-oxides precipitate as a result of enzymatic oxidation of Mn^{II} to Mn^{III} or Mn^{IV} (Tebo et al., 2004; Webb et al., 2005b). Mn^{II} oxidation by microbes occurs much more rapidly than when Mn^{II} is oxidized without the influence of microbial enzymes (Tebo et al., 1997; Tebo et al., 2004; Webb et al., 2005b). This observation leads to the conclusion that most Mn-oxides that occur in surface environments are of biogenic origin (Shiller and Stephens, 2005; Tebo et al., 1997; Tebo et al., 2004). These biogenic Mn-oxides tend to be highly reactive with respect to metal sorption and oxidation (Tani et al., 2004; Toner et al., 2006; Villalobos et al., 2003; Villalobos et al., 2006; Webb et al., 2005a; Zhu et al., 2010a; Zhu et al., 2010b).

Because of the widespread occurrence and high reactivity of biogenic Mn-oxides, it is important to understand their structure, especially as it relates to reactivity. Many of the biogenic Mn-oxides studied to date exhibit the same structure as hexagonal birnessite (Villalobos et al., 2003; Webb et al., 2005a; Zhu et al., 2010b).

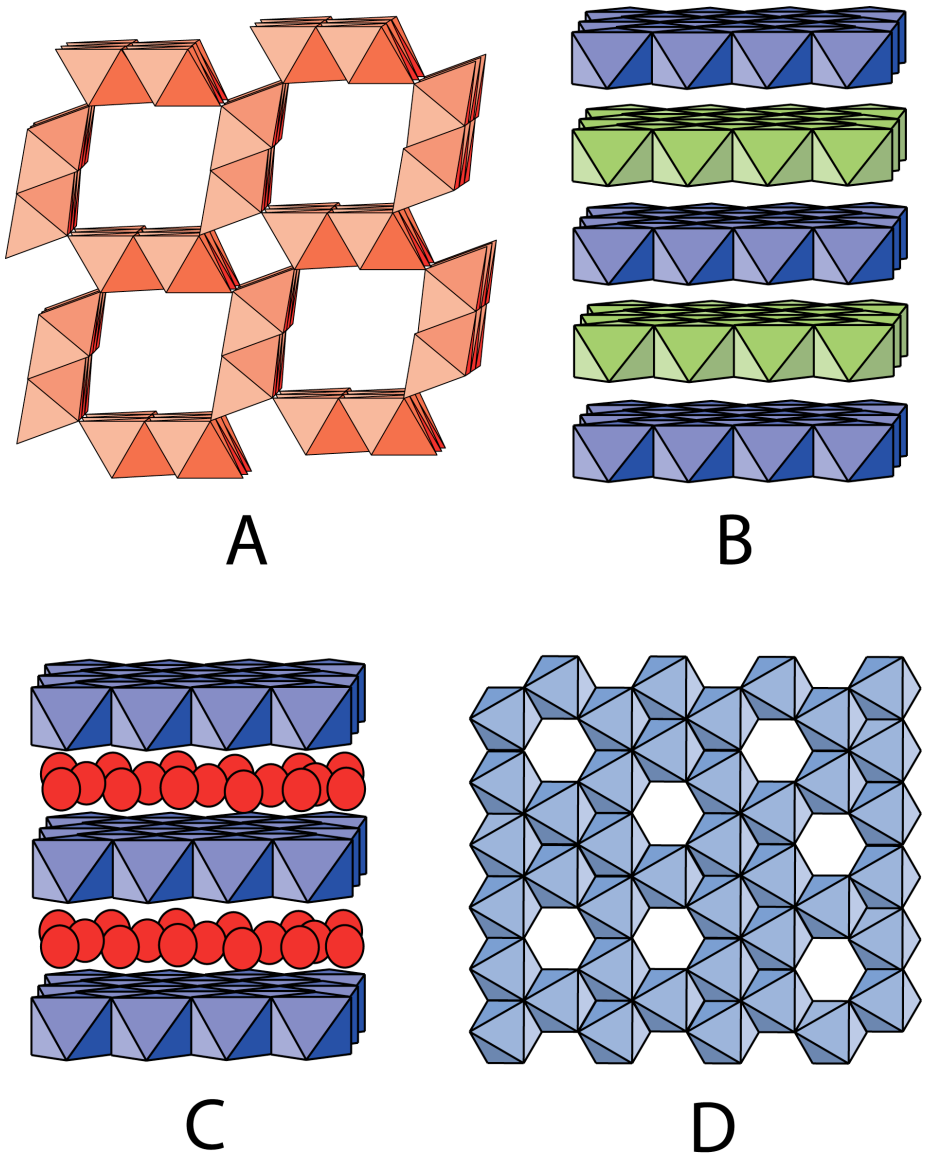

Figure 1. Schematic representations of: A. hollandite, a 2x2 tectomanganate, B. lithiophorite, a phyllomanganate with alternating layers of MnO_6 octahedra (blue) and (Al / Li) $(OH)_6$ octahedra (green), C. Na birnessite with unstructured hydrated Na^+ in interlayers (red) to balance the negative charge of Mn octahedral layers (blue), and D. top view of one Mn octahedral sheet in hexagonal birnessite with vacancy sites.

Hexagonal birnessite is a phyllomanganate composed of sheets of edge sharing Mn octahedra stacked vertically (in the *c* direction) (Drits et al., 1997; Silvester et al., 1997). The Mn octahedral sheets in hexagonal birnessite are almost exclusively composed of Mn^{IV}, and some of the sites in the Mn octahedral sheets that should be occupied by Mn^{IV} are vacant (Figure 1d) (Drits et al., 1997; Silvester et al., 1997; Villalobos et al., 2003). These vacancy sites in hexagonal birnessite are the primary source of negative charge, and also contribute to the higher reactivity of hexagonal birnessite compared to other forms of birnessite (Drits et al., 1997). Because Mn-oxides precipitated on microbial surfaces are thought to be the most important Mn-oxide minerals in the environment, studies investigating Mn-oxide reactivity in the environment should focus on birnessite minerals with hexagonal symmetry.

Arsenic

Arsenic (As) is a metalloid with toxic effects that have been known for centuries. It has been used for medicinal purposes, as a poison, and has even been called "inheritance powder." Although As has a relatively low elemental abundance in the Earth's crust, it is distributed widely in both terrestrial and marine environments (Nriagu, 2002). At present, anthropogenic activities as well as natural geological weathering processes are acting to increase the concentration of As in and near human

populations around the world, causing increased concern about the affect of As exposure on human health.

Some sources of As contamination in the environment are natural, primarily the release of inorganic As from weathering of minerals (Tamaki and Frankenberger, 1992). Groundwater contamination caused by the weathering of As bearing minerals in Southeast Asia is currently causing what some have called the largest mass poisoning in history (Nickson et al., 1998; Smedley et al., 2001). Although most naturally occurring As is introduced to the environment as inorganic As, these species can also be transformed by organisms in the environment. Some marine organisms can transform inorganic As, into a variety of organic As compounds (Cullen and Reimer, 1989). These organic As compounds are produced primarily by phytoplankton and algae, and are a major source of As in human diets through consumption of marine macrofauna. The global As cycle also includes anthropogenic sources of As, including coal burning stoves, metal smelting, industrial agriculture, and industrial mining (Mukhopadhyay et al., 2002). For example, methylated forms of As are used in the agriculture industry as defoliants, herbicides, and pesticides (Cullen and Reimer, 1989), and an organic arsenical is added to poultry feed as an antibiotic (Jackson and Bertsch, 2001).

Although As is present in the environment as several different species, the inorganic forms of As tend to be predominant (Cullen and Reimer, 1989). In most environmental systems, inorganic As occurs in either the +5 oxidation state as the oxyanion arsenate (AsO_4^{3-}, hereafter abbreviated As^V) or in the +3 oxidation state as

the arsenite ion (AsO_3^{3-}, hereafter abbreviated As^{III}). As^V is usually partially protonated and exists as AsO_4H^{1-} or AsO_4H^{2-} (pK_{a1} = 12.19, pK_{a2} = 6.94, and pK_{a3} = 2.24), while below pH 9.2, As^{III} is fully protonated and is present as $H_3AsO_3^0$ (Sadiq, 1997). Therefore, under most environmental conditions, As^{III} exhibits neutral charge, and As^V is negatively charged.

The toxicity of As is widely known; however, the mode of As toxicity is dependent on its speciation. As^{III} toxicity arises from its inhibition of dehydrogenases (and other proteins) by reaction with thiol or sulfhydryl groups in many proteins (Ehrlich, 2002). Alternatively, the toxic effects of As^V are due to its tendency to compete with phosphate in cells. In the presence of As^V, oxidative phosphorilation can be disrupted, causing cellular energy generation to become hindered (Winship, 1984). Of the inorganic forms of As, As^{III} is considered to be the most toxic (i.e. more toxic than As^V) (Winship, 1984). The primary As exposure to humans is through consumption of As contaminated drinking water, thus the United States Environmental Protection Agency (USEPA) has set the maximum contaminant level for As in drinking water at 10 $\mu g\ L^{-1}$ (USEPA, 2001).

The mobility of As in terrestrial environments is generally determined by the extent to which it is adsorbed on mineral surfaces. Metal oxides tend to be the primary sorbents of As in the environment, especially the oxides of iron (Fe) and aluminum (Al) (Anderson et al., 1976; Arai et al., 2001; Dixit and Hering, 2003; Gupta and Chen, 1978; Hingston et al., 1971; Raven et al., 1998). Mn-oxides can also sorb As to some extent (Foster et al., 2003; Manning et al., 2002; Parikh et al., 2008;

Tani et al., 2004). Although, metal oxides are generally thought to bind As^{V} more readily than As^{III}, the extent to which each species is sorbed depends greatly on pH. For example, As^{V} sorption by Fe-oxides is greater at acidic pH values, whereas As^{III} sorption by Fe-oxides is greater at basic pH values (Dixit and Hering, 2003; Raven et al., 1998). Although As sorption is pH dependent, As^{III} is generally regarded as more mobile than its oxidized counterpart under many environmental conditions.

The processes controlling oxidation and reduction of inorganic As in the environment are likely to be the primary factors controlling As speciation and thus mobility. Several processes affect the oxidation state of inorganic As in the environment. Microbial As^{V} reduction occurs in environments ranging from soil, to mine tailings, to marine systems and can be responsible for releasing As from solid phases via direct reduction of sorbed As or dissolution of As mineral phases (Oremland and Stolz, 2003). Also, As^{III} oxidizing bacteria have been isolated from environments ranging from soil to As contaminated hot-springs and lakes (Oremland and Stolz, 2003). As^{III} oxidation and As^{V} reduction can be carried out by a variety of bacteria under both aerobic and anaerobic conditions (Oremland and Stolz, 2003). Abiotically, oxidation of As^{III} to As^{V} can also be carried out by Mn-oxide minerals commonly found in the environment (Oscarson et al., 1980; Oscarson et al., 1981a).

As^{III} Oxidation by Phyllomanganates

In some environments, sediments are capable of oxidizing As^{III} to As^{V} without biological activity (Oscarson et al., 1980). The minerals responsible for As^{III} oxidation in the environment are Mn-oxides (Oscarson et al., 1981a; Oscarson et al., 1981b). However, Mn-oxide reactivity varies with mineralogy. Specifically, phyllomanganates are more reactive, in terms of As^{III} oxidation, than other types of Mn-oxides (Oscarson et al., 1983). Among phyllomanganates, birnessite minerals have shown the greatest ability to oxidize As^{III} (Chiu and Hering, 2000; Manning et al., 2002; Oscarson et al., 1983; Scott and Morgan, 1995; Tournassat et al., 2002).

The mechanisms of As^{III} oxidation by phyllomanganates can be quite complex, involving several simultaneous reactions. For example, As^{III} oxidation by birnessite produces As^{V} and Mn^{II} as reaction products (Equation 1) (Ginder-Vogel et al., 2009; Oscarson et al., 1983; Parikh et al., 2008; Scott and Morgan, 1995; Tournassat et al., 2002). Also, both As^{V} and Mn^{II} can be

$$Mn^{IV}O_2 + H_3As^{III}O_3 + 2H^+ \rightarrow Mn^{II} + H_3As^{V}O_4 + H_2O \quad [1]$$

adsorbed by birnessite (represented by $>Mn^{IV}O_2$, Equations 2 and 3) (Oscarson et al., 1983; Scott and Morgan, 1995). However, sorption of As^{V} and Mn^{II} by birnessite could occur at different reaction sites on the mineral surface (Manceau et al., 2002;

Tournassat et al., 2002). A common observation during As^{III} oxidation by phyllomanganates, is a decrease in the rate of oxidation

$$Mn^{II} + >Mn^{IV}O_2 \rightarrow >Mn^{IV}O_2\text{-}Mn^{II} \quad [2]$$

$$As^{V} + >Mn^{IV}O_2 \rightarrow >Mn^{IV}O_2\text{-}As^{V} \quad [3]$$

(i.e. the Mn-oxide surface becomes passivated) (Ginder-Vogel et al., 2009; Manning et al., 2002; Moore et al., 1990; Oscarson et al., 1981a; Oscarson et al., 1983; Parikh et al., 2008; Scott and Morgan, 1995; Tani et al., 2004; Tournassat et al., 2002).

Several causes have been attributed to the Mn-oxide passivation observed during As^{III} oxidation. One potential mechanism for passivation of Mn-oxide surfaces is sorption of Mn^{II} (Equation 2) (Oscarson et al., 1981a; Scott and Morgan, 1995). Typically As^{V} and Mn^{II} are not released into solution in stoichometric amounts during As^{III} oxidation, indicating that some Mn^{II} is sequestered through re-adsorption to the Mn-oxide surface (Scott and Morgan, 1995). Sorption of some Mn^{II} is thought to occur at the reactive sites where As^{III} is oxidized, thus physically blocking those sites on the mineral surface (Oscarson et al., 1981a; Scott and Morgan, 1995). However, no spectroscopic data exists to implicate Mn^{II} in Mn-oxide surface passivation.

Most As^{V} produced during As^{III} oxidation by phyllomanganates is released into solution, however, some As^{V} remains sorbed on the mineral surface during these reactions (Foster et al., 2003; Manning et al., 2002). Interestingly, more As tends to sorb on Mn-oxides during As^{III} oxidation than when As^{V} is sorbed without

simultaneous As^{III} oxidation (Manning et al., 2002; Parikh et al., 2008; Tani et al., 2004). Molecular modeling data indicate that As^{V} is more competitive for Mn-oxide surface sites than As^{III} (Zhu et al., 2009). Therefore, it is possible that As^{V} sorption on the Mn-oxide surface during As^{III} oxidation could result in Mn-oxide passivation.

Passivation of phyllomanganates could also occur by the formation of a Mn/As precipitate under certain reaction conditions. A Mn/As^{V} precipitate compositionally close to the mineral krautite ($Mn^{II}HAs^{V}O_4 \cdot H_2O$) has been observed during As^{III} oxidation by birnessite (Tournassat et al., 2002). Although other studies have not observed this precipitate, it could potentially be a source of Mn-oxide passivation under highly contaminated conditions in the environment.

Most recent attention has been given to the formation of a Mn^{III} intermediate, produced during As^{III} oxidation by phyllomanganates as a cause of Mn-oxide passivation (Nesbitt et al., 1998; Tournassat et al., 2002). During As^{III} oxidation by birnessite, X-ray photoelectron spectroscopy (XPS) observes the proportion of Mn^{III} and OH^- at the mineral surface increase, (Nesbitt et al., 1998). The observed increase in Mn^{III} content at the Mn-oxide surface leads to the conclusion that oxidation of As^{III} by birnessite proceeds as two discrete electron transfers, where Mn^{III} reactive sites are an intermediate reaction product (MnOOH in Equations 4 and 5).

$$2Mn^{IV}O_2 + H_3As^{III}O_3 + H_2O \rightarrow 2Mn^{III}OOH + H_3As^{V}O_4 \quad [4]$$

$$2Mn^{III}OOH + H_3As^{III}O_3 + 4H^+ \rightarrow 2Mn^{II}(aq) + H_3As^{V}O_4 + 3H_2O \quad [5]$$

These results offer spectroscopic evidence for the non-stoichometric release of As^{V} and Mn^{II} during As^{III} oxidation by Mn-oxides. However, unlike previous studies, XPS data suggest that the differences in As^{V} and Mn^{II} appearance in solution is not due to Mn^{II} blocking reaction sites, but rather the formation of a Mn^{III} intermediate (Nesbitt et al., 1998). Mn^{III} reactive sites could contribute to Mn-oxide passivation because they are less reactive than Mn^{IV} reactive sites in Mn-oxides (Chiu and Hering, 2000; Zhu et al., 2009).

Research Objectives

Contamination of soils and waters with As is a major concern throughout the world and is a threat to human health. The fate, transport and bioavailability of As in the environment is primarily impacted by sorption on metal oxides and redox reactions. There is a need to better understand the role that the most environmentally relevant mineral surfaces play in controlling As speciation in the environment. Biogenic Mn-oxides are arguably some of the most reactive and important natural materials that impact As speciation, and thus its toxicity and bioavailability.

Although several studies have investigated As^{III} oxidation by Mn-oxides, very few have used poorly-crystalline phyllomanganates representative of the most environmentally important Mn-oxide minerals (e.g. poorly crystalline hexagonal birnessite). Thus, the mechanisms of As oxidation and sorption on poorly crystalline, environmentally representative Mn-oxides have not been fully elucidated. Also,

discrepancies in the cause of Mn-oxide passivation during As^{III} oxidation exist in the literature. In addition, the mobility of As sorbed on phyllomanganate surfaces has not been fully explored. To date, there is has not been a through study of the reaction mechanisms of As^{III} oxidation, As sorption, and Mn-oxide passivation over time. An increased understanding of these reactions is needed in order to better understand the overall reaction mechanism for As^{III} oxidation, and more accurately predict processes that may occur in natural systems.

The goal of this research is to provide insight into the complexity of As^{III} oxidation by poorly crystalline hexagonal birnessite and the impacts of this reaction on As transformations in the environment. Three objectives are central to achieving this goal:

I. Determine the mechanisms of As^{III} oxidation and As sorption on poorly crystalline hexagonal birnessite.

II. Determine the mechanisms of Mn-oxide surface passivation during As^{III} oxidation.

III. Determine the mobility of As^{V} sorbed on poorly crystalline hexagonal birnessite.

References

Anderson, M.A., J.F. Ferguson, and J. Gavis. 1976. Arsenate adsorption on amorphous aluminum hydroxide. J. Colloid Interface Sci. 54:391-399.

Arai, Y., E.J. Elzinga, and D.L. Sparks. 2001. X-ray absorption spectroscopic investigation of arsenite and arsenate adsorption at the aluminum oxide-water interface. J. Colloid Interface Sci. 235:80-88.

Chiu, V.Q., and J.G. Hering. 2000. Arsenic adsorption and oxidation at manganite surfaces. 1. Method for simultaneous determination of adsorbed and dissolved arsenic species. Environ. Sci. Technol. 34:2029-2034.

Cullen, W.R., and K.J. Reimer. 1989. Arsenic speciation in the environment. Chem. Rev. 89:713-764.

Dixit, S., and J.G. Hering. 2003. Comparison of arsenic(V) and arsenic(III) sorption onto iron oxide minerals: Implications for arsenic mobility. Environ. Sci. Technol. 37:4182-4189.

Dixon, J.B., and G.N. White. 2002. Manganese oxides, p. 367-388, *In* J. B. Dixon and D. G. Schulze, eds. Soil mineralogy with environmental implications. Soil Science Society of America, Inc., Madison, Wisconsin.

Drits, V.A., E. Silvester, A.I. Gorshkov, and A. Manceau. 1997. Structure of synthetic monoclinic Na-rich birnessite and hexagonal birnessite. 1. Results from X-ray diffraction and selected-area electron diffraction. Am. Mineral. 82:946-961.

Ehrlich, H.L. 2002. Bacterial oxidation of As(III) compounds, p. 313-328, *In* J. W.T. Frankenberger, ed. Environmental chemistry of arsenic. Marcel Dekker, New York.

Fendorf, S.E., and R.J. Zasoski. 1992. Chromium(III) oxidation by δ-manganese oxide (MnO_2). 1. Characterization. Environ. Sci. Technol. 26:79-85.

Foster, A.L., G.E. Brown, and G.A. Parks. 2003. X-ray absorption fine structure study of As(V) and Se(IV) sorption complexes on hydrous Mn oxides. Geochim. Cosmochim. Ac. 67:1937-1953.

Ginder-Vogel, M., G. Landrot, J.S. Fischel, and D.L. Sparks. 2009. Quantification of rapid environmental redox processes with quick-scanning x-ray absorption spectroscopy (Q-XAS). Proc. Natl. Acad. Sci. 106:16124-16128.

Gupta, S.K., and K.Y. Chen. 1978. Arsenic removal by adsorption. J. Water Pollut. Control 50:493-506.

Hess, R.E., and R.W.B. Blanchar. 1976. Arsenic stability in contaminated soils. Soil Sci. Soc. Am. J. 40:847-852.

Hingston, F.J., A.M. Posner, and J.P. Quirk. 1971. Competitive adsorption of negatively charged ligands on oxide surfaces. Faraday Discussions 52:334-342.

Jackson, B.P., and P.M. Bertsch. 2001. Determination of arsenic speciation in poultry wastes by IC-ICP-MS. Environ. Sci. Technol. 35:4868-4873.

Jenne, E.A. 1968. Controls on Mn, Fe, Co, Ni, Cu, and Zn concentraitons in soils and water: The significant role of hydrous Mn and Fe oxides. Adv. Chem. Ser. 73:337-387.

Manceau, A., B. Lanson, and V.A. Drits. 2002. Structure of heavy metal sorbed birnessite. Part III: Results from powder and polarized extended X-ray absorption fine structure spectroscopy. Geochim. Cosmochim. Acta 66:2639-2663.

Manning, B.A., S.E. Fendorf, B. Bostick, and D.L. Suarez. 2002. Arsenic(III) oxidation and arsenic(V) adsorption reactions on synthetic birnessite. Environ. Sci. Technol. 36:976-981.

McKenzie, R.M. 1972. Sorption of some heavy metals by lower oxides of manganese. Geoderma 8:29-35.

Moore, J.N., J.R. Walker, and T.H. Hayes. 1990. Reaction scheme for the oxidation of As(III) to As(V) by birnessite. Clay. Clay Miner. 38:549-555.

Mukhopadhyay, R., B.P. Rosen, L.T. Pung, and S. Silver. 2002. Microbial arsenic: From geocycles to genes and enzymes. FEMS Microbiol. Rev. 26:311-325.

Murray, J.W. 1975a. Interaction of cobalt with hydrous manganese dioxide. Geochim. Cosmochim. Ac. 39:635-647.

Murray, J.W. 1975b. Interaction of metal-ions at manganese dioxide solution interface. Geochim. Cosmochim. Ac. 39:505-519.

Murray, J.W., and J.G. Dillard. 1979. Oxidation of cobalt(II) adsorbed on manganese dioxide. Geochim. Cosmochim. Ac. 43:781-787.

Nesbitt, H.W., G.W. Canning, and G.M. Bancroft. 1998. XPS study of reductive dissolution of 7 angstrom-birnessite by H_3AsO_3, with constraints on reaction mechanism. Geochim. Cosmochim. Ac. 62:2097-2110.

Nickson, R.T., J.M. McArthur, W. Burgess, and K.M. Ahmed. 1998. Arsenic poisoning of Bangladesh groundwater. Nature 395:338.

Nriagu, J.O. 2002. Arsenic poisoning through the ages, p. 1-27, *In* J. W.T. Frankenberger, ed. Environmental chemistry of arsenic. Marcel Deker, New York.

Oremland, R.S., and J.F. Stolz. 2003. The ecology of arsenic. Science 300:939-944.

Oscarson, D.W., P.M. Huang, and W.K. Liaw. 1980. The oxidation of arsenite by aquatic sediments. J. Environ. Qual. 9:700-703.

Oscarson, D.W., P.M. Huang, and W.K. Liaw. 1981a. Role of manganese in the oxidation of arsenite by freshwater sediments. Clay. Clay Miner. 29:219-225.

Oscarson, D.W., P.M. Huang, C. Defosse, and A. Herbillon. 1981b. Oxidative power of Mn(IV) and Fe(III) oxides with respect to As(III) in terrestrial and aquatic environments. Nature 291:50-51.

Oscarson, D.W., P.M. Huang, W.K. Liaw, and U.T. Hammer. 1983. Kinetics of oxidation of arsenite by various manganese dioxides. Soil Sci. Soc. Am. J. 47:644-648.

Parikh, S.J., B.J. Lafferty, and D.L. Sparks. 2008. An ATR-FTIR spectroscopic approach for measuring rapid kinetics at the mineral/water interface. J. Colloid Interface Sci. 320:177.

Posselt, H.S., F.J. Anderson, and W.J. Weber. 1968. Cation sorption on colloidal hydrous manganese dioxide. Environ. Sci. Technol. 2:1087-1093.

Post, J.E. 1999. Manganese oxide minerals: Crystal structures and economic and environmental significance. Proc. Natl. Acad. Sci. 96:3447-3454.

Raven, K.P., A. Jain, and R.H. Loeppert. 1998. Arsenite and arsenate adsorption on ferrihydrite: kinetics, equilibrium, and adsorption envelopes. Environ. Sci. Technol. 32:344-349.

Sadiq, M. 1997. Arsenic chemistry in soils: An overview of thermodynamic predictions and field observations. Water Air Soil Poll. 93:117-136.

Scott, M.J., and J.J. Morgan. 1995. Reactions at oxide surfaces. 1. Oxidation of As(III) by synthetic birnessite. Environ. Sci. Technol. 29:1898-1905.

Shiller, A.M., and T.H. Stephens. 2005. Microbial manganese oxidation in the lower Mississippi river: methods and evidence. Geomicrobiol. J. 22:117-125.

Silvester, E., A. Manceau, and V.A. Drits. 1997. Structure of synthetic monoclinic Na-rich birnessite and hexagonal birnessite. 2. Results from chemical studies and EXAFS spectroscopy. Am. Mineral. 82:962-978.

Smedley, P.L., D.G. Kinniburgh, I. Huq, Z. Luo, and H. Nicolli. 2001. International perspective on naturally occurring arsenic problems in groundwater, p. 9-25, *In* W. R. Chappell, et al., eds. Arsenic exposure and health effects IV. Elsevier, Amsterdam.

Tamaki, S., and W.T. Frankenberger. 1992. Environmental chemistry of arsenic, p. 79-110 Reviews of environmental contamination and toxicology, Vol. 124. Springer, Verlag, New York.

Tani, Y., N. Miyata, M. Ohashi, T. Ohnuki, H. Seyama, K. Iwahori, and M. Soma. 2004. Interaction of Inorganic Arsenic with Biogenic Manganese Oxide Produced by a Mn-Oxidizing Fungus, Strain KR21-2. Environ. Sci. Technol. 38:6618-6624.

Tebo, B.M., W.C. Ghiorse, L.G.v. Waasbergen, P.L. Siering, and R. Caspi. 1997. Bacterially-mediated mineral formation: Insights into manganese(II) oxidation from molecular genetic and biochemical studies, p. 225-266, *In* J. F. Banfield

and K. H. Nealson, eds. Geomicrobiology: Interactions between microbes and minerals, Vol. 35. Mineral. Soc. Am., Washington D.C.

Tebo, B.M., J.R. Bargar, B.G. Clement, G.J. Dick, K.J. Murray, D. Parker, R. Verity, and S.M. Webb. 2004. Biogenic manganese oxides: Properties and mechanisms of formation. Ann. Rev. Earth and Plan. Sci. 32:287-328.

Toner, B., A. Manceau, S.M. Webb, and G. Sposito. 2006. Zinc sorption to biogenic hexagonal-birnessite particles within a hydrated bacterial biofilm. Geochim. Cosmochim. Acta 70:27-43.

Tournassat, C., L. Charlet, D. Bosbach, and A. Manceau. 2002. Arsenic(III) oxidation by birnessite and precipitation of manganese(II) arsenate. Environ. Sci. Technol. 36:493-500.

USEPA. 2001. National primary drinking water regulations; arsenic and clarifications to compliance and new source contaminants monitoring, pp. 6976-7065, Vol. Rule 66 FR 6976. Federal Register.

Villalobos, M., B. Toner, J. Bargar, and G. Sposito. 2003. Characterization of the manganese oxide produced by *Pseudomonas putida* strain MnB1. Geochim. Cosmochim. Acta 67:2649-2662.

Villalobos, M., B. Lanson, A. Manceau, B. Toner, and G. Sposito. 2006. Structural model for the biogenic Mn oxide produced by Pseudomonas putida. Am. Mineral. 91:489-502.

Webb, S.M., B.M. Tebo, and J.R. Bargar. 2005a. Structural characterization of biogenic Mn oxides produced in seawater by the marine bacillus sp. strain SG-1. Am. Mineral. 90:1342-1357.

Webb, S.M., G.J. Dick, J.R. Bargar, and B.M. Tebo. 2005b. Evidence for the presence of Mn(III) intermediates in the bacterial oxidation of Mn(II). Proc. Natl. Acad. Sci. 102:5558-5563.

Winship, K.A. 1984. Toxicity of inorganic arsenic salts. Adv. Drug React. Ac. Pois. Rev. 3:129-60.

Zhu, M., M. Ginder-Vogel, and D.L. Sparks. 2010a. Ni(II) sorption on biogenic Mn-oxides with varying Mn octahedral layer structure. accepted to Environ. Sci. Technol.

Zhu, M., K.W. Paul, J.D. Kubicki, and D.L. Sparks. 2009. Quantum chemical study of arsenic (III, V) adsorption on Mn-oxides: Implications for arsenic(III) oxidation. Environ. Sci. Technol. 43:6655-6661.

Zhu, M., M. Ginder-Vogel, S.J. Parikh, X.-H. Feng, and D.L. Sparks. 2010b. Cation effects on the layer structure of biogenic Mn-oxides. Accepted to Environ. Sci. Technol.

Chapter 1

ARSENITE OXIDATION BY A POORLY-CRYSTALLINE MANGANESE OXIDE: STIRRED-FLOW EXPERIMENTS

Abstract

Manganese-oxides (Mn-oxides) are quite reactive, with respect to arsenite (As^{III}) oxidation. However, studies regarding the pathways of As^{III} oxidation, over a range of time scales, by poorly-crystalline Mn-oxides, are lacking. In stirred-flow experiments, As^{III} oxidation by δ-MnO_2 (a poorly crystalline hexagonal birnessite) is initially rapid but slows appreciably after several hours of reaction. Mn^{II} is the only reduced product of δ-MnO_2 formed by As^{III} oxidation during the initial, most rapid phase of the reaction. There seems to be evidence that the formation of Mn^{III} observed in previous studies is a result of conproportionation of Mn^{II} sorbed onto Mn^{IV} reaction sites rather than from direct reduction of Mn^{IV} by As^{III}. The only evidence of arsenic (As) sorption is during the initial period of rapid As^{III} oxidation by δ-MnO_2, and As sorption is greater when As^{V} and Mn^{II} occur simultaneously in solution. Our findings indicate that As^{III} oxidation by poorly-crystalline δ-MnO_2 involves several simultaneous reactions and reinforces the importance of Mn oxidation state in the reactivity of Mn-oxides, as well as the value of studying reaction mechanisms over a range of time scales.

Introduction

Manganese-oxide (Mn-oxide) minerals are powerful oxidizing agents, and they play an important role in many redox processes in the environment. Specifically, Mn-oxides have been observed as the primary oxidizing agent of arsenic (As) in some environments (Oscarson et al., 1981a; Oscarson et al., 1981b). The oxidation of arsenite (As^{III}) to arsenate (As^{V}) is an important reaction in the environment because it decreases As mobility by increasing its tendency to be sorbed to mineral surfaces (Dixit and Hering, 2003; Gupta and Chen, 1978; Hingston et al., 1971). Also, since As^{V} is less toxic than As^{III} (Petrick et al., 2000), Mn-oxides can act as detoxifying agents.

The reactivity of Mn-oxide minerals varies with their mineralogy, and layered Mn-oxide minerals (i.e. phyllomanganates) are more reactive, in terms of As^{III} oxidation, than other types of Mn-oxides (Chiu and Hering, 2000; Manning et al., 2002; Oscarson et al., 1983; Scott and Morgan, 1995; Tournassat et al., 2002). During reaction with As^{III}, phyllomanganates become passivated, i.e. As^{III} oxidization initially proceeds rapidly, followed by a decrease in oxidation rate (Ginder-Vogel et al., 2009; Manning et al., 2002; Moore et al., 1990; Oscarson et al., 1981a; Parikh et al., 2008; Scott and Morgan, 1995; Tani et al., 2004; Tournassat et al., 2002). In early studies, passivation of the Mn-oxide surface (represented by $>Mn^{IV}O_2$ in Equation 1.1) was attributed to sorption of Mn^{II} (Equation 1.1), which is created during As^{III} oxidation (Equation 1.2) (Oscarson et al., 1981a; Scott and Morgan, 1995). However, discovery

of a Mn^{III} intermediate, produced during As^{III} oxidation by phyllomanganates (Nesbitt et al., 1998), has been proposed as

$$Mn^{II} + >Mn^{IV}O_2 \rightarrow >Mn^{IV}O_2\text{-}Mn^{II} \quad [1.1]$$

$$Mn^{IV}O_2 + H_3As^{III}O_3 + 2H^+ \rightarrow Mn^{II} + H_3As^{V}O_4 + H_2O \quad [1.2]$$

another cause of Mn-oxide passivation (Nesbitt et al., 1998; Tournassat et al., 2002) (Equations 1.3 and 1.4). The Mn^{III} reactive site ($Mn^{III}OOH$ in Equations 1.3 and 1.4) on a Mn-oxide surface is expected to be less reactive than a Mn^{IV} reactive site, in terms of As^{III} oxidation (Zhu et al., 2009).

$$2Mn^{IV}O_2 + H_3As^{III}O_3 + H_2O \rightarrow 2Mn^{III}OOH + H_3As^{V}O_4 \quad [1.3]$$

$$2Mn^{III}OOH + H_3As^{III}O_3 + 4H^+ \rightarrow 2Mn^{II}(aq) + H_3As^{V}O_4 + 3H_2O \quad [1.4]$$

Although most As^{V} produced during As^{III} oxidation by phyllomanganates is released into solution, it is also possible that some As^{V} is sorbed by the solid phase and thus can also contribute to passivation of the mineral surface (Foster et al., 2003; Manning et al., 2002; Zhu et al., 2009). Passivation of phyllomanganates can also occur by the formation of a Mn/As precipitate under certain reaction conditions (Tournassat et al., 2002).

Although several Mn-oxide minerals have the ability to oxidize As^{III}, the most reactive Mn-oxides have a great potential to affect As speciation, even when present in

small quantities. There is evidence that a large number of Mn-oxides found in surface environments are poorly-crystalline and of biogenic origin (Shiller and Stephens, 2005; Tebo et al., 2004). Also, these poorly-crystalline biogenic Mn-oxides may be among the most reactive Mn-oxides in the environment (Tebo et al., 2004). Therefore, it is important to understand the reactivity of poorly-crystalline Mn-oxides, as it relates to As speciation, not only because of their higher reactivity, but also because of their abundance in the environment.

Because the reactivity of phyllomanganates can decrease over time, it is important to understand the causes of this passivation and how it affects As speciation. A number of studies have investigated As^{III} oxidation by Mn-oxides; however the fundamental mechanisms controlling the reactions between As^{III} and poorly-crystalline, environmentally representative Mn-oxides are not entirely clear. Accordingly, in this study, the reactions of As^{III} with a poorly-crystalline hexagonal birnessite, δ-MnO_2, are investigated, using a stirred-flow technique over a range of time scales, in order to better understand the kinetics and mechanisms of reaction processes and their influence on the speciation and mobility of As in natural systems. A unique benefit of stirred-flow techniques in measuring reaction kinetics is that reaction products are removed from the reactor, thus limiting potential reactions between these products and the mineral surface being studied.

Materials and Methods

δ-MnO_2 Synthesis and Characterization

δ-MnO_2, a poorly-crystalline, phyllomanganate, was used in the studies presented here because of its high reactivity as well as its similarities to biogenic Mn-oxides (Villalobos et al., 2003). δ-MnO_2 is a form of hexagonal birnessite with a low degree of stacking of phyllomanganate sheets (Drits et al., 1997; Silvester et al., 1997). δ-MnO_2, was synthesized by drop wise addition of a 100 mL solution containing 11.29 g $Mn(NO_3)_2{\cdot}4H_2O$ to a 100 mL solution containing 2.4 g NaOH and 4.74 g $KMnO_4$, corresponding to a final Mn^{II}:Mn^{VII}:OH ratio of 3:2:4 (Morgan and Stumm, 1964). After adding Mn^{II} to the basic permanganate solution, the resulting suspension was stirred overnight (at least 12 hours) to allow complete conproportionation of Mn^{II} and Mn^{VII} to Mn^{IV}. Following synthesis, δ-MnO_2 was washed with 18.2 MΩ deionized (DI) water via centrifugation (10,000 RCF for 15 min) three times and then dialyzed (Spectra/Por, 12,000–14,000 MWCO, Spectrum) in DI water until the conductivity of dialysis water remained unchanged for 12 hours (usually 2 days). Following dialysis, δ-MnO_2 was transferred to a polypropylene bottle, suspended in DI water, and stored at 4 ^oC prior to use in experiments. Experiments were conducted using δ-MnO_2 within three weeks of synthesis.

The average oxidation state of Mn in the δ-MnO_2 structure used in these experiments was determined, by oxalate titration (Villalobos et al., 2003), to be 3.95. The point of zero charge (PZC) of δ-MnO_2 is 1.85 using the prolonged salt titration

method (PST) appropriate for Mn-oxides as outlined by Tan et al. (2008) (Figure 1.1). X-ray diffraction (XRD) confirmed that the only product of the synthesis was poorly-crystalline δ-MnO_2 (Figure 2.3, Chapter 2). The surface area of δ-MnO_2 was 273.5 m^2 g^{-1}, using BET analysis in which air-dried δ-MnO_2 was purged with a dry He atmosphere at room temperature (~25 ^oC) for 16 hours to remove as much water as possible without heating the mineral. An average δ-MnO_2 particle size of 450 nm was determined by dynamic light scattering (Zetasizer ® Nano Series, Malvern Instruments Ltd.). High-resolution transmission electron microscopy (HRTEM) further showed that δ-MnO_2 had few, small crystalline domains surrounded by poorly-crystalline (i.e. TEM amorphous) material, all of which were aggregated together into larger particles that varied in size (Figure 1.2).

Stirred-Flow Experiments

As^{III} oxidation by δ-MnO_2 was investigated using a modified version of the stirred-flow reactor described by Wielinga et al. (2001). The original reactor was modified to reduce the reaction chamber volume to 30 mL for use in these experiments. The reaction suspension was mixed at 100 rpm via a magnetic stir bar suspended in the reaction chamber. During stirred-flow experiments, δ-MnO_2 suspensions were retained in the reactor at the inlet by solution flowing into the reactor at 1 mL/min and at the outlet by a 0.22 μm pore size filter. Effluent solution was collected by a fraction collector and stored at 4 ^oC in the dark until analysis.

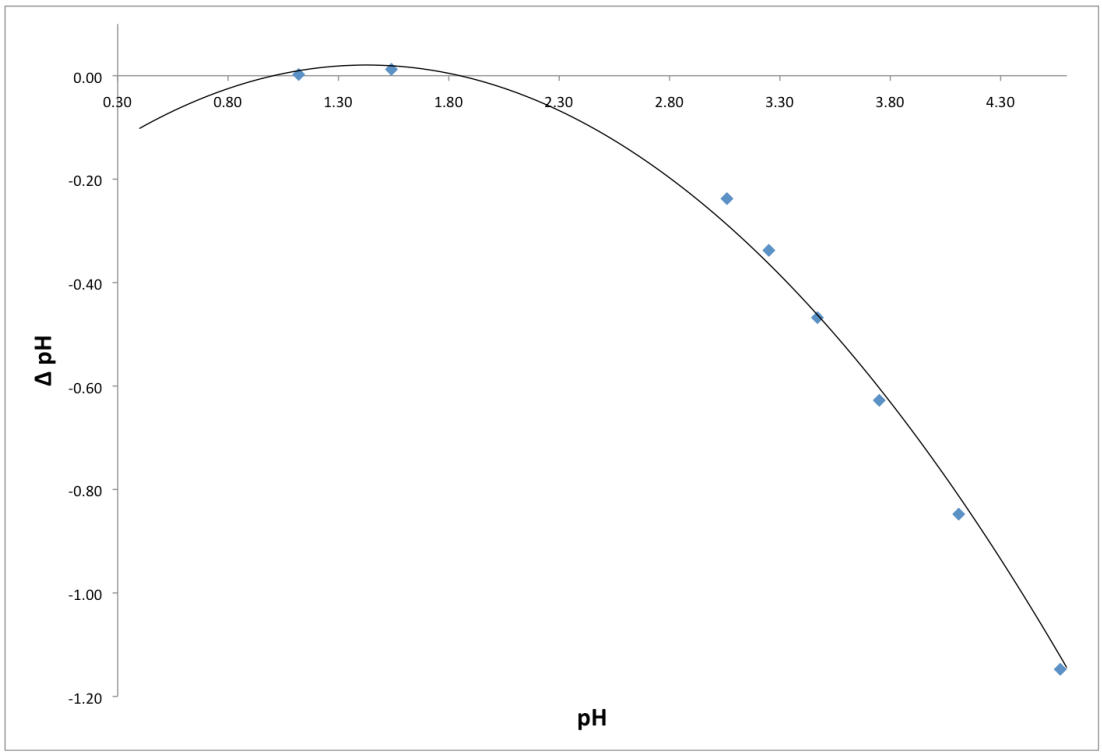

Figure 1.1. Point of zero charge of δ-MnO_2 measured by the prolonged salt titration method.

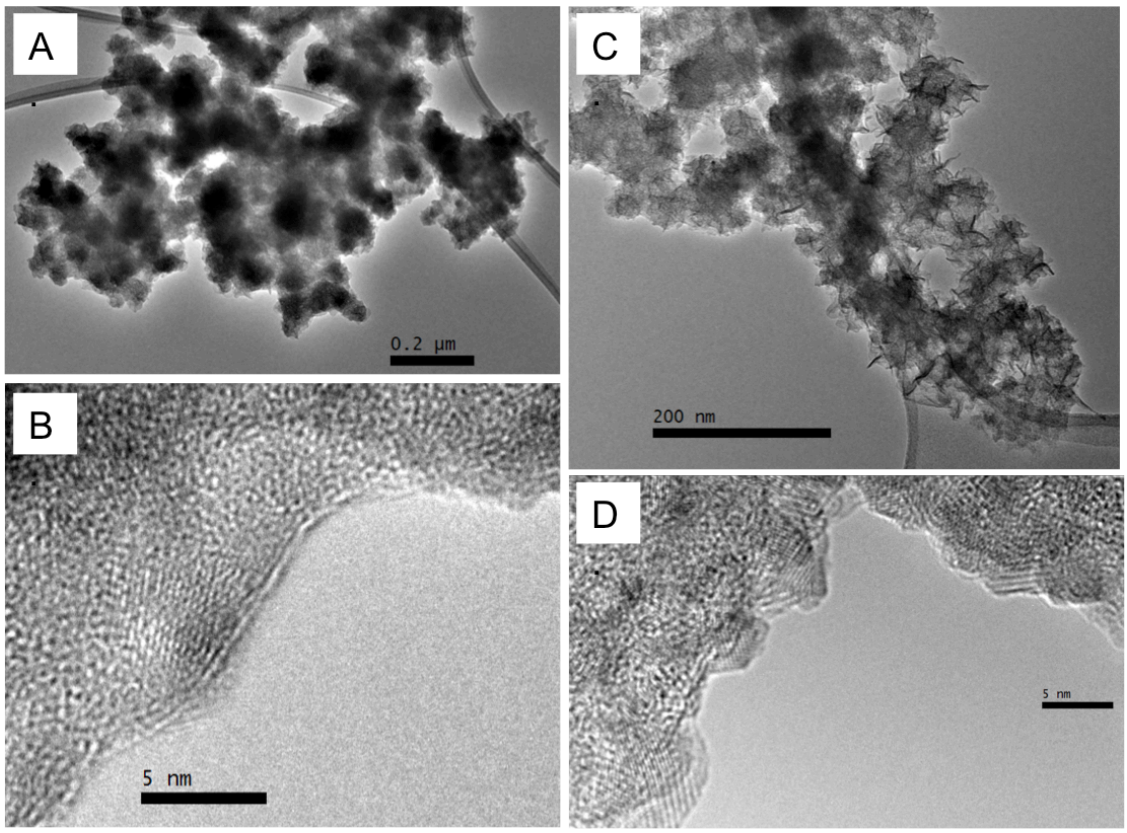

Figure 1.2. Transmission electron micrographs of unreacted δ-MnO_2 (A and B), and δ-MnO_2 reacted with As^{III} for 48 hours (C and D).

All reactions were conducted in a background electrolyte solution of 10mM NaCl and 5mM MOPS adjusted to pH 7.2. The δ-MnO_2 concentration in stirred-flow reactions was 1 g/L (corresponding to 30 mg δ-MnO_2 in the reactor). Before each experiment, background electrolyte solution was introduced into the reactor at a flow rate of 1 mL/min for at least 2 hours. Each experiment was conducted by flowing solution consisting of the background electrolyte and a reactant (i.e. As^{III}, As^{V}, or Mn^{II}) into the reaction chamber by a peristaltic pump at 1 mL/min for the duration of the experiment. All stirred-flow experiments were conducted at least in duplicate. A stopped-flow test was conducted (Bar-Tal et al., 1990), and it was determined that kinetic processes were being observed.

The flow rate used for all stirred-flow reactions in this study was 1 mL/min, and the concentration of reactants when each reaction started (i.e. t = 0) was zero. Thus, when a reactant was introduced into the stirred-flow reactor, some time was required before the reactant concentration in the reactor reached equilibrium (i.e. concentration of a reactant entering the reactor equaled the concentration of that same reactant leaving the reactor, assuming no retention of that reactant in the stirred-flow reactor). For example, when 100 μM As^{III} was introduced to the stirred-flow reactor, 3.4 hours were required for the concentration of total As flowing out of the reactor to equal 100 μM (assuming no As sorption). To minimize confusion caused by this dilution during the first 3.4 hours, it is useful to consider the concentration of each As species as a % of the total As in the reactor (Figure 1.3b).

In all experiments, As^{III} and As^{V} were quantified by liquid chromatography inductively coupled plasma mass spectrometry (LC-ICP-MS), and Mn in the stirred-flow reactor effluent was quantified by ICP-MS. By measuring both reactants and products in the stirred-flow effluent, a mass balance relationship for As and Mn could be calculated at any given time point. The amount of As sorbed during the reaction was determined by calculating the difference between the mass of As (nmol) introduced into the reactor and the mass of As (nmol) removed from the reactor in the effluent at each sampling point.

Results and Discussion

As^{III} Oxidation by δ-MnO_2

We hypothesize that four possible pathways exist for the oxidation of As^{III} by δ-MnO_2, with each pathway using a different combination of Mn reactive sites on the δ-MnO_2 surface for As^{III} oxidation. In the first pathway, one As^{III} molecule reacts with one Mn^{IV} reactive site (represented by $>Mn^{IV}$-OH in Equations 1.5 – 1.7; protonation state based on Peacock and Sherman (2007)) producing one As^{V} molecule and one Mn^{II} molecule (Equation 1.5). One As^{III} molecule could also react with two Mn^{IV} reactive sites producing one As^{V} molecule and two Mn^{III} reactive sites (represented by $>Mn^{III}$-OH_2 in Equations 1.6 – 1.8; protonation state based on Ramstedt et al. (2004)) (Equation 1.6).

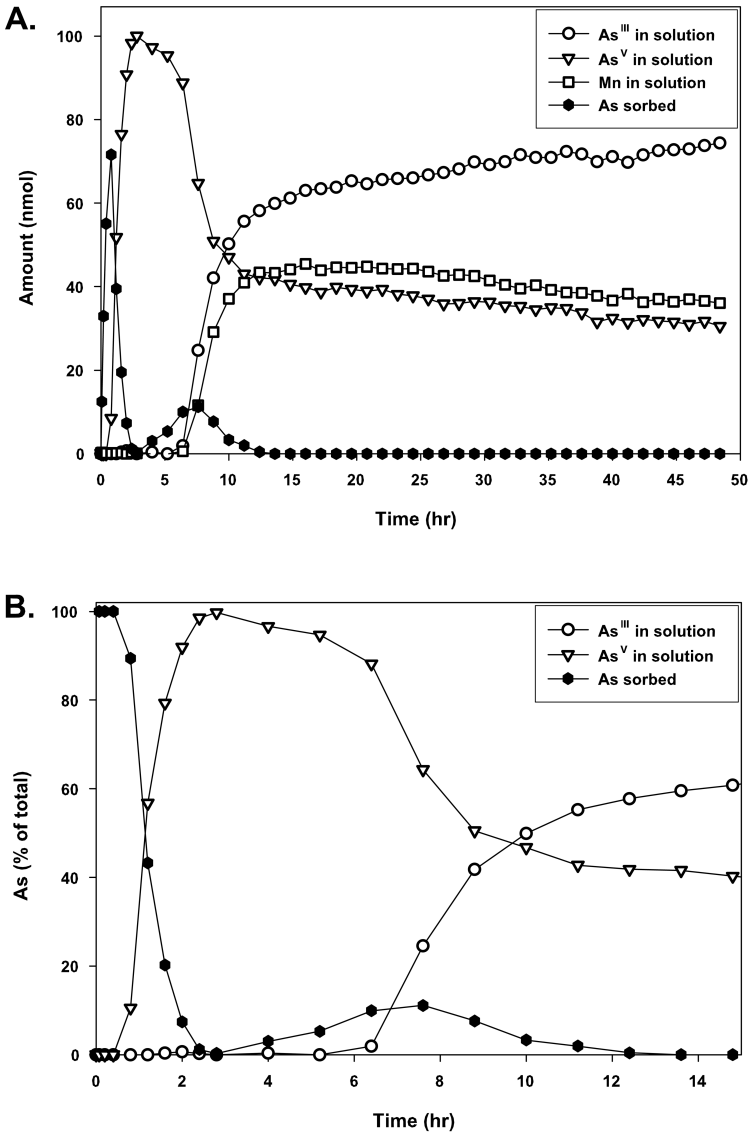

Figure 1.3. (A.) The amount (nmol) of As sorbed as well as amounts (nmol) of As^{III}, As^{V}, and Mn^{II} in the effluent of a stirred-flow experiment reacting 1 g/L δ-MnO_2 with 100 µM As^{III} flowing at 1 mL/min for 48 hours. (B.) The proportion (%) of As as As^{III}, As^{V}, and As sorbed to δ-MnO_2 during the first 15 hours of the same stirred-flow experiment.

$$>Mn^{IV}\text{-}OH + H_3As^{III}O_3(aq) \rightarrow Mn^{II}(aq) + HAs^{V}O_4^{2-}(aq) + 3H^+ \quad [1.5]$$

$$2(>Mn^{IV}\text{-}OH) + H_3As^{III}O_3(aq) + H_2O \rightarrow 2(>Mn^{III}\text{-}OH_2) + HAs^{V}O_4^{2-}(aq) + 2H^+ \quad [1.6]$$

The third and fourth potential As^{III} oxidation pathways require that the δ-MnO_2 surface first contain Mn^{III} reactive sites. One proposed mechanism is for Mn^{III} to be formed directly through As^{III} oxidation (Equations 1.3 and 1.6) (Nesbitt et al., 1998). However, recent studies have indicated that Mn^{III} can be formed by conproportionation of Mn^{II} and Mn^{IV} at the δ-MnO_2 surface. In this conproportionation reaction, Mn^{II} is oxidized, Mn^{IV} is reduced, and the resulting product is Mn^{III} (Perez-Benito, 2002; Webb et al., 2005). Mn^{III} produced by conproportionation of Mn^{II} and Mn^{IV} could produce soluble Mn^{III}, but with no ligand to stabilize Mn^{III} in the reactions discussed here, any soluble Mn^{III} should quickly disproportionate back into Mn^{II} and Mn^{IV} (Morgan, 2000). Therefore, we assume all Mn^{III} in these reactions is associated with the δ-MnO_2 surface.

One possibility for As^{III} to be oxidized by Mn^{III} is through the reaction of one As^{III} molecule with one Mn^{III} reactive site and one Mn^{IV} reactive site, resulting in one As^{V} molecule, one Mn^{II} molecule and one Mn^{III} reactive site (Equation 1.7). The final potential pathway for As^{III} oxidation by δ-MnO_2 is for one As^{III} molecule to react with two Mn^{III} reactive sites forming one As^{V} molecule and two Mn^{II} molecules (Equation 1.8). When 100 μM As^{III} is reacted with 1 g/L δ-MnO_2, there are two clear reaction

$$>Mn^{IV}\text{-}OH + >Mn^{III}\text{-}OH_2 + H_3As^{III}O_3(aq) \rightarrow$$

$$Mn^{II}(aq) + >Mn^{III}\text{-}OH_2 + HAs^{V}O_4^{2-}(aq) + 3H^+ \quad [1.7]$$

$$2(>Mn^{III}\text{-}OH_2) + H_3As^{III}O_3(aq) \rightarrow 2Mn^{II}(aq) + HAs^{V}O_4^{2-}(aq) + H_2O + 4H^+ \quad [1.8]$$

phases. During the initial 6.4 hours of reaction, only As^V appears in the reactor effluent, indicating that all As^{III} introduced into the reactor during this period is oxidized to As^V or sorbed onto the δ-MnO_2 surface (Figure 1.3). After 6.4 hours of reaction, a second phase of the reaction begins, in which the oxidation rate of As^{III} slows, as indicated by the appearance and subsequent increase of As^{III} in the reactor effluent from 6.4 - 48 hours (Figure 1.3). Thus, the first 6.4 hours of reaction between As^{III} and δ-MnO_2 represents the period of highest reactivity and the most rapid rate of As^{III} oxidation. Although the rate decreases from 6.4 - 48 hours, As^{III} oxidation is continuous throughout the experiment.

The observed decrease in reactivity of δ-MnO_2 when reacted with As^{III} (Figure 1.3) can be attributed to passivation of the δ-MnO_2 surface. As discussed previously, passivation of phyllomanganates is likely caused by formation of less reactive Mn^{III} sites, sorption of Mn^{II}, or sorption of As^V. Passivation caused by physically blocking reaction sites likely occurs by Mn^{II} or As^V sorbing at δ-MnO_2 edge sites, which likely is the location of As^{III} oxidation (Tournassat et al., 2002). The net effect of physically blocking some surface sites where As^{III} can be oxidized is that fewer reaction sites are

available for As^{III} oxidation, resulting in an apparent slowing in As^{III} oxidation rate. On the other hand, passivation by the formation of Mn^{III} sites on the δ-MnO_2 surface should not decrease the number of available reactive sites, but rather replace more reactive Mn^{IV} sites with less reactive Mn^{III} sites. The roles of both As and Mn in passivation of δ-MnO_2 is discussed in the following sections.

During As^{III} oxidation by δ-MnO_2, As retained on the solid phase via precipitation of a Mn^{II}/As^{V} precipitate (Tournassat et al., 2002) could also lead to passivation. The data in Figure 1.3 suggest that a precipitate is not formed during As^{III} oxidation by δ-MnO_2 because there is no increase in As associated with δ-MnO_2 beyond 12.4 hours of reaction. Also, TEM images of δ-MnO_2 reacted with As^{III} do not reveal a change in particle morphology as is expected with the precipitation of a new mineral phase (Figure 1.2).

Arsenic Sorption

When As^{III} is oxidized by δ-MnO_2 in a stirred-flow reactor, two periods of As sorption are observed. Initially (0 - 0.4 hours) all As added to the reactor is completely sorbed, followed by continuous decrease in As sorption until 2.8 hours, at which point no As is sorbed by δ-MnO_2 (Figure 1.3b). Subsequently, a second period of As sorption occurs from 2.8 – 13.6 hours. During this second period of As sorption, less As is sorbed than during the initial period of As sorption (Figure 1.3b), and no further As sorption occurs after 13.6 hours. Interestingly, the peak of the

second period of As sorption during As^{III} oxidation by δ-MnO_2, coincides with the first appearance of As^{III} and Mn^{II} in the reactor effluent (Figure 1.3), which is also the point at which δ-MnO_2 reactivity decreases. Sorption of As at δ-MnO_2 edge sites could play a role in δ-MnO_2 passivation. It is unlikely, however, that As sorption is the only cause of δ-MnO_2 passivation since the rate of As^{III} oxidation continues to decrease well after As sorption has stopped (Figure 1.3).

While As^{III} must be sorbed to the δ-MnO_2 surface prior to its oxidation, previous experimental results indicate that when either As^{V} or As^{III} is reacted with phyllomanganates, As is retained only as As^{V} on the mineral surface (Manning et al., 2002). Although stirred-flow techniques have the unique benefit of removing products from the reactor (in this case, As^{V}), sorption of As^{V} onto the surface of Mn-oxides can be more rapid than the 3.4 hours required to completely remove it from the reactor in these experiments (Manning et al., 2002). The sorption of As during As^{III} oxidation is evidence that As^{V} cannot be removed from the stirred-flow reactor in these experiments quickly enough to completely prevent its interaction with the δ-MnO_2 surface (Figure 1.3). Therefore, in order to understand the reaction mechanisms controlling As^{III} oxidation by δ-MnO_2, specifically δ-MnO_2 passivation, one must also understand the interactions between As^{V} and the δ-MnO_2 surface.

In order to better understand As sorption mechanisms that occur during As^{III} oxidation, stirred flow experiments were conducted by reacting pristine δ-MnO_2 with As^{V} alone and with As^{V} and Mn^{II} simultaneously, in addition to reacting Mn^{II}-

saturated δ-MnO_2 with As^{III}. To produce Mn^{II}-saturated δ-MnO_2, 50 μM Mn^{II} was reacted with δ-MnO_2 for 48 hours, followed immediately by reaction with 100 μM As^{III} for an additional 48 hours. The purpose of reacting δ-MnO_2 with Mn^{II} for 48 hours was to ensure that the δ-MnO_2 surface was saturated with Mn^{II}, thus allowing Mn^{II} to block as many δ-MnO_2 reaction sites as possible. After 22 hours of reaction, Mn^{II} appeared in the stirred-flow reactor effluent, confirming that δ-MnO_2 was saturated with Mn^{II} (data not shown).

In all experiments, an initial period of high As sorption occurs (Figure 1.4). However, when pristine δ-MnO_2 is reacted with 100 μM As^{V} or when Mn^{II}-saturated δ-MnO_2 is reacted with 100 μM As^{III}, no second period of As sorption is seen, unlike As^{III} oxidation by pristine δ-MnO_2 (Figure 1.4). Also, the second period of As sorption observed when As^{III} is oxidized by pristine δ-MnO_2 does occur when As^{V} and Mn^{II} are reacted simultaneously with pristine δ-MnO_2 (Figure 1.4). A comparison of the total As sorbed in these experiments reveals that more As is sorbed when As^{III} is reacted with pristine δ-MnO_2 (130.7 $nmol_{As\ sorbed}$) or when As^{V} and Mn^{II} are reacted with pristine δ-MnO_2 simultaneously (425.5 $nmol_{As\ sorbed}$) than when As^{V} is reacted with pristine δ-MnO_2 (87.6 $nmol_{As\ sorbed}$) or As^{III} is reacted with Mn^{II}-saturated δ-MnO_2 (111.0 $nmol_{As\ sorbed}$). The increase in As sorption during As^{III} oxidation compared to the As sorbed during the reaction of As^{V} with phyllomanganates has been reported previously (Manning et al., 2002; Oscarson et al., 1983; Parikh et al., 2008;

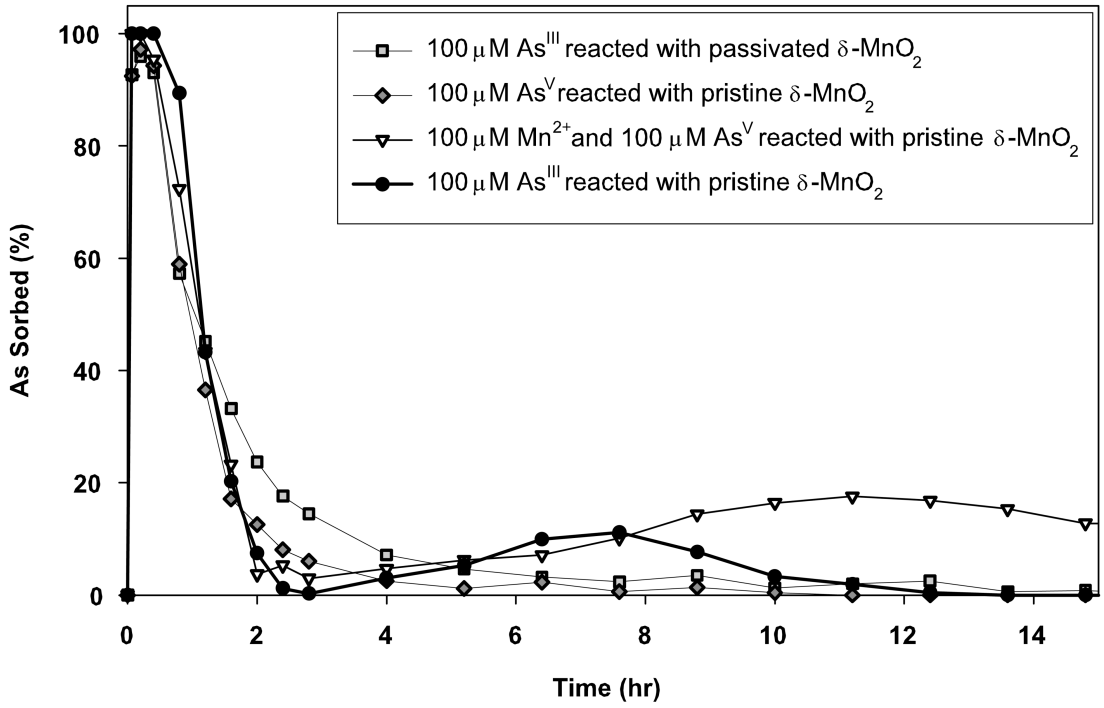

Figure 1.4. Percentage of As sorbed by δ-MnO_2 over time in four stirred-flow experiments. Three stirred-flow experiments were conducted by reacting 1 g/L of pristine δ-MnO_2 with 100 μM As^{III}, 100 μM As^{V}, or 100 μM As^{V} and 100 μM Mn^{II} simultaneously, while the other experiment was conducted by reacting 1 g/L of Mn^{II}-saturated δ-MnO_2 with 100 μM As^{III}.

Tani et al., 2004). Also, an increase in Mn^{II} concentration in solution simultaneously with As^{V} enhances As sorption while saturating δ-MnO_2 with Mn^{II} prior to As^{III} oxidation leads to an intermediate increase in As sorption, compared to As^{V} sorbed to δ-MnO_2 alone. δ-MnO_2 is expected to possess two types of reaction sites: vacancy sites within phyllomanganate sheets and edge sites at the edges of Mn octahedral sheets (Drits et al., 1997). Arsenic is probably oxidized and sorbed only at edge sites of δ-MnO_2 (Tournassat et al., 2002), while heavy metal (including Mn^{II}) sorption probably occurs both on edge sites as well as vacancy sites of δ-MnO_2 (Manceau et al., 2007; Peacock and Sherman, 2007). Because of their high density of negative charge, it is likely that vacancy sites are the primary location of Mn^{II} sorption, until they are all occupied. After all vacancy sites are saturated, Mn^{II} can potentially compete with As for edge sites. It is possible that the initial period of As sorption during As^{III} oxidation (i.e. 0 – 2.8 hours), occurs during the period that Mn^{II} reacts only with vacancy sites, and the second period of As sorption (2.8-13.2 hours) is when Mn^{II} begins to react with edge sites. This scenario explains the overall decrease in As sorption during As^{III} oxidation by δ-MnO_2, but fails to account for the two observed periods of sorption.

There are two previously observed reactions that can potentially explain the second period of As sorption during As^{III} oxidation by δ-MnO_2. First, as Mn^{II} begins to react with δ-MnO_2 edge sites, a ternary Mn^{II}-As^{V} sorption complex might form, causing an increase in As sorption. It is also known that Mn^{II} can undergo

conproportionation with Mn^{IV} on the δ-MnO_2 surface, forming Mn^{III} reactive sites (discussed in detail later), which may occur when Mn^{II} begins to react at δ-MnO_2 edge sites. A newly formed Mn^{III} reactive site on the δ-MnO_2 surface could create new sorption sites for As, which might explain the second period of As sorption. However, without spectroscopic data of As sorption complexes, elucidating the As sorption mechanisms is difficult.

Role of Mn Speciation in δ-MnO_2 Reactivity

Mn speciation plays a crucial, determining role in both As sorption by δ-MnO_2 and passivation of the δ-MnO_2 surface during As^{III} oxidation. Therefore, one must understand the reactions controlling Mn speciation at the δ-MnO_2 surface in order to understand the mechanisms involved in As oxidation and sorption by δ-MnO_2. Although it is important to understand Mn speciation at the δ-MnO_2 surface, direct characterization of Mn in the δ-MnO_2 solid phase is not possible using only the aqueous phase data presented here. However, inferences can be made regarding Mn speciation at the δ-MnO_2 surface by examining possible reaction pathways using aqueous phase data from stirred-flow reactions.

To investigate the role of Mn^{II} sorption in δ-MnO_2 passivation, a stirred-flow experiment was conducted measuring As^{III} oxidation by Mn^{II}-saturated δ-MnO_2 (described previously). When Mn^{II}-saturated δ-MnO_2 is reacted with As^{III}, the initial rapid oxidation of As^{III} observed during As^{III} oxidation by pristine δ-MnO_2, does not

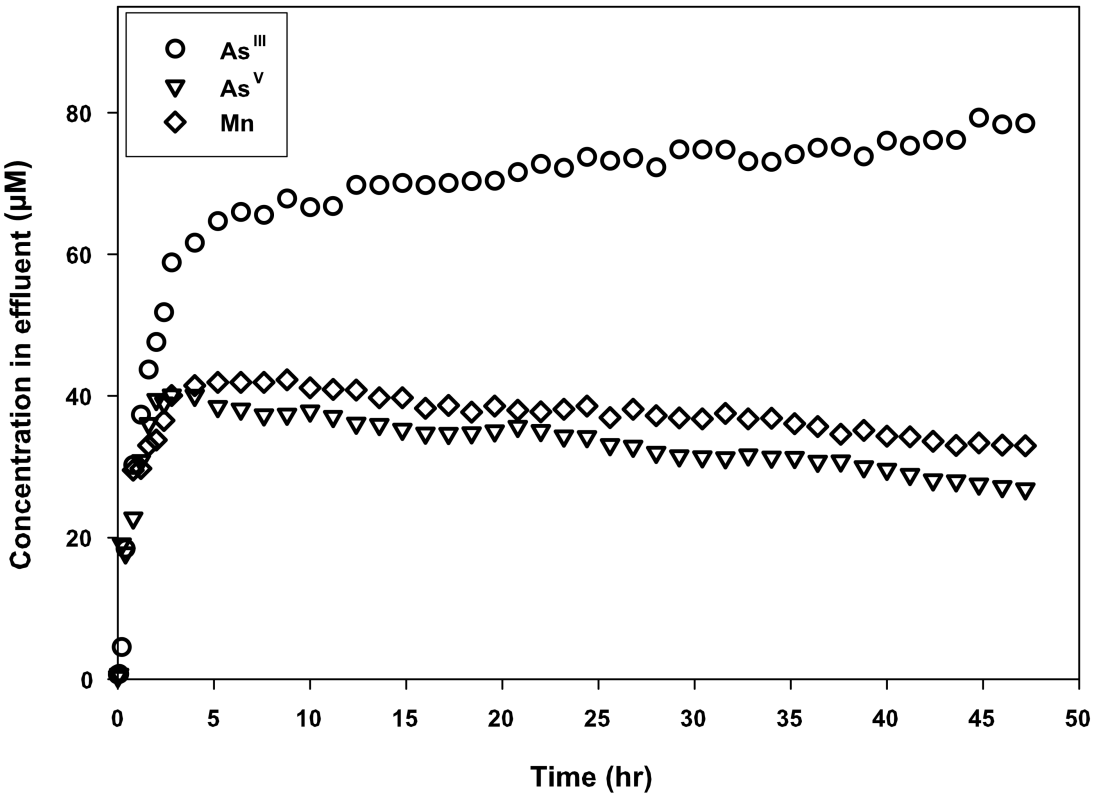

Figure 1.5. As^{V}, As^{III}, and Mn^{II} concentrations in the effluent of a stirred-flow reaction in which a 1 g/L suspension of Mn^{II}-saturated δ-MnO_2 was reacted with 100 µM As^{III} flowing at 1 mL/min for 48 hours. δ-MnO_2 was saturated by reaction with 50 µM Mn^{II}, and no Mn was added to the stirred-flow reactor during the time period shown.

occur (Figures 1.3 and 1.5), however, the initial reactivity of Mn^{II}-saturated δ-MnO_2 is nearly identical to that of pristine δ-MnO_2 beyond 6.4 hours (Figures 1.3 and 1.5). These results seem to indicate that reaction of Mn^{II} with the δ-MnO_2 surface plays an important role in the passivation of pristine δ-MnO_2 during the first ~6 hours of As^{III} oxidation. Although initial reactivity is decreased when δ-MnO_2 is saturated with Mn^{II}, δ-MnO_2 is still able to oxidize As^{III} when saturated with Mn^{II}. This indicates that there are still some reaction sites on the δ-MnO_2 surface that are not blocked by As^{V} and Mn^{II}, for which As^{III} is competitive. The ability of Mn^{II} sorption to passivate δ-MnO_2 similar to passivation during As^{III} oxidation seems to imply that As^{V} sorption plays a limited role in passivation of δ-MnO_2 during As^{III} oxidation.

When considering surface passivation in the initial phases of As^{III} oxidation by δ-MnO_2, it is important to determine the importance of Mn^{II} sorption versus formation of less reactive Mn^{III} surface sites. During the first 5.2 hours of As^{III} oxidation by δ-MnO_2, when the highest amounts of As^{V} occur in the reactor, no Mn appears in the reactor effluent (Figure 1.3a). The lack of Mn in the reactor effluent early in the reaction, when Mn^{IV} predominates the δ-MnO_2 structure (average Mn oxidation state of pristine δ-MnO_2 = 3.95), indicates that As^{III} oxidation produces either Mn^{III} reactive sites at the δ-MnO_2 surface (Equation 1.6), or Mn^{II} (Equation 1.5) which is completely retained by the δ-MnO_2 surface. It is difficult to distinguish Mn^{II} versus Mn^{III} formation by As data in the stirred-flow effluent alone.

One possible way to decipher the prevalence of Mn^{III} reactive sites produced versus the prevalence of Mn^{II} produced by As^{III} oxidation is by utilizing the Mn^{II} sorption capacity of δ-MnO_2. Sorption capacity of δ-MnO_2 can be evaluated by sorbing Mn^{II} to pristine δ-MnO_2 in a stirred-flow reactor. By assuming that Mn^{II} will not appear in the stirred-flow reactor effluent until δ-MnO_2 is saturated with Mn^{II}, the time at which Mn^{II} appears in the effluent can be considered the time at which δ-MnO_2 is (very nearly) saturated. By comparing the time required for Mn^{II} to appear in the reactor effluent when 100 μM Mn^{II} is reacted with pristine δ-MnO_2 to the time required for Mn^{II} to appear in the reactor effluent during 100 μM As^{III} oxidation by δ-MnO_2, conclusions can be made regarding how much Mn^{II} versus Mn^{III} is produced by As^{III} oxidation. This comparison requires the assumption that Mn^{II} will not appear in the reactor effluent of either reaction until the δ-MnO_2 surface is saturated (or very nearly saturated) with Mn^{II}. When 100 μM Mn^{II} is reacted with δ-MnO_2, dissolved Mn appears in the reactor effluent after 7.6 hours of reaction, which is similar to the time that Mn^{II} appears in stirred-flow effluent during the reaction of 100 μM As^{III} with δ-MnO_2 (6.4 hours) (Figure 1.6). The most probable reason for Mn^{II} appearance in the reactor effluent at a slightly earlier time when As^{III} is oxidized than during Mn^{II} sorption, is dissolution of the δ-MnO_2 surface during As^{III} oxidation, which results in fewer sorption sites for Mn^{II}. On the other hand, when 50 μM Mn^{II} is reacted with δ-MnO_2, dissolved Mn does not appear in the reactor effluent until 12.4 hours of reaction. The appearance of Mn^{II} in the stirred-flow reactor effluent at approximately

the same time during oxidation of 100 μM As^{III} and during the sorption of 100 μM Mn^{II} indicates that during the initial phase of rapid As^{III} oxidation by δ-MnO_2, a nearly equal amount of Mn^{II} is sorbed by δ-MnO_2. Therefore, it is reasonable to conclude that Mn^{II} is the primary reduced Mn product of As^{III} oxidation.

However, there is more than one pathway that can produce Mn^{II} from the oxidation of As^{III} by δ-MnO_2. Either a combination of equations 6 and 8, or equation 1.5 alone can produce the same amount of Mn^{II} from the oxidation of As^{III}. If equation 1.5 is solely responsible, all As^{III} oxidation produces Mn^{II} with no Mn^{III} intermediate, and if equations 1.6 and 1.8 are solely responsible the net result is the same, with the exception of the formation of a Mn^{III} intermediate. Batch experiments were conducted under the same reaction conditions as stirred-flow experiments, using manganite (γ-$Mn^{III}OOH$) as a proxy for Mn^{III} reaction sites on δ-MnO_2, and they indicate that As^{III} oxidation by Mn^{III} is negligible within 48 hours (Figure 1.7). Thus, we can infer that As^{III} oxidation by Mn^{III} reactive sites on the δ-MnO_2 surface (Equations 1.7 and 1.8) is too slow to be significant during the first 6.4 hours of reaction between As^{III} and δ-MnO_2. Therefore, we conclude that As^{III} oxidation occurs as a 2 electron transfer with δ-MnO_2, and does not proceed through a Mn^{III} intermediate early in the reaction. Luther and Popp (2002) have also proposed a 2 electron transfer in the oxidation of an oxyanion (nitrite) by a Mn-oxide similar to δ-MnO_2. The data presented here do not preclude the presence of Mn^{III} sites on δ-MnO_2 during the first 6.4 hours of reaction, but they seem to indicate that Mn^{III} formed

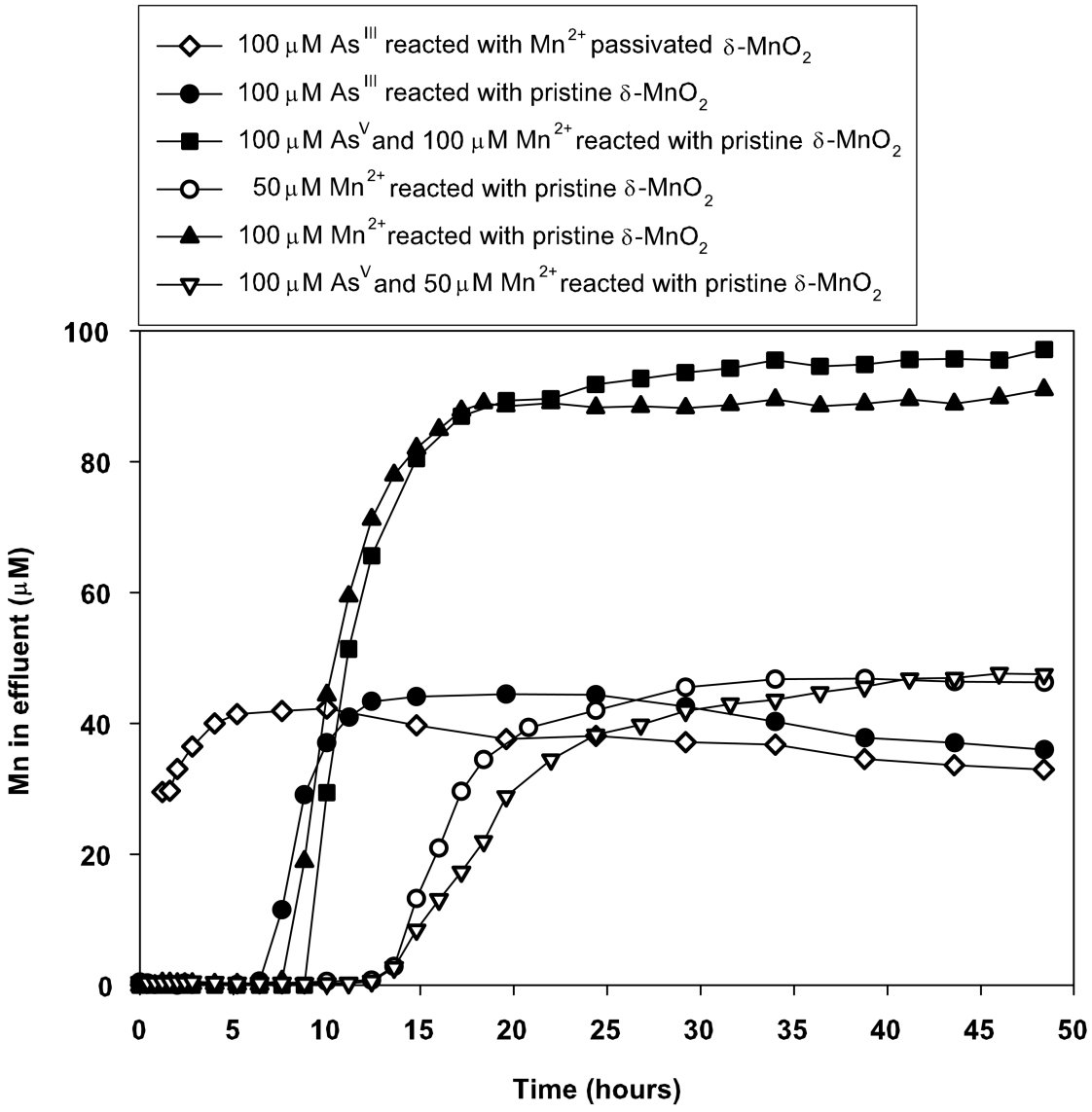

Figure 1.6. Change in Mn^{II} concentration over time in the effluent of six stirred-flow reactions. Stirred-flow experiments were conducted by reacting 1 g/L of pristine δ-MnO_2 with: 50 µM Mn^{II}, or 100 µM Mn^{II}, or 100 µM As^{III}, or 100 µM Mn^{II} and 50 µM As^{V} simultaneously, or 100 µM Mn^{II} and 100 µM As^{V} simultaneously. Also, one stirred-flow reaction was conducted by reacting 100 µM As^{III} with 1 g/L of Mn^{II}-saturated δ-MnO_2.

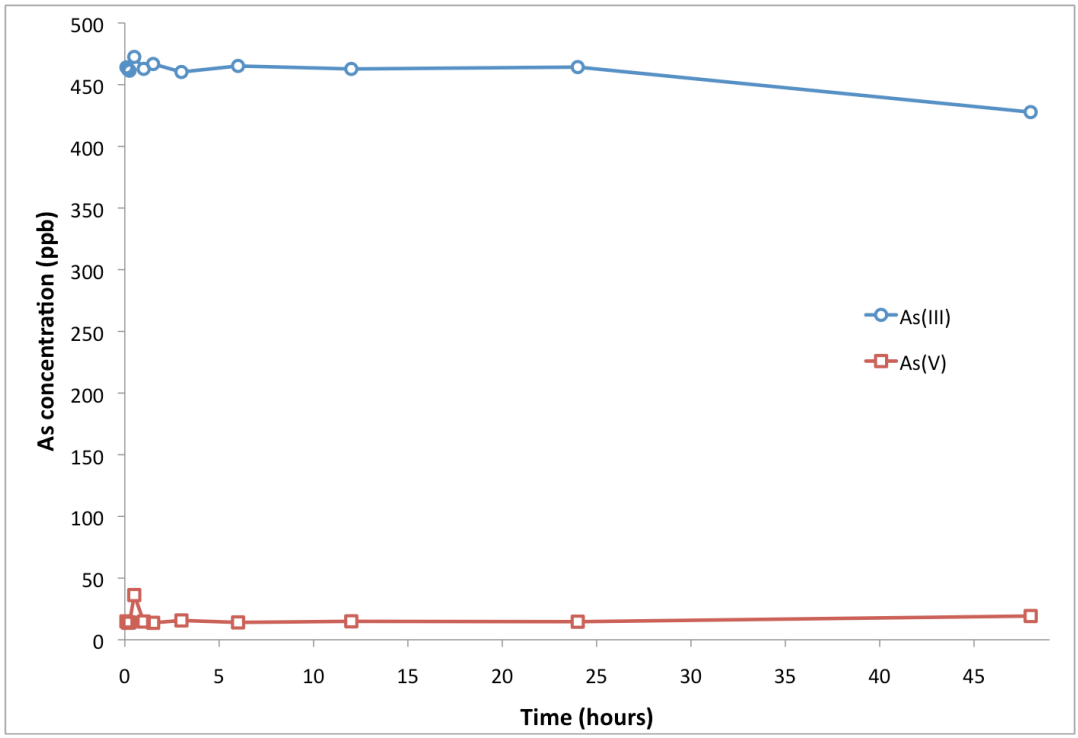

Figure 1.7. Batch reaction of As^{III} with manganite (γ-$Mn^{III}OOH$) in the presence of 10 mM NaCl and 5 mM MOPS (pH = 7.2).

during this time is from $Mn^{II/IV}$ conproportionation rather than As^{III} reduction of Mn^{IV}.

After the δ-MnO_2 surface becomes passivated (i.e. after 6.4 hours), the reaction pathways are less clear. Both the rate of Mn release and As^{V} production by δ-MnO_2 stabilize after 16 hours and begin to decrease at approximately the same rate for the remainder of the experiment. For the pathway represented in equation 1.5 to be solely responsible for As^{III} oxidation (i.e. all Mn^{IV} oxidized directly to Mn^{II} with no Mn^{III} intermediate), an As^{V}: Mn^{II} molar ratio of 1:1 is expected in the reactor effluent (assuming no net Mn^{II} sorption, which is expected at this point in the reaction due to surface saturation by Mn^{II}). If the pathway represented by equations 1.6 and 1.8 is solely responsible for As^{III} oxidation (i.e. all Mn^{IV} is reduced to Mn^{III} before further reduction to Mn^{II}), an As^{V}: Mn^{II} ratio of 1:1 is also expected in the reactor effluent. However, if Mn^{III} reactive sites on the surface of δ-MnO_2, are solely responsible for As^{III} oxidation (Equation 1.8), an As^{V}: Mn^{II} ratio of 1:2 is expected in the reactor effluent. Interestingly, from 16 - 48 hours of reaction there is an average of 5.2 nmols more Mn^{II} than As^{V} in the reactor effluent, corresponding to an As^{V}: Mn^{II} ratio of 1:1.15. Therefore, a single reaction pathway cannot definitively describe the stirred-flow effluent As^{V} and Mn concentrations from 16 - 48 hours. One possible explanation for the presence of more Mn^{II} than As^{V} in stirred-flow effluent from 16 - 48 hours (Figure 1.3) is heterogeneous As^{III} oxidation by Mn^{III} and Mn^{IV} reactive sites (i.e. a combination of Equations 1.5 – 1.8). Assuming slow oxidation of As^{III} by Mn^{III}

sites, (either from Equation 1.8 or from Mn^{II}/Mn^{IV} conproportionation), slightly more Mn^{II} could be released than As^{V} if the pathway represented in equation 1.5 is also operational. The As^{V}: Mn^{II} ratio of 1:1.15 could also be a result of the slow release of sorbed Mn^{II} during the reductive dissolution of δ-MnO_2.

The stirred flow experiments discussed here indicate that As^{III} oxidation by pristine δ-MnO_2 initially favors the formation of Mn^{II} rather than Mn^{III} reactive sites. However, when As^{III} is oxidized by passivated δ-MnO_2 (by reaction with Mn^{II} or As^{III}), the reaction is more complex and probably involves several reaction pathways occurring simultaneously. Also, As^{III} oxidation by passivated δ-MnO_2 probably includes As^{III} oxidation by Mn^{III} reactive sites, which likely come from conproportionation of sorbed Mn^{II} rather than from As^{III} oxidation. Spectroscopic data are required to verify the origin of Mn^{III} reactive sites on δ-MnO_2, which is discussed in Chapter 2. When Mn-oxide minerals become passivated, as is expected in natural environments, their reactivity can decrease significantly. Overall, the results presented here show that As^{III} oxidation by δ-MnO_2 can be quite complex, and the reactions involved vary in their importance over time. This study clearly demonstrates the value of investigating As^{III} oxidation by Mn-oxides over time.

References

Bar-Tal, A., S. Feigenbaum, D.L. Sparks, and J.D. Pesek. 1990. Analyses of adsorption kinetics using a stirred-flow chamber: I. Theory and critical tests. Soil Sci. Soc. Am. J. 54:1273-1278.

Chiu, V.Q., and J.G. Hering. 2000. Arsenic adsorption and oxidation at manganite surfaces. 1. Method for simultaneous determination of adsorbed and dissolved arsenic species. Environ. Sci. Technol. 34:2029-2034.

Dixit, S., and J.G. Hering. 2003. Comparison of arsenic(V) and arsenic(III) sorption onto iron oxide minerals: Implications for arsenic mobility. Environ. Sci. Technol. 37:4182-4189.

Drits, V.A., E. Silvester, A.I. Gorshkov, and A. Manceau. 1997. Structure of synthetic monoclinic Na-rich birnessite and hexagonal birnessite. 1. Results from X-ray diffraction and selected-area electron diffraction. Am. Mineral. 82:946-961.

Foster, A.L., G.E. Brown, and G.A. Parks. 2003. X-ray absorption fine structure study of As(V) and Se(IV) sorption complexes on hydrous Mn oxides. Geochim. Cosmochim. Ac. 67:1937-1953.

Ginder-Vogel, M., G. Landrot, J.S. Fischel, and D.L. Sparks. 2009. Quantification of rapid environmental redox processes with quick-scanning x-ray absorption spectroscopy (Q-XAS). Proc. Natl. Acad. Sci. 106:16124-16128.

Gupta, S.K., and K.Y. Chen. 1978. Arsenic removal by adsorption. J. Water Pollut. Control 50:493-506.

Hingston, F.J., A.M. Posner, and J.P. Quirk. 1971. Competitive adsorption of negatively charged ligands on oxide surfaces. Faraday Discussions 52:334-342.

Luther, G., and J. Popp. 2002. Kinetics of the abiotic reduction of polymeric manganese dioxide by nitrite: An anaerobic nitrification reaction. Aquatic Geochem. 8:15-36.

Manceau, A., M. Lanson, and N. Geoffroy. 2007. Natural speciation of Ni, Zn, Ba, and As in ferromanganese coatings on quartz using X-ray fluorescence, absorption, and diffraction. Geochim. Cosmochim. Acta 71:95-128.

Manning, B.A., S.E. Fendorf, B. Bostick, and D.L. Suarez. 2002. Arsenic(III) oxidation and arsenic(V) adsorption reactions on synthetic birnessite. Environ. Sci. Technol. 36:976-981.

Moore, J.N., J.R. Walker, and T.H. Hayes. 1990. Reaction scheme for the oxidation of As(III) to As(V) by birnessite. Clay. Clay Miner. 38:549-555.

Morgan, J.J. 2000. Manganese in natural waters and Earth's crust: its availability to organisms, p. 1-33, *In* A. Sigel and H. Sigel, eds. Metal ions in boilogical systems, manganese and its role in biological processes, Vol. 37. Marcel Dekker, New York.

Morgan, J.J., and W. Stumm. 1964. Colloid-chemical properties of manganese dioxide. J. Colloid Sci. 19:347-359.

Nesbitt, H.W., G.W. Canning, and G.M. Bancroft. 1998. XPS study of reductive dissolution of 7 angstrom-birnessite by H_3AsO_3, with constraints on reaction mechanism. Geochim. Cosmochim. Ac. 62:2097-2110.

Oscarson, D.W., P.M. Huang, and W.K. Liaw. 1981a. Role of manganese in the oxidation of arsenite by freshwater sediments. Clay. Clay Miner. 29:219-225.

Oscarson, D.W., P.M. Huang, C. Defosse, and A. Herbillon. 1981b. Oxidative power of Mn(IV) and Fe(III) oxides with respect to As(III) in terrestrial and aquatic environments. Nature 291:50-51.

Oscarson, D.W., P.M. Huang, W.K. Liaw, and U.T. Hammer. 1983. Kinetics of oxidation of arsenite by various manganese dioxides. Soil Sci. Soc. Am. J. 47:644-648.

Parikh, S.J., B.J. Lafferty, and D.L. Sparks. 2008. An ATR-FTIR spectroscopic approach for measuring rapid kinetics at the mineral/water interface. J. Colloid Interface Sci. 320:177.

Peacock, C.L., and D.M. Sherman. 2007. Sorption of Ni by birnessite: Equilibrium controls on Ni in seawater. Chemical Geology 238:94-106.

Perez-Benito, J.F. 2002. Reduction of colloidal manganese dioxide by manganese(II). J. Colloid Innterf. Sci. 248:130-135.

Petrick, J.S., F. Ayala-Fierro, W.R. Cullen, D.E. Carter, and H.V. Aposhian. 2000. Monomethylarsonous acid (MMA(III)) is more toxic than arsenite in Chang human hepatocytes. Toxicol. Appl. Pharmacol. 163:203-207.

Ramstedt, M., B.M. Andersson, A. Shchukarev, and S. Sjoberg. 2004. Surface properties of hydrous manganite (MnOOH). A potentiometric, electroacoustic, and X-ray photoelectron spectroscopy study. Langmuir 20:8224-8229.

Scott, M.J., and J.J. Morgan. 1995. Reactions at oxide surfaces. 1. Oxidation of As(III) by synthetic birnessite. Environ. Sci. Technol. 29:1898-1905.

Shiller, A.M., and T.H. Stephens. 2005. Microbial manganese oxidation in the lower Mississippi river: methods and evidence. Geomicrobiol. J. 22:117-125.

Silvester, E., A. Manceau, and V.A. Drits. 1997. Structure of synthetic monoclinic Na-rich birnessite and hexagonal birnessite. 2. Results from chemical studies and EXAFS spectroscopy. Am. Mineral. 82:962-978.

Tan, W.-F., S.-J. Lu, F. Liu, X.-H. Feng, J.-Z. He, and L.K. Koopal. 2008. Determination of the point-of-zero charge of manganese oxides with different methods including an improved salt titration method. Soil Sci. 173:277-286.

Tani, Y., N. Miyata, M. Ohashi, T. Ohnuki, H. Seyama, K. Iwahori, and M. Soma. 2004. Interaction of inorganic arsenic with biogenic manganese oxide produced by a Mn-oxidizing fungus, strain KR21-2. Environ. Sci. Technol. 38:6618-6624.

Tebo, B.M., J.R. Bargar, B.G. Clement, G.J. Dick, K.J. Murray, D. Parker, R. Verity, and S.M. Webb. 2004. Biogenic manganese oxides: Properties and mechanisms of formation. Ann. Rev. Earth and Plan. Sci. 32:287-328.

Tournassat, C., L. Charlet, D. Bosbach, and A. Manceau. 2002. Arsenic(III) oxidation by birnessite and precipitation of manganese(II) arsenate. Environ. Sci. Technol. 36:493-500.

Villalobos, M., B. Toner, J. Bargar, and G. Sposito. 2003. Characterization of the manganese oxide produced by *Pseudomonas putida* strain MnB1. Geochim. Cosmochim. Acta 67:2649-2662.

Webb, S.M., G.J. Dick, J.R. Bargar, and B.M. Tebo. 2005. Evidence for the presence of Mn(III) intermediates in the bacterial oxidation of Mn(II). Proc. Natl. Acad. Sci. 102:5558-5563.

Wielinga, B., M.M. Mizuba, C.M. Hansel, and S. Fendorf. 2001. Iron promoted reduction of chromate by dissimilatory iron reducing bacteria. Environ. Sci. Technol. 35:522-527.

Zhu, M., K.W. Paul, J.D. Kubicki, and D.L. Sparks. 2009. Quantum chemical study of arsenic (III, V) adsorption on Mn-oxides: Implications for arsenic(III) oxidation. Environ. Sci. Technol. 43:6655-6661.

Chapter 2

ARSENITE OXIDATION BY A POORLY-CRYSTALLINE MANGANESE OXIDE: RESULTS FROM X-RAY ABSORPTION SPECTROSCOPY AND X-RAY DIFFRACTION

Abstract

Arsenite (As^{III}) oxidation by manganese oxides (Mn-oxides) serves to detoxify and, under many conditions, immobilize arsenic (As) by forming arsenate (As^{V}). As^{III} oxidation by Mn^{IV}-oxides can be quite complex, involving many simultaneous forward reactions and subsequent back reactions. During As^{III} oxidation by Mn-oxides, a reduction in oxidation rate is often observed, which is attributed to Mn-oxide surface passivation. X-ray absorption spectroscopy (XAS) and X-ray diffraction (XRD) data show that Mn^{II} sorption on a poorly-crystalline hexagonal birnessite (δ-MnO_2) is important in passivation early during the reaction. Also, it appears that Mn^{III} in the δ-MnO_2 structure is formed by conproportionation of sorbed Mn^{II} and Mn^{IV} in the mineral structure. The content of Mn^{III} within the δ-MnO_2 structure appears to increase as the reaction proceeds. Binding of As^{V} to δ-MnO_2 also changes as Mn^{III} becomes more prominent in the δ-MnO_2 structure. The data presented indicate that As^{III} oxidation and As^{V} sorption by poorly-crystalline δ-MnO_2 is greatly affected by

Mn oxidation state in the δ-MnO_2 structure, and emphasize the value of studying reaction mechanisms over a range of time scales.

Introduction

Manganese-oxides (Mn-oxides) commonly occur as fine-grained particles or coatings in terrestrial and aquatic environments, usually exhibiting high reactivity due to their large surface area and negative charge (Post, 1999). They tend to exhibit a high sorption capacity for metals, and are among the most potent oxidants in terrestrial and aquatic environments (Post, 1999). Thus, Mn-oxides can influence the environment much more than some other, more abundant minerals. Biological Mn^{II} oxidation proceeds much more rapidly than abiotic Mn^{II} oxidation, which has led to the conclusion that many Mn-oxides in the environment are formed by microorganisms (i.e. are biogenic) (Tebo et al., 2004). Many biogenic Mn-oxides are phyllomanganates with structures similar to hexagonal birnessite, and are highly reactive with respect to metal sorption and oxidation (Toner et al., 2006; Villalobos et al., 2003; Villalobos et al., 2006; Webb et al., 2005a; Zhu et al., 2010a).

Arsenic (As) is a toxic element commonly occurring in the environment via natural processes and anthropogenic activities. In soils and sediments, the toxicity and mobility of As are determined, to a great extent, by its speciation. Specifically, arsenite (As^{III}) is more toxic than arsenate (As^{V}) (Petrick et al., 2000), and the sorption of As by oxide minerals can be heavily dependent on pH and its speciation (Dixit and Hering, 2003; Raven et al., 1998). Several Mn-oxides, including phyllomanganates, are able to oxidize As^{III} to As^{V} (Chiu and Hering, 2000; Ginder-Vogel et al., 2009; Manning et al., 2002; Moore et al., 1990; Parikh et al., 2008; Scott and Morgan, 1995;

Tournassat et al., 2002), and because As^{III} is more toxic than As^{V} this process can be important as an As detoxification pathway in the environment. Along with detoxifying As, As^{III} oxidation by Mn-oxides can alter As mobility, often making it less mobile (Dixit and Hering, 2003; Raven et al., 1998).

Mechanisms of As^{III} oxidation by Mn-oxides can be quite complex, involving several reactions simultaneously. For example, As^{III} oxidation by birnessite produces As^{V} and Mn^{II} as reaction products (Ginder-Vogel et al., 2009; Oscarson et al., 1983; Parikh et al., 2008; Scott and Morgan, 1995; Tournassat et al., 2002). However, both As^{V} and Mn^{II} can be adsorbed by birnessite (Oscarson et al., 1983; Scott and Morgan, 1995). Also, a Mn^{III} intermediate can form during As^{III} oxidation by Mn-oxides (Nesbitt et al., 1998; Tournassat et al., 2002). A phenomenon commonly observed during the oxidation of As^{III} by birnessite is passivation of the mineral surface (Ginder-Vogel et al., 2009; Manning et al., 2002; Oscarson et al., 1981; Parikh et al., 2008; Scott and Morgan, 1995; Tani et al., 2004; Tournassat et al., 2002). That is to say, as the reaction between birnessite and As^{III} proceeds, the rate of As^{III} oxidation decreases with time. There have been three proposed mechanisms for Mn-oxide passivation during As^{III} oxidation. First, sorption of As^{V} produced by oxidation of As^{III} can sorb to the mineral surface and block reactive sites, thus decreasing the reactive surface area and causing an apparent decrease in As^{III} oxidation rate (Foster et al., 2003; Manning et al., 2002; Zhu et al., 2009). In a similar fashion, sorption of Mn^{II}, produced by reducing Mn^{IV} in the mineral structure, can also block reactive sites on the mineral surface (Oscarson et al., 1981; Scott and Morgan, 1995). Lastly, the

formation of Mn^{III} on Mn-oxide surfaces, which are considered to be less reactive than Mn^{IV} sites, can decrease As^{III} oxidation rate (Nesbitt et al., 1998; Tournassat et al., 2002; Zhu et al., 2009).

As^{III} oxidation by δ-MnO_2 occurs in two distinct phases in the stir-flow reactions presented in this study (Chapter 1). The first phase, from 0 to 6.4 hours of reaction, is the period of highest δ-MnO_2 reactivity and the most rapid rate of As^{III} oxidation. Beyond 6.4 hours, δ-MnO_2 becomes passivated, and reactivity decreases, as evidenced by the decrease in As^{III} oxidation rate and decrease in Mn^{II} sorption. The majority of As sorption by δ-MnO_2 during As^{III} oxidation, under these conditions, occurs only before δ-MnO_2 becomes passivated, and it also occurs in two distinct phases. Passivation of δ-MnO_2 when reacted with As^{III} can be attributed primarily to sorption of Mn^{II} (Chapter 1). It is hypothesized that Mn^{II} passivates δ-MnO_2 by directly blocking reaction sites, or by the formation of less reactive Mn^{III} sites through conproportionation of Mn^{II} sorbed on Mn^{IV} sites on the mineral surface. However, using only data from the aqueous phase of stirred-flow reactions, determination of the mechanism of δ-MnO_2 passivation is impossible.

In this study, the speciation of As and Mn in the solid phase are investigated during As^{III} oxidation by δ-MnO_2. To achieve this, stirred-flow reactions are stopped after various reaction times and reacted δ-MnO_2 is collected for analysis by spectroscopic, diffraction, and microscopic techniques. A primary focus of this study is to characterize As sorption, Mn^{II} sorption, and Mn^{III} formation on δ-MnO_2 as they

change over time by analyzing samples of the solid phase throughout the reaction. Also, this research aims to clarify the passivation mechanism(s) of birnessite during As^{III} oxidation. It is important to understand the mechanism(s) responsible for birnessite passivation in nature in order to better predict Mn-oxide reactivity and contaminant mobility in natural systems.

Materials and Methods

δ-MnO_2 Synthesis and Characterization

δ-MnO_2, a poorly-crystalline Mn-oxide mineral, was synthesized for the experiments presented in this work. The procedures used to synthesize δ-MnO_2 as well as a description of characterization procedures are included in Chapter 1.

Stirred-Flow Experiments

As^{III} oxidation by δ-MnO_2 was investigated using the same stirred-flow protocol and reaction conditions described in Chapter 1. Briefly, the stirred-flow experiments were carried out by flowing a solution containing 100 μM As^{III} and background electrolyte (10 mM NaCl and 5 mM MOPS adjusted to pH 7.2) into the reactor at 1 mL/min for varying lengths of time. Initial δ-MnO_2 concentration in stirred-flow reactions was 1 g/L (corresponding to 30 mg δ-MnO_2 in the reactor). In order to monitor changes occurring in the solid phase during As^{III} oxidation by δ-MnO_2, the reaction was stopped and solid phase collected for analysis after 0.5, 4, 10,

24, and 48 hours of reaction (Figure 2.1). 0.5 hours corresponds to the greatest amount of As sorption during As^{III} oxidation by δ-MnO_2, while 4 hours is the time at which the maximum As^{V} appears in the stirred-flow effluent. The sample at 10 hours is near the end of As sorption during As^{III} oxidation, and also occurs early in the second phase of the reaction. The samples at 24 and 48 hours are both during the less reactive phase of the reaction.

To stop the reaction, influent solution was removed, and the suspension in the reaction chamber was immediately filtered (0.22 μm) to remove any background electrolyte, Mn, and As not bound to δ-MnO_2. After filtration, some of the residual wet paste was immediately covered by Kapton tape, and stored for less than 5 days prior to spectroscopic analysis. The remaining wet paste from each sample was refrigerated in sealed test tubes in the dark for less than 5 days for analysis by high resolution transmission electron microscopy (TEM) and synchrotron based X-ray diffraction (XRD). As^{V} sorption standards were prepared by reacting 100 μM As^{V} with 1g/L δ-MnO_2 or manganite (γ-MnOOH) for 24 hours in the same background electrolyte used in stirred-flow reactions. Sorption standards were filtered and the residual wet paste was immediately covered with Kapton tape and stored for less than 5 days for spectroscopic analysis.

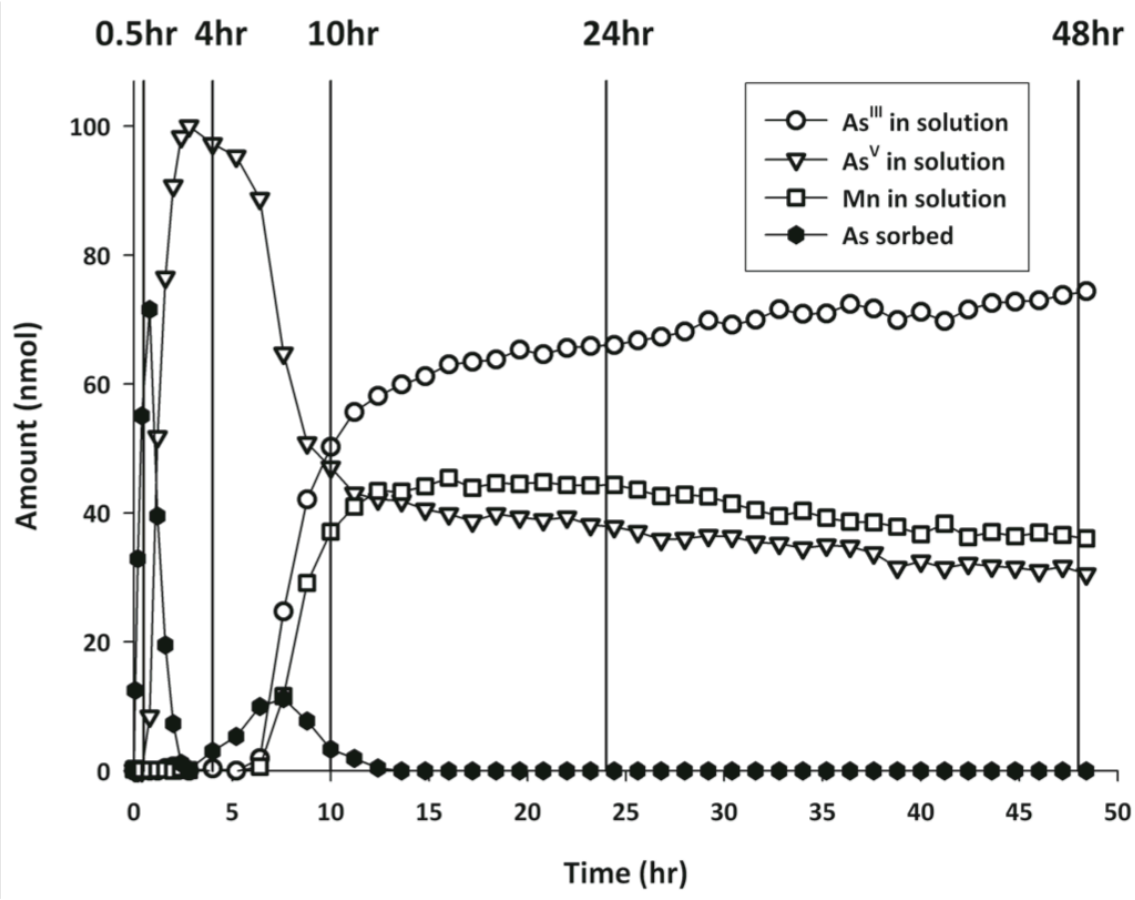

Figure 2.1. Vertical lines represent the duration of five stirred-flow reactions measuring As^{III} oxidation by δ-MnO_2 (1 g/L δ-MnO_2 and 100 µM As^{III}). Each reaction was stopped at the time indicated at the top of the graph (0.5, 4, 10, 24, or 48 hours), at which point all remaining δ-MnO_2 was collected for analysis. Data show the amount (nmol) of As sorbed by δ-MnO_2, as well as amounts (nmol) of As^{III}, As^{V}, and Mn^{II} in the effluent from the stirred-flow experiment.

Solid-Phase Characterization

Transmission electron microscopy (TEM) analyses were performed on a Philips CM 300 FEG (field emission gun) operating at 297 kV. The spatial resolution of the CM 300 is 0.2 nm. Digital images were acquired using a 1024 X 1024 pixel CCD camera mounted on a Gatan GIF 200 EELS spectrometer.

X-ray diffraction (XRD) analysis was conducted at beamline 11-3 at the Stanford Synchrotron Radiation Laboratory (SSRL, Stanford University, Palo Alto, California). Data were collected at a X-ray wavelength of 0.97584Å using an image plate in transmission mode. All samples were analyzed as wet pastes in aluminum sample holders with Lexan windows. XRD data were processed using the Fit2D software package (Hammersley, 1998), which was calibrated using XRD patterns of LaB_6. Background contributions of Lexan and water in the XRD spectra of all samples were subtracted using XRD-bs (Samuel Webb, SSRL).

Extended X-ray absorption fine structure (EXAFS) and X-ray absorption near edge (XANES) spectroscopic data were collected at beamline 4-1 at SSRL. The electron storage ring operates 3.0 GeV with a current ranging from 100 to 90 mA. The monochromator consisted of two parallel Si-(220) crystals with a vertical entrance slit separation of 0.5 mm. As (11.9 keV) and Mn (6.5 keV) K-edge EXAFS spectra were collected. All samples were oriented at 45° to the incident beam and a Lytle detector was used to collect Mn spectra in fluorescence mode while a germanium (Ge)

multi-element detector was used to collect As spectra in fluorescence mode. The monochromator crystals were detuned by 30% for As and 50 % for Mn in I_0 to reject higher order harmonics. A 3-path length Ge (for As) or chromium (Cr) (for Mn) filter, and Sollier slits were used for signal optimization and removal of elastically scattered radiation. The monochromator angle was calibrated to the As(V) K-edge (11.874 keV) using diluted $Na_2HAs^VO_4$ as a standard (10 wt % BN) or the Mn(0) K-edge (6.539 keV) using a Mn metal foil. These standards were monitored in transmission mode simultaneous to sample collection to check for potential shifts in their respective K-edges. Multiple scans were collected at room temperature for each sample to improve the signal-to-noise ratio for data analysis.

EXAFS and XANES data were processed using the SixPACK (Webb, 2005) interface to IFEFFIT (Newville, 2001). XANES data were background-subtracted and normalized to a unit-edge step. After background subtraction and normalization, the EXAFS data were extracted and k^3-weighted. For both As and Mn, theoretical phase shift and amplitude functions for shell-by-shell fitting were generated using FEFF 7.20 (Ankudinov and Rehr, 1997). EXAFS fitting for Mn was based on the model described by Webb et al. (2005a). Phase and amplitude functions for As shell-by-shell fitting were generated from theoretically calculated As-Mn sorption complexes, and As-O multiple scattering paths were included in the fits. For Mn XANES, a set of reference standards (δ-$Mn^{IV}O_2$, Mn_2O_3, and $Mn^{II}SO_4$) was utilized to perform linear combination spectral fitting, using Six-PACK's least-squares fitting module, which is a graphical interface for IFEFFIT's minimization function (Newville, 2001). Linear

combination fitting routines were used to reconstruct the experimental spectrum to determine relative Mn oxidation state. Shell-by-shell and linear combination fits were optimized by minimizing reduced σ^2 (Newville et al., 1995).

Results and Discussion

δ-MnO_2 Structure

The method used to synthesize δ-MnO_2 in this study produces a phyllomanganate composed of sheets of edge sharing Mn^{IV} octahedra, and little order in vertical stacking arrangement (i.e. turbostratic) (Villalobos et al., 2003; Villalobos et al., 2006). The Mn K-edge EXAFS spectra has the three features between 4 and 6 $Å^{-1}$ (Figure 2.2a), which is common for EXAFS patterns of phyllomanganates (Marcus et al., 2004). XRD analysis of the δ-MnO_2 synthesized for this study shows only two predominant peaks (37˚ and 66˚ 2θ (Cu Kα)), and a broad feature between them, also characteristic of turbostratic phyllomanganates (Figure 2.3) (Drits et al., 2007; Villalobos et al., 2006). The absence of shoulders or splitting in the two predominant XRD peaks (37˚ and 66˚, Figure 2.3) along with the presence of single peaks at 8.1 and 9.25 $Å^{-1}$ in the Mn EXAFS pattern of pristine δ-MnO_2 (0 hours, Figure 2.2a) confirms that δ-MnO_2 exhibits hexagonal symmetry rather than triclinic (Drits et al., 2007; Manceau et al., 2005; Marcus et al., 2004). Also, in the XRD pattern of unreacted δ-MnO_2, the absence of a dip at 45˚ (Figure 2.3) indicates very little $Mn^{II / III}$ sorbed in interlayers (at vacancy sites) (Drits et al., 2007; Villalobos et al., 2006), and

the absence of a shoulder at ~6.5 $Å^{-1}$ in the Mn EXAFS agrees with this observation (0 hours, Figure 2.2a) (Toner et al., 2006). One can also conclude that little Mn^{III} is present within pristine δ-MnO_2 layers, due to the average oxidation state of the starting material (3.95) (Chapter 1), as well as the sharp peak at 9.25 $Å^{-1}$ in the Mn EXAFS (0 hours, Figure 2.2a) (Manceau et al., 2004).

A characteristic of hexagonal symmetry in the octahedral layer of birnessite minerals (e.g. δ-MnO_2), is the presence of vacancy sites. Vacancy sites resulting from the absence of a positively charged Mn^{IV} atom in the Mn octahedral layer, are negatively charged, and tend to sorb cations readily (Drits et al., 1997; Manceau et al., 2002; Manceau et al., 2007; Silvester et al., 1997). When edge sites are present in large amounts on phyllomanganates (which occurs for minerals with small particle sizes), they can be important reactive sites as well (Foster et al., 2003; Manning et al., 2002; Tournassat et al., 2002; Villalobos et al., 2005). δ-MnO_2 used in this research consists of small crystalline domains surrounded by TEM amorphous material (Chapter 1, Figure 1.2). However, it is difficult to accurately determine the size of crystalline domains in δ-MnO_2 by TEM because crystalline particles are surrounded by TEM-amorphous material making them difficult to delineate. However, it is reasonable to conclude that the small particle size of δ-MnO_2 used in this study leads to the presence of a significant amount of edge sites. Therefore, we conclude that the δ-MnO_2 used here has two predominant reaction sites: vacancy sites within Mn octahedral layers, and edge sites at Mn octahedral layer edges.

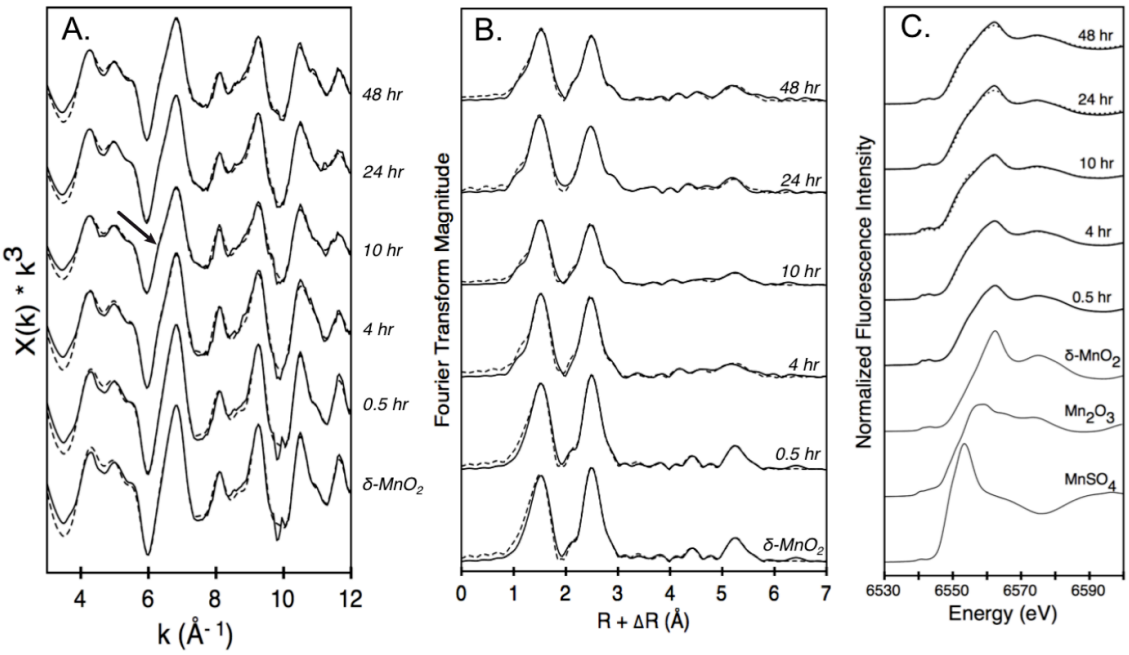

Figure 2.2. Manganese K-edge EXAFS (A.), Fourier transformed EXAFS (B.), and XANES (C.) of unreacted δ-MnO_2 and δ-MnO_2 (1 mg/L) reacted with As^{III} (100 μM) in a stirred-flow reactor for 0.5, 4, 10, 24, and 48 hours. XAS data is presented as solid lines and fits are presented as dashed lines (fit data provided in Table 2.2). Arrow in panel A indicates the shoulder at ~ 6.5 $Å^{-1}$ which is present beyond 0.5 hours.

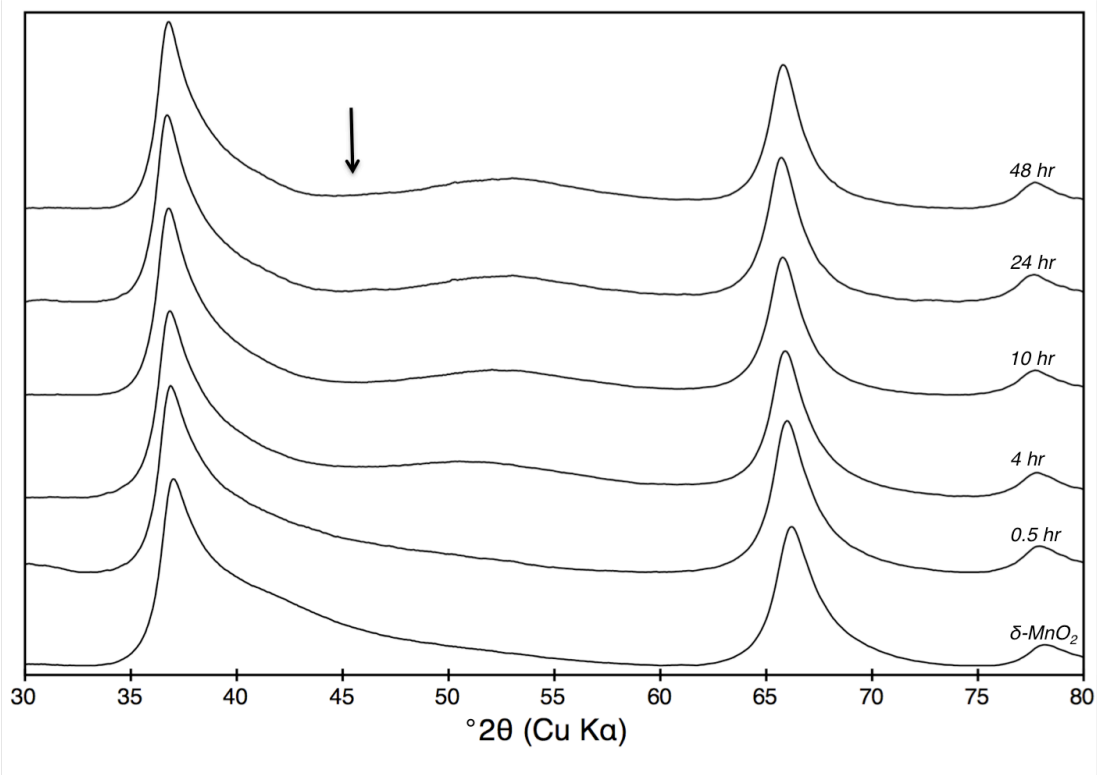

Figure 2.3. Synchrotron XRD patterns of unreacted δ-MnO_2 and δ-MnO_2 (1 mg/L) reacted with As^{III} (100 μM) in a stirred-flow reactor for 0.5, 4, 10, 24, and 48 hours. Arrow indicates the position of the 'dip' at 45° that increases with reaction time.

As δ-MnO_2 is reacted with As^{III}, the XRD peaks at 37˚ and 66˚ shift to lower values (Figure 2.3), with the shift being more pronounced between 0 and 4 hours than from 4 to 48 hours of reaction (Figure 2.3). XRD simulations show that a leftward shift in these peaks can be attributed to an increase in particle size (i.e. coherent scattering domains) (Villalobos et al., 2006). The XRD peaks at 37˚ and 66˚ to lower values could possibly be due to a higher rate of dissolution of the less crystalline fraction of δ-MnO_2 during the first 4 hours of As^{III} oxidation. However, if the amount of poorly crystalline δ-MnO_2 decreases, the remaining mineral would necessarily have a greater degree of crystallinity than the starting material, and thus a sharpening of the peaks at 37˚ and 66˚ as they shift would be expected. This sharpening is quite noticeable on the low angle side of the 37˚ peak in XRD simulations with a 4nm increase in particle size (Villalobos et al., 2006). In the XRD patterns presented here, no detectable sharpening of the 37˚ peak occurs. It should also be noted that a large amount of TEM amorphous δ-MnO_2 remains after 48 hours of reaction with As^{III} (Chapter 1, Figure 1.2). Since there is no evidence for increasing δ-MnO_2 particle size during As^{III} oxidation, one must assume that the shift in XRD peaks at 37˚ and 66˚ to lower 2θ values is caused by some other change in the δ-MnO_2 structure.

Mn Sorption on δ-MnO_2 During As^{III} Oxidation

When As^{III} is oxidized by δ-MnO_2 under the conditions studied here, only Mn^{II} is produced initially (Chapter 1). However, Mn^{II} produced by As^{III} reaction with Mn^{IV}

in δ-MnO_2 can undergo a 'back reaction' by sorbing on the δ-MnO_2 surface (Oscarson et al., 1981; Scott and Morgan, 1995). Heavy metals tend to preferentially sorb at vacancy sites rather than edge sites in hexagonal birnessite (Manceau et al., 2002). Thus, in this system, we expect Mn^{II} to sorb at δ-MnO_2 vacancy sites until they are filled (or nearly filled) followed by sorption at available δ-MnO_2 edges sites.

When Mn^{II} sorbs at layer vacancy sites in hexagonal birnessite, it tends to form triple corner sharing complexes (Manceau et al., 2002). In triple corner sharing complexes, Mn^{II} shares corners of its octahedral coordination shell with corners of Mn^{IV} octahedra surrounding vacancy sites in Mn octahedral layers (Drits et al., 2007). Mn^{III} octahedra can also form triple corner sharing complexes when sorbed at δ-MnO_2 vacancy sites. A dip at 45˚ in XRD patterns of turbostratic phyllomanganates has previously been attributed to an increase in corner-sharing $Mn^{II\ /\ III}$ at vacancy sites (Drits et al., 2007; Villalobos et al., 2006). When As^{III} is reacted with δ-MnO_2, this characteristic 'dip' in the XRD pattern of δ-MnO_2 appears at 45˚ (Figure 2.3). After 0.5 hours, the dip at 45˚ is slight, however, it becomes more pronounced after 4 and 10 hours (Figure 2). Beyond 10 hours of As^{III} oxidation, the dip at 45˚ remains constant. Thus, XRD patterns of δ-MnO_2 confirm that as Mn^{II} is produced in the most reactive, early phase of As^{III} oxidation, it begins to sorb at δ-MnO_2 vacancy sites immediately. Also, XRD data indicate that δ-MnO_2 vacancy sites are nearly fully occupied by $Mn^{II\ /\ III}$ in triple corner sharing complexes within 4 hours of reaction, and are completely occupied between 4 and 10 hours.

Mn sorbed at δ-MnO_2 vacancies in triple corner sharing complexes can also be detected in Mn EXAFS data. Specifically, the shoulder at ~ 6.5 $Å^{-1}$ in EXAFS spectra (Figure 2.2a), and the peak at 2.9 Å (R + ΔR) in the Fourier transformed data (Figure 2.2b) can be attributed to $Mn^{II\ /\ III}$ sorbed at vacancy sites in triple corner sharing complexes (Gaillot et al., 2003; Manceau et al., 1997; Toner et al., 2006). A slight increase is observed in the shoulder at ~ 6.5 $Å^{-1}$ in Mn EXAFS patterns during As^{III} oxidation (Figure 2.2a), and this trend can also be seen as an increase of the 2.9 Å (R + ΔR) peak in the Fourier transformed data (Figure 2.2b). The 2.9 Å (R + ΔR) peak of the Fourier transformed data, exhibits its largest increase from 0 – 4 hours, with a small increase between 4 and 10 hours, and appears stable from 10 – 48 hours (Figure 2.2a). Although difficult to discern, the trend in the 6.5 $Å^{-1}$ peak of the EXAFS data shows the same trend (Figure 2.2a). A decrease in the amplitude of first shell Mn-O and Mn-Mn peaks (1.53 and 2.49 Å (R + ΔR) respectively) is also caused by $Mn^{II\ /\ III}$ sorption at vacancy sites (Toner et al., 2006), and both of these peaks decrease until 10 hours of As^{III} oxidation by δ-MnO_2, providing further evidence that maximum $Mn^{II\ /\ III}$ sorption at vacancy sites occurs between 4 and 10 hours (Figures 2.2b and 2.4).

In Chapter 1, it is concluded that the decrease in As^{V} sorption after ~3 hours of reaction is due to increased competition between As^{V} and Mn^{II} for δ-MnO_2 edge sites. Both XRD and EXAFS analyses indicate vacancy sites are nearly fully occupied by $Mn^{II\ /\ III}$ after 4 hours of As^{III} oxidation, which implies that, at least beyond 4 hours, Mn^{II} produced during As^{III} oxidation increasingly competes with As for δ-MnO_2 edge

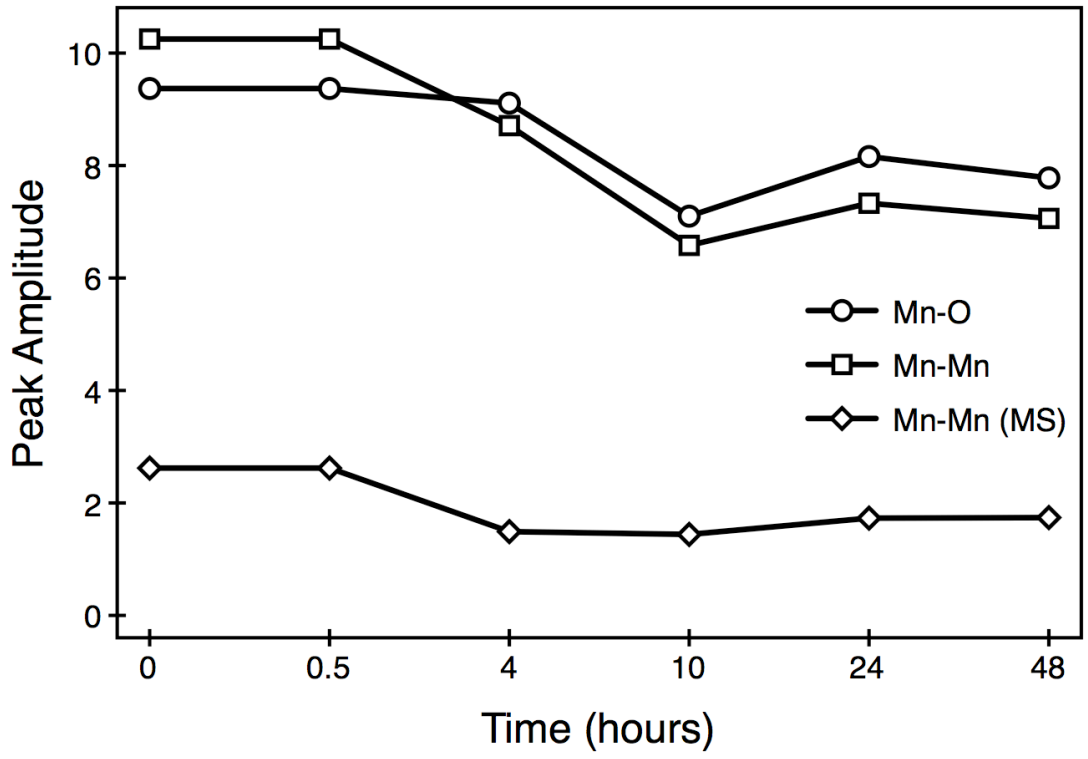

Figure 2.4. The amplitude of first Mn-O, first Mn-Mn, and Mn-Mn multiple scattering shell from Fourier transformed Mn-EXAFS data.

sites. Also, XRD and EXAFS data show that δ-MnO_2 vacancy sites are fully occupied by Mn^{II} between 4 and 10 hours of reaction, which is consistent with the first appearance of Mn^{II} in the stirred-flow effluent at 6.4 hours (Figure 2.1).

Mn^{III} Formation During As^{III} Oxidation

Although initially, δ-MnO_2 has very little Mn^{III} within its layers, the amount of Mn^{III} in its structure appears to increase as As^{III} oxidation proceeds. A broadening and decrease in peak height of the 9.25 $Å^{-1}$ peak in Mn EXAFS can be attributed to an increase in the Mn^{III} content within phyllomanganate layers (Manceau et al., 2005; Marcus et al., 2004; Zhu et al., 2010b). Mn^{III} content of up to ~20% in δ-MnO_2 has been observed by this change in the EXAFS spectra (with no splitting or leftward shift in the spectra reported until higher amounts of Mn^{III} are present) (Manceau et al., 2005; Marcus et al., 2004). In the time-series data presented in Figure 2.2a, one can see the largest proportions of Mn^{III} in δ-MnO_2 layers occurring in the 10, 24, and 48 hour samples, with a slight increase observed between 0.5 and 4 hours as well as between 4 and 10 hours. The broadening of the peak at 9.25 $Å^{-1}$ coincides with a decrease in the Mn-Mn multiple scattering peak in the Fourier transformed data at 5.2 Å (R + ΔR) (Figures 2.2b and 2.4). The Mn-Mn multiple scattering peak is not expected to be greatly affected by $Mn^{II\ /\ III}$ sorption at vacancy sites (Toner et al., 2006), however, it should be dramatically affected by the presence of Mn^{III} within octahedral layers (Webb et al., 2005a). Therefore, we can conclude from Mn EXAFS

data that Mn^{III} is not present in δ-MnO_2 layers in significant quantities before 0.5 hours, and is greatest from 10 to 48 hours.

Using Mn XANES to measure Mn oxidation states in Mn minerals with mixed II / III / IV oxidation states is difficult, however, the overall trend observed in XANES analysis agrees with EXAFS and XRD findings. Results from linear combination fitting of Mn XANES indicate that the amount of Mn^{II} associated with the solid increases from 0 to 10 hours of reaction, and beyond 10 hours of reaction, Mn^{II} content decreases with a corresponding increase in Mn^{III} (Figure 2.2c and Table 2.1). An increase in Mn sorbed on vacancy sites (presumably as Mn^{II}) was observed from 0 to 10 hours by XRD and EXAFS, while EXAFS also indicates an increase in Mn^{III} within δ-MnO_2 layers, especially beyond 10 hours. Therefore, although Mn XANES is not an adequate indicator of Mn oxidation state in this system on its own, it does complement the findings from both XRD and EXAFS data.

Table 2.1. Percentages of Mn^{II}, Mn^{III}, and Mn^{IV} in the solid phase after reacting δ-MnO_2 with As^{III} for 0.5, 4, 10, 24, and 48 hours. Percentages are calculated from linear combination fits of standard compounds ($MnSO_4$, Mn_2O_3, and δ-MnO_2).

Time (hours)	Mn(IV)	Mn(III)	Mn(II)
0	100	0	0
0.5	95	5	0
4	89	5	6
10	81	5	14
24	79	13	8
48	80	10	10

There are two possible mechanisms for formation of Mn^{III} during As^{III} oxidation by δ-MnO_2. First, Mn^{III} could be formed directly through Mn^{IV} oxidation of As^{III} (Equation 2.1).

$$2(>Mn^{IV}\text{-}OH) + H_3As^{III}O_3(aq) + H_2O \rightarrow 2(>Mn^{III}\text{-}OH_2) + HAs^{V}O_4^{2-}(aq) + 2H^+ \quad [2.1]$$

Although this process does not occur in the first 10 hours of reaction in this study (Chapter 1), it has been reported previously in As^{III} oxidation by birnessite (Nesbitt et al., 1998; Tournassat et al., 2002). Another possible pathway for Mn^{III} formation is through conproportionation of Mn^{II} sorbed at Mn^{IV} sites on the δ-MnO_2 surface (Equation 2.2).

$$>Mn^{IV}\text{-}OH + Mn^{II}(aq) + H_2O + H^+ \rightarrow 2(>Mn^{III}\text{-}OH_2) \quad [2.2]$$

This process has also been observed under reaction conditions similar to those used in this study (Webb et al., 2005b). Although the mechanism of Mn^{III} formation within Mn octahedral sheets is not certain, EXAFS data indicates that as Mn^{III} is formed, at least some is arranged in edge sharing complexes on δ-MnO_2 edge sites (i.e. as part of the mineral structure), or around vacancy sites in octahedral layers of δ-MnO_2. Although its value is associated with rather large error, the trend in the fraction of Mn

sites occupied in the δ-MnO_2 structure (f_{occ} from Mn EXAFS fitting) indicates that some Mn^{III} formed during As^{III} oxidation could enter into δ-MnO_2 vacancy sites (Table 2.2) (Zhu et al., 2010b).

As Speciation and Binding Mechanisms During As^{III} Oxidation

As K-edge XANES first derivative spectra show only As^{V} associated with δ-MnO_2 during As^{III} oxidation (Figure 2.5a). Shell-by-shell fits of the As EXAFS spectra indicate a first shell As-O distance of 1.7 Å exclusively (Table 2.3). An As-O bond distance of 1.7 Å is consistent with previously observed As^{V} bound to phyllomanganates (Foster et al., 2003; Manning et al., 2002), and similar to As^{V} bound to Fe-oxides (Fendorf et al., 1997; Waychunas et al., 1993). Previous studies have also found that during As^{III} oxidation by birnessite, As is bound to the solid phase only as As^{V} with no evidence of As^{III} (Manning et al., 2002; Tournassat et al., 2002).

As K-edge EXAFS spectra exhibit a single major frequency (Figure 2.5b) which is due to the presence of four oxygen atoms surrounding As in tetrahedral coordination (Foster et al., 2003). This major frequency produces the predominant feature in the Fourier transformed data, an As-O peak at 1.3 Å (R + ΔR) (Figure 2.5c). In addition to the As-O shell, several As-Mn shells occur between 2.2 and 3.2 Å (R + ΔR) (Figure 2.5c). When As^{V} is reacted with δ-MnO_2 (sorption standard), two As-Mn

Table 2.2. Structural parameters derived from least-squares fits to raw k^3-weighted Mn-EXAFS spectra of unreacted δ-MnO_2 and δ-MnO_2 reacted with As^{III} for 0.5, 4, 10, 24, and 48 hours.

Sample	R	f_{occ}	Shell	CN	Dist (Å)	σ^2	Sample	R	f_{occ}	Shell	CN	Dist (Å)	σ^2
δ-MnO2	0.03	0.7(2)	Mn-O	4	1.90(8)	0.006(7)	*10 hrs*	0.02	0.8(2)	Mn-O	4	1.91(1)	0.013(2)
(0 hrs)			Mn-O	2	1.91(6)	0.006				Mn-O	2	1.90(1)	0.002(1)
			Mn-Mn	2	2.79(3)	0.010(5)				Mn-Mn	2	2.81(3)	0.010(8)
			Mn-Mn	4	2.87(0)	0.003(1)				Mn-Mn	4	2.88(1)	0.005(1)
			Mn-O	4	3.42(3)	0.008(4)				Mn-O	4	3.42(3)	0.002(2)
			Mn-O	2	3.7(1)	0.01(2)				Mn-O	2	3.8(1)	
			Mn-Na inter	2(2)	4.07(5)	0.006				Mn-Na inter	0.8(7)	4.02(7)	0.002
			Mn-Mn corn	0	3.32	0.006				Mn-Mn corn	1.4(9)	3.63(7)	0.006
			Mn-O	4	5.0(3)	0.01(1)				Mn-O	4	4.37(7)	0.010(5)
			Mn-O	8	4.61(9)					Mn-O	8	4.65(5)	
			Mn-Mn	4	4.87(6)	0.007(3)				Mn-Mn	4	4.91(8)	0.015(8)
			Mn-Mn	2	5.32(8)					Mn-Mn	2	5.4(3)	
			Mn-Mn	2	5.33	0.006(4)				Mn-Mn	2	5.48	0.009(5)
			Mn-Mn	4	5.5					Mn-Mn	4	5.88	

Sample	R	f_{occ}	Shell	CN	Dist (Å)	σ^2	Sample	R	f_{occ}	Shell	CN	Dist (Å)	σ^2
0.5 hrs	0.04	0.8(1)	Mn-O	4	1.89(2)	0.010(2)	*24 hrs*	0.04	1.0(3)	Mn-O	4	1.88(2)	0.007(3)
			Mn-O	2	1.90(1)	0.003(1)				Mn-O	2	1.91(3)	0.003(2)
			Mn-Mn	2	2.79(3)	0.010(5)				Mn-Mn	2	2.77(5)	0.014(9)
			Mn-Mn	4	2.87(0)	0.003(1)				Mn-Mn	4	2.87(1)	0.005(2)
			Mn-O	4	3.42(3)	0.008(3)				Mn-O	4	3.42(7)	0.003(5)
			Mn-O	2	3.69(7)					Mn-O	2	3.8(2)	
			Mn-Na inter	1(1)	4.07(4)	0.003				Mn-Na inter	1(1)	4.03(6)	0.002
			Mn-Mn corn	0	3.32	0.006				Mn-Mn corn	1(1)	3.6(3)	0.006
			Mn-O	4	5.0(3)	0.01(1)				Mn-O	4	5(25)	0.0(4)
			Mn-O	8	4.62(8)					Mn-O	8	5(13)	
			Mn-Mn	4	4.87(6)	0.007(3)				Mn-Mn	4	4.87(5)	0.013(8)
			Mn-Mn	2	5.32(7)					Mn-Mn	2	5.3(2)	
			Mn-Mn	2	5.34	0.005(3)				Mn-Mn	2	5.46	0.012(9)
			Mn-Mn	4	5.51					Mn-Mn	4	5.89	

Sample	R	f_{occ}	Shell	CN	Dist (Å)	σ^2	Sample	R	f_{occ}	Shell	CN	Dist (Å)	σ^2
4 hrs	0.03	0.9(3)	Mn-O	4	1.89(2)	0.015(2)	*48 hrs*	0.06	1.0(3)	Mn-O	4	1.88(1)	0.008(2)
			Mn-O	2	1.90(1)	0.002(1)				Mn-O	2	1.91(1)	0.002(1)
			Mn-Mn	2	2.8(1)	0.02(1)				Mn-Mn	2	2.77(4)	0.011(7)
			Mn-Mn	4	2.86(0)	0.005(1)				Mn-Mn	4	2.88(1)	0.005(2)
			Mn-O	4	3.43(4)	0.004(3)				Mn-O	4	3.40(4)	0.003(2)
			Mn-O	2	3.7(1)					Mn-O	2	3.7(1)	
			Mn-Na inter	1(2)	4.1(2)	0.009				Mn-Na inter	1(1)	4.09(6)	0.002
			Mn-Mn corn	0.5(7)	3.6(1)	0.003				Mn-Mn corn	1(1)	3.59(9)	0.006
			Mn-O	4	4.47(6)	0.005(4)				Mn-O	4	4.46(6)	0.005(4)
			Mn-O	8	4.68(3)					Mn-O	8	4.67(4)	
			Mn-Mn	4	4.92(6)	0.011(8)				Mn-Mn	4	4.91(6)	0.010(4)
			Mn-Mn	2	5.2(1)					Mn-Mn	2	5.3(3)	
			Mn-Mn	2	5.36	0.008(5)				Mn-Mn	2	5.5(2)	0.007(7)
			Mn-Mn	4	5.88					Mn-Mn	4	5.85(5)	

* Coordination number (CN), interatomic distance (r), and Debye-Waller factor (σ^2) were obtained by fitting data with theoretical phase and amplitude functions. Estimated errors at 95% confidence interval from the least-squares fit are given in parentheses. For a further description of fitted parameters, see Webb et al. (2005).

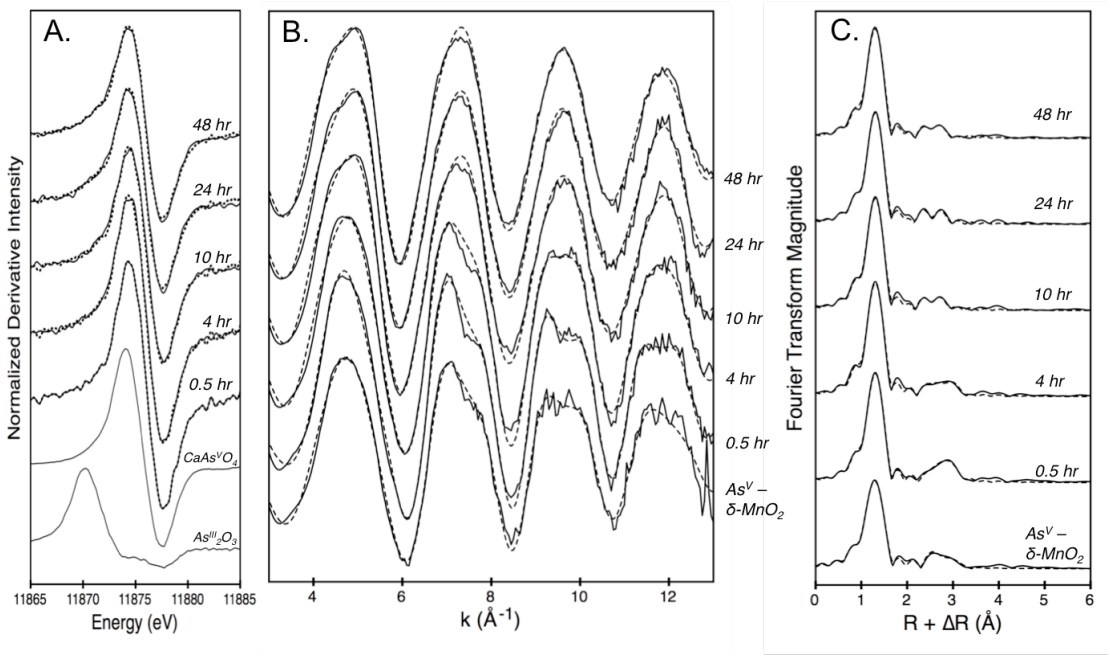

Figure 2.5. Arsenic K-edge derivative XANES (A.), As K-edge EXAFS (B.), and Fourier transformed EXAFS (C.) of unreacted δ-MnO_2 and δ-MnO_2 (1 mg/L) reacted with As^{III} (100 μM) in a stirred-flow reactor for 0.5, 4, 10, 24, and 48 hours. XAS data is presented as solid lines and fits are presented as dashed lines (fit data provided in Table 2.3).

Table 2.3. Structural parameters derived from least-square fits to raw k^3-weighted As-EXAFS spectra for sorption standards and As^{III} oxidation samples taken at 0.5, 4, 10, 24, and 48 hours of reaction.

Sample	*As-O*			*As-Mn*			*As-Mn*			*As-Mn*		
Time	*CN* *	*r* *	σ^{2} *	*CN* *	*r* *	σ^{2} *	*CN* *	*r* *	σ^{2} *	*CN* *	*r* *	σ^{2} *
0.5 hours	4.8(2)	1.70(0)	0.004(0)				1.3(2)	3.12(1)	0.005(2)	2.9(5)	3.42(1)	0.002(1)
4 hours	3.8(3)	1.69(1)	0.003(1)				1.2(5)	3.13(4)	0.005(5)	1.4(6)	3.47(6)	0.009(3)
10 hours	3.9(5)	1.69(1)	0.003(1)	0.3(2)	2.71(4)	0.006(3)	0.9(4)	3.20(3)	0.006(3)	0.4(5)	3.39(2)	0.006(3)
24 hours	3.8(3)	1.69(1)	0.003(1)	0.4(2)	2.72(3)	0.006(3)	1.0(4)	3.23(3)	0.006(2)	0.4(5)	3.42(6)	0.006(3)
48 hours	3.9(2)	1.69(1)	0.003(1)	0.21(3)	2.71(4)	0.006(2)	1.0(4)	3.19(3)	0.006(3)	0.6(4)	3.34(6)	0.006(4)
As^{V} - Manganite	4.0(1)	1.69(1)	0.004(1)	0.1(1)	2.78(6)	0.006(3)	0.6(4)	3.35(1)	0.004(2)			
As^{V} - δ-MnO_2	3.9(2)	1.70(1)	0.004(1)				0.9(5)	3.13(2)	0.003(2)	0.3(3)	3.48(4)	0.002(1)

* Coordination number (CN), interatomic distance (r), and Debye-Waller factor (σ^2) were obtained by fitting data with theoretical phase and amplitude functions. Estimated errors at 95% confidence interval from the least-squares fit are given in parentheses.

distances are present (Table 2.3). The As-Mn distance of 3.13 Å, is similar to that observed (3.16 Å) by Foster et al. (2003), which was attributed to a bidentate-binuclear complex with δ-MnO_2. However, the observed 3.13 Å As-Mn distance is shorter than the ~3.22 Å As-Mn distance attributed to a bidentate-binuclear complex by both Manceau et al. (2007) and Manning et al. (2002). Quantum chemical calculations of As^V sorption in a bidentate-binuclear complex on Mn^{IV} also predict an As^V-Mn^{IV} distance of 3.20 Å (Zhu et al., 2009). One possible explanation for the longer As-Mn distances observed by Manceau (2007) and Manning (2002) could be the presence of Mn^{III} on the surface (i.e. at edge sites) of the Mn-oxides used in these studies. Mn^{III} octahedra undergo Jahn-Teller distortion that is exhibited in a lengthening of 2 of the 6 Mn-O bonds in the octahedra. If some As^V is bound to Mn^{III} on the mineral surfaces used by Manceau et al. (2007) and Manning et al. (2002), it is reasonable to assume the resulting As-Mn distance would increase. We can reasonably describe the 3.13 Å As-Mn distance observed here as representing a bidentate-binuclear complex between As^V and δ-MnO_2.

A second As-Mn distance of 3.48 Å is also present when As^V is reacted with δ-MnO_2 (Table 2.3). An As-Mn distance similar to this has not been previously observed for As^V bound to Mn-oxides. However, Foster et al. (2003) modeled As^V sorption on δ-MnO_2 in a monodentate-mononuclear complex, and predicted an As-Mn distance of 3.6 Å, similar to the As^V-Fe distance observed for the same type of complex (Fendorf et al., 1997; Waychunas et al., 1993). The Fe-O distance in an Fe octahedra (Waychunas et al., 1993) is 2.1 Å, while the Mn-O distance in Mn octahedra

in this study are 1.9 Å (Table 2.2). Taking this difference into account, it is reasonable to conclude that the As-Mn distance of 3.48 Å observed in the As^V sorption standard represents a monodentate-mononuclear sorption complex between As^V and the δ-MnO_2 surface.

When As^{III} is reacted with δ-MnO_2, As^V is present on the δ-MnO_2 surface in the same sorption complexes (bidentate-binuclear and monodentate-mononuclear) for the first four hours, as when As^V is sorbed on δ-MnO_2 (Table 2.3, Figure 2.6b). One can clearly see in the As Fourier transformed data (Figure 2.5c), that As^V sorbed on δ-MnO_2, and the samples representing 0.5 and 4 hours of reaction between As^{III} and δ-MnO_2 differ from 10, 24, and 48 hour samples in the 2.2 and 3.2 Å region (R + ΔR). However, the Fourier transformed data obtained after 10, 24, and 48 hours, are quite similar (Figure 2.5). Also, the monodentate-mononuclear complex between As^V and the δ-MnO_2 surface is present when As^V is sorbed as well as throughout As^{III} oxidation with a relatively consistent As-Mn distance (Table 2.3).

A change in As bonding environment on the δ-MnO_2 surface occurs between 4 and 10 hours of reaction. This change occurs simultaneously with maximum Mn sorption at vacancy sites and the greatest Mn^{III} increase in the δ-MnO_2 structure (Figure 2.6c and d). From 10 to 48 hours, an As-Mn distance of 2.7 Å appears, which corresponds to a bidentate-mononuclear (edge-sharing) complex between As^V and the δ-MnO_2 surface. The same complex observed on Fe-oxides is characterized by a Fe-O distance of 2.85 Å (Fendorf et al., 1997), which is longer than in this study, possibly

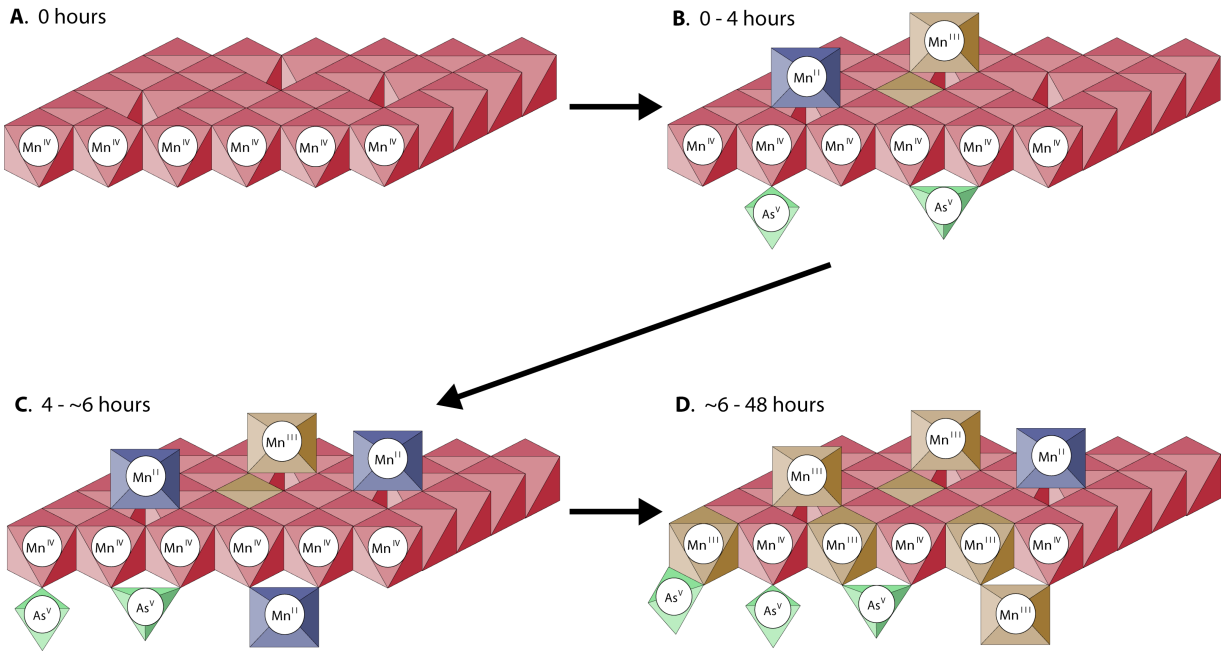

Figure 2.6. Proposed reaction mechanism for As^{III} oxidation by δ-MnO_2 over 48 hours in a stirred-flow reactor. Throughout the reaction, As^{III} is oxidized by Mn^{IV} at δ-MnO_2 edge sites, producing Mn^{II} and As^{V}. (A.) Unreacted δ-MnO_2 octahedral layers consist of primarily Mn^{4+}, and have reaction sites at layer edges (edge sites) and vacancy sites. (B.) During the first 4 hours of As^{III} oxidation, Mn^{II} sorbs at δ-MnO_2 vacancy sites, and As^{V} sorbs at edge sites in bidentate-binuclear and monodentate-mononuclear complexes. Also, a portion of sorbed Mn^{II} reacts with Mn^{IV} at vacancy sites to form Mn^{III}. (C.) Between 4 and ~ 6 hours of reaction, vacancy sites become filled with $Mn^{II\,/\,III}$, Mn^{II} begins to sorb at δ-MnO_2 edge sites, and As^{V} sorption continues in the same sorption complexes. (D.) Beyond ~ 6 hours of reaction, Mn^{II} at edge sites (and probably vacancy sites) reacts with Mn^{III} in δ-MnO_2 octahedral layers to form Mn^{III}. The resulting Mn^{III} changes the bonding environment of As^{V}, which begins to sorb in bidentate-mononuclear complexes and the As-Mn distance in As^{V} bidentate-binuclear complexes increases slightly.

due to the larger size of Fe^{III} octahedra compared to Mn^{IV} octahedra. However, the As-Mn distance of 2.7 Å can be reproduced by sorbing As^{V} on γ-$Mn^{III}OOH$ (Table 2.3), which might indicate that the bidentate-mononuclear complex observed during As^{III} oxidation by δ-MnO_2 is caused by As^{V} binding to Mn^{III} on the δ-MnO_2 surface rather than Mn^{IV} (Figure 2.6d).

Also observed between 4 and 10 hours of reaction is a lengthening of the As-Mn distance attributed to a bidentate-binuclear complex from 3.13 Å to 3.21 Å (Table 2.3). This longer As-Mn distance (3.21 Å) is similar to the distances attributed to As bidentate-binuclear complexes on other phyllomanganates (Manceau et al., 2007; Manning et al., 2002). In our system it is possible that the increased As-Mn distance from 3.13 Å to 3.21 Å is due to As being bound, in part, to Mn^{III} rather than Mn^{IV} on the δ-MnO_2 surface (Figure 2.6d). This seems likely since the change in the As-Mn distance associated with bidentate-binuclear adsorption complexes coincides with the greatest increase in Mn^{III} on the δ-MnO_2 surface as discussed previously. Figure 4d includes a schematic representation of all observed As^{V} sorption complexes on the δ-MnO_2 surface.

Although, in this study, As^{III} oxidation probably does not directly form Mn^{III} on the δ-MnO_2 surface, it seems that the presence of Mn^{III} on a Mn-oxide surface can significantly alter the As local bonding environment. It also appears that Mn^{II}

produced via reductive dissolution of δ-MnO_2 can passivate the δ-MnO_2 surface via sorption and conproportionation with Mn^{IV} to form Mn^{III} in the mineral structure. Passivation could be an important process in the environment because of its potential to decrease the sorption and oxidative capacities of some of the most reactive minerals in nature.

References

Ankudinov, A.L., and J.J. Rehr. 1997. Relativistic calculations of spin-dependent X-ray-absorption spectra. Phys. Rev. B 56:R1712.

Chiu, V.Q., and J.G. Hering. 2000. Arsenic adsorption and oxidation at manganite surfaces. 1. Method for simultaneous determination of adsorbed and dissolved arsenic species. Environ. Sci. Technol. 34:2029-2034.

Dixit, S., and J.G. Hering. 2003. Comparison of arsenic(V) and arsenic(III) sorption onto iron oxide minerals: Implications for arsenic mobility. Environ. Sci. Technol. 37:4182-4189.

Drits, V.A., B. Lanson, and A.C. Gaillot. 2007. Birnessite polytype systematics and identification by powder X-ray diffraction. Am. Mineral. 92:771-788.

Drits, V.A., E. Silvester, A.I. Gorshkov, and A. Manceau. 1997. Structure of synthetic monoclinic Na-rich birnessite and hexagonal birnessite. 1. Results from X-ray diffraction and selected-area electron diffraction. Am. Mineral. 82:946-961.

Fendorf, S., M.J. Eick, and P. Grossl. 1997. Arsenate and chromate retention mechanisms on goethite. 1. Surface structure. Environ. Sci. Technol. 31:315-320.

Foster, A.L., G.E. Brown, and G.A. Parks. 2003. X-ray absorption fine structure study of As(V) and Se(IV) sorption complexes on hydrous Mn oxides. Geochim. Cosmochim. Ac. 67:1937-1953.

Gaillot, A.C., D. Flot, V.A. Drits, A. Manceau, M. Burghammer, and B. Lanson. 2003. Structure of synthetic K-rich birnessite obtained by high-temperature decomposition of $KMnO_4$. I. Two-layer polytype from 800 ^{o}C experiment. Chem. Mat. 15:4666-4678.

Ginder-Vogel, M., G. Landrot, J.S. Fischel, and D.L. Sparks. 2009. Quantification of rapid environmental redox processes with quick-scanning x-ray absorption spectroscopy (Q-XAS). Proc. Natl. Acad. Sci. 106:16124-16128.

Hammersley, A.P. 1998. FIT2D V9.129 Reference Manual V3.1. ESRF Internal Report ESRF98HA01T.

Manceau, A., B. Lanson, and V.A. Drits. 2002. Structure of heavy metal sorbed birnessite. Part III: Results from powder and polarized extended X-ray absorption fine structure spectroscopy. Geochim. Cosmochim. Acta 66:2639-2663.

Manceau, A., M. Lanson, and N. Geoffroy. 2007. Natural speciation of Ni, Zn, Ba, and As in ferromanganese coatings on quartz using X-ray fluorescence, absorption, and diffraction. Geochim. Cosmochim. Acta 71:95-128.

Manceau, A., V.A. Drits, E. Silvester, C. Bartoli, and B. Lanson. 1997. Structural mechanism of Co^{2+} oxidation by the phyllomanganate buserite. Am. Mineral. 82:1150-1175.

Manceau, A., M.A. Marcus, N. Tamura, O. Proux, N. Geoffroy, and B. Lanson. 2004. Natural speciation of Zn at the micrometer scale in a clayey soil using X-ray fluorescence, absorption, and diffraction. Geochim. Cosmochim. Acta 68:2467-2483.

Manceau, A., C. Tommaseo, S. Rihs, N. Geoffroy, D. Chateigner, M. Schlegel, D. Tisserand, M.A. Marcus, N. Tamura, and Z.-S. Chen. 2005. Natural speciation of Mn, Ni, and Zn at the micrometer scale in a clayey paddy soil using X-ray fluorescence, absorption, and diffraction. Geochim. Cosmochim. Acta 69:4007-4034.

Manning, B.A., S.E. Fendorf, B. Bostick, and D.L. Suarez. 2002. Arsenic(III) oxidation and arsenic(V) adsorption reactions on synthetic birnessite. Environ. Sci. Technol. 36:976-981.

Marcus, M.A., A. Manceau, and M. Kersten. 2004. Mn, Fe, Zn and As speciation in a fast-growing ferromanganese marine nodule. Geochim. Cosmochim. Acta 68:3125-3136.

Moore, J.N., J.R. Walker, and T.H. Hayes. 1990. Reaction scheme for the oxidation of As(III) to As(V) by birnessite. Clay. Clay Miner. 38:549-555.

Nesbitt, H.W., G.W. Canning, and G.M. Bancroft. 1998. XPS study of reductive dissolution of 7 angstrom-birnessite by H_3AsO_3, with constraints on reaction mechanism. Geochim. Cosmochim. Ac. 62:2097-2110.

Newville, M. 2001. IFEFFIT : Interactive XAFS analysis and FEFF fitting. J. Synchrotron Radiat. 8:322-324.

Newville, M., B. Ravel, D. Haskel, J.J. Rehr, E.A. Stern, and Y. Yacoby. 1995. Analysis of multiple-scattering XAFS data using theoretical standards. Physica B: Condensed Matter 208-209:154-156.

Oscarson, D.W., P.M. Huang, and W.K. Liaw. 1981. Role of manganese in the oxidation of arsenite by freshwater sediments. Clay. Clay Miner. 29:219-225.

Oscarson, D.W., P.M. Huang, W.K. Liaw, and U.T. Hammer. 1983. Kinetics of oxidation of arsenite by various manganese dioxides. Soil Sci. Soc. Am. J. 47:644-648.

Parikh, S.J., B.J. Lafferty, and D.L. Sparks. 2008. An ATR-FTIR spectroscopic approach for measuring rapid kinetics at the mineral/water interface. J. Colloid Interface Sci. 320:177.

Petrick, J.S., F. Ayala-Fierro, W.R. Cullen, D.E. Carter, and H.V. Aposthian. 2000. Monomethylarsonous acid (MMA(III)) is more toxic than arsenite in Chang human hepatocytes. Toxicol. Appl. Pharmacol. 163:203-207.

Post, J.E. 1999. Manganese oxide minerals: Crystal structures and economic and environmental significance. Proc. Natl. Acad. Sci. 96:3447-3454.

Raven, K.P., A. Jain, and R.H. Loeppert. 1998. Arsenite and arsenate adsorption on ferrihydrite: kinetics, equilibrium, and adsorption envelopes. Environ. Sci. Technol. 32:344-349.

Scott, M.J., and J.J. Morgan. 1995. Reactions at oxide surfaces. 1. Oxidation of As(III) by synthetic birnessite. Environ. Sci. Technol. 29:1898-1905.

Silvester, E., A. Manceau, and V.A. Drits. 1997. Structure of synthetic monoclinic Na-rich birnessite and hexagonal birnessite. 2. Results from chemical studies and EXAFS spectroscopy. Am. Mineral. 82:962-978.

Tani, Y., N. Miyata, M. Ohashi, T. Ohnuki, H. Seyama, K. Iwahori, and M. Soma. 2004. Interaction of inorganic arsenic with biogenic manganese oxide produced by a Mn-oxidizing fungus, strain KR21-2. Environ. Sci. Technol. 38:6618-6624.

Tebo, B.M., J.R. Bargar, B.G. Clement, G.J. Dick, K.J. Murray, D. Parker, R. Verity, and S.M. Webb. 2004. Biogenic manganese oxides: Properties and mechanisms of formation. Ann. Rev. Earth and Plan. Sci. 32:287-328.

Toner, B., A. Manceau, S.M. Webb, and G. Sposito. 2006. Zinc sorption to biogenic hexagonal-birnessite particles within a hydrated bacterial biofilm. Geochim. Cosmochim. Acta 70:27-43.

Tournassat, C., L. Charlet, D. Bosbach, and A. Manceau. 2002. Arsenic(III) oxidation by birnessite and precipitation of manganese(II) arsenate. Environ. Sci. Technol. 36:493-500.

Villalobos, M., J. Bargar, and G. Sposito. 2005. Mechanisms of Pb(II) sorption on a biogenic manganese oxide. Environ. Sci. Technol. 39:569-576.

Villalobos, M., B. Toner, J. Bargar, and G. Sposito. 2003. Characterization of the manganese oxide produced by *Pseudomonas putida* strain MnB1. Geochim. Cosmochim. Acta 67:2649-2662.

Villalobos, M., B. Lanson, A. Manceau, B. Toner, and G. Sposito. 2006. Structural model for the biogenic Mn oxide produced by Pseudomonas putida. Am. Mineral. 91:489-502.

Waychunas, G.A., B.A. Rea, C.C. Fuller, and J.A. Davis. 1993. Surface chemistry of ferrihydrite, Part l. EXAFS studies of the geometry of coprecipitated and adsorbed arsenate. Geochim. Cosmochim. Acta. 57:2251-69.

Webb, S.M. 2005. SIXpack: a graphical user interface for XAS analysis using IFEFFIT. Physica Scripta T115:1011-1014.

Webb, S.M., B.M. Tebo, and J.R. Bargar. 2005a. Structural characterization of biogenic Mn oxides produced in seawater by the marine bacillus sp. strain SG-1. Am. Mineral. 90:1342-1357.

Webb, S.M., G.J. Dick, J.R. Bargar, and B.M. Tebo. 2005b. Evidence for the presence of Mn(III) intermediates in the bacterial oxidation of Mn(II). Proc. Natl. Acad. Sci. 102:5558-5563.

Zhu, M., M. Ginder-Vogel, and D.L. Sparks. 2010a. Ni(II) sorption on biogenic Mn-oxides with varying Mn octahedral layer structure. accepted to Environ. Sci. Technol.

Zhu, M., K.W. Paul, J.D. Kubicki, and D.L. Sparks. 2009. Quantum chemical study of arsenic (III, V) adsorption on Mn-oxides: Implications for arsenic(III) oxidation. Environ. Sci. Technol. 43:6655-6661.

Zhu, M., M. Ginder-Vogel, S.J. Parikh, X.-H. Feng, and D.L. Sparks. 2010b. Cation effects on the layer structure of biogenic Mn-oxides. Accepted to Environ. Sci. Technol.

Chapter 3

DESORPTION OF ARSENIC AND MANGANESE FROM A POORLY CRYSTALLINE MANGANESE OXIDE

Abstract

It is crucial to understand arsenic (As) mobility in the environment because of its toxicity and potential to negatively affect human health. Sorption by metal oxides, and speciation are the primary factors that determine As mobility in the environment. Manganese oxides (Mn-oxides) are powerful oxidants in soils and sediments, and are known to oxidize toxic arsenite (As^{III}) to less toxic arsenate (As^{V}). Mn-oxides also have the ability to sorb As, potentially decreasing its mobility. However, the effect of competing ions on the mobility of As sorbed on Mn-oxides is not well understood. In this study, desorption of As^{V}, As^{III}, and Mn^{II} from poorly crystalline hexagonal birnessite (δ-MnO_2) by a common cation and anion is investigated using a stirred-flow technique. No As^{III} is desorbed under any conditions studied, which agrees with previous studies showing As sorbed on Mn-oxides exists as As^{V}. As^{V} is desorbed to a large extent (> 50 %) under all conditions studied. However, some As^{V} consistently remains sorbed on δ-MnO_2. Mn^{II} desorption only occurs after 10 hours of As^{III} oxidation, probably at δ-MnO_2 edge sites. Overall, δ-MnO_2 has the potential to decrease As mobility through As^{III} oxidation and As^{V} sorption.

Introduction

Arsenic (As) is an element with toxic properties, and is common in the environment. Elevated levels of As in soil can result from natural weathering processes, or anthropogenic activities such as mining, agriculture, and manufacturing. In several locations throughout the world, As contamination of soil and water occurs near human populations, thus posing a significant threat to human health. Therefore, understanding the chemical reactions controlling As mobility in the environment is critical.

A major factor controlling As behavior in the environment is its chemical speciation. Typically, As occurs as one of two inorganic oxyanions: arsenite (As^{III}) or arsenate (As^{V}). Below pH 9, As^{III} appears predominately in its fully protonated form (H_3AsO_3), while at circumneutral pH values, As^{V} occurs as a mixture of $H_2AsO_4^-$ and $HAsO_4^{2-}$ (Sadiq, 1997). A significant pathway affecting speciation of As is oxidation of As^{III} by Mn-oxide minerals. Several Mn-oxides can readily oxidize As^{III} to As^{V}, most notably layered Mn-oxides (i.e. phyllomanganates) such as birnessite (Driehaus et al., 1995; Ginder-Vogel et al., 2009; Moore et al., 1990; Nesbitt et al., 1998; Oscarson et al., 1981a; Oscarson et al., 1981b; Oscarson et al., 1983; Parikh et al., 2008; Scott and Morgan, 1995; Tournassat et al., 2002). Oxidation of As^{III} by Mn-oxides not only changes As mobility, this process can also detoxify As since As^{III} is more toxic than As^{V} (Petrick et al., 2000).

The mobility of As in terrestrial environments is generally determined by the extent to which it is adsorbed by metal oxides, especially the oxides of iron (Fe) and aluminum (Al) (Anderson et al., 1976; Arai et al., 2001; Dixit and Hering, 2003; Gupta and Chen, 1978; Hingston et al., 1971; Raven et al., 1998). Although, metal oxides are generally thought to bind As^{V} more readily than As^{III}, the extent to which each species is sorbed depends greatly on pH. For example, As^{V} sorption by Fe-oxides is greater at acidic pH values, whereas As^{III} sorption by Fe oxides is greater at basic pH values (Dixit and Hering, 2003; Raven et al., 1998).

Mn-oxides also have the ability to sorb As. Several studies have observed As^{V} sorption both when As^{V} (Foster et al., 2003; Manning et al., 2002), and As^{III} are reacted with phyllomanganates (Manning et al., 2002; Oscarson et al., 1983; Parikh et al., 2008; Tani et al., 2004). Increased As sorption is often observed during As^{III} oxidation by phyllomanganates than when As^{V} is sorbed without simultaneous As^{III} oxidation (Driehaus et al., 1995; Manning et al., 2002; Oscarson et al., 1983; Parikh et al., 2008; Tani et al., 2004). Some studies have also observed As binding to phyllomanganates through a tertiary Mn^{II}-As^{V} 'bridging' complex (Parikh et al., 2008; Tani et al., 2004)..

Because Mn-oxides can play an important role in controlling As speciation, it is important to understand the mobility of As when it is sorbed on Mn-oxide surfaces. When As is sorbed by phyllomanganates, it is present as As^{V} and can form multiple surface complexes (Chapter 2) (Foster et al., 2003; Manning et al., 2002). Thus, it is possible that the lability As^{V} bound to Mn-oxide surfaces depends on the type of

surface complex. In nature, As co-exists with other ions which can compete for sorption sites on mineral surfaces, thus understanding As mobility in the environment requires understanding the potential for competing ions to desorb As from Mn-oxide surfaces. To date, few studies have investigated the ability of common environmental ions to desorb As from the surface of Mn-oxides. The purpose of this study is to determine to what extent a common cation (Ca^{2+}), and oxyanion in the environment ($H_2PO_4^-/HPO_4^{2-}$) are able to desorb As from a poorly crystalline hexagonal birnessite (δ-MnO_2).

Materials and Methods

Stirred Flow Method

Stirred flow experiments were conducted using the same 30 mL reactor described previously (Chapter 1). Each experiment was conducted at least in duplicate, and the presented data are averages. All stirred flow reactions were conducted in a constant background electrolyte concentration (10 mM NaCl), buffered at pH 7.2 (5 mM MOPS), and had a constant flow rate of 1 mL/min. Also, all experiments were mixed via a magnetic stir bar with a constant rate of stirring (100 rpm).

In all desorption reactions, 100 μM As^{III} was reacted (i.e. oxidized and sorbed) with 1g/L δ-MnO_2 for 4, 10, or 24 hours, followed immediately by reaction (i.e. desorbed) with 100 μM calcium chloride ($CaCl_2$, abbreviated Ca^{2+}), 100 μM sodium phosphate (NaH_2PO_4, abbreviated PO_4), or background electrolyte alone (10 mM

NaCl and 5mM MOPS). It is important to emphasize that desorption by Ca^{2+} and PO_4 was also conducted in the presence of background electrolyte (10 mM NaCl and 5mM MOPS). Prior to the start of each reaction, background electrolyte was introduced into the stirred flow reactor for at least two hours and was kept constant throughout As^{III} oxidation and subsequent As and Mn desorption. As^{III} oxidation in each reaction was stopped after 4, 10, or 24 hours by removing As^{III} influent solution from the stirred flow reactor, and desorption was immediately initiated by introducing desorbing solution to the reactor. A plot showing the full data from one experiment is presented in the supporting information (Figure 3.1).

As, Mn, Ca, and P Analysis

Arsenic in stirred flow influent was analyzed via liquid chromatography inductively coupled plasma mass spectrometry (LC-ICP-MS), and aqueous Mn was analyzed by ICP-MS as described in (Chapter 1). Total aqueous P and Ca were analyzed by ICP-OES to verify the concentration of desorptive present in the stirred-flow reactor.

Sorption and Desorption Calculations

To determine the mass of As adsorbed as well as the mass of As and Mn subsequently desorbed, curves representing ideal behavior of the stirred flow reactor influent solution were calculated (i.e. perfect mixing and no retention of reactant

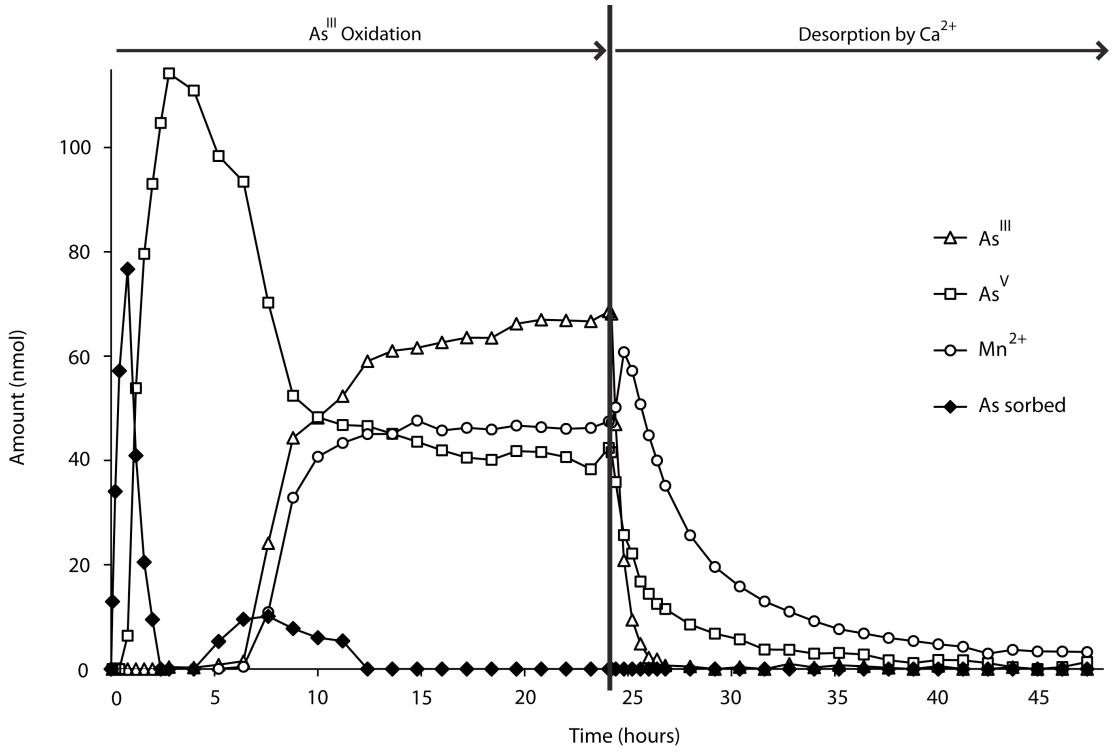

Figure 3.1. Raw data from one replicate of As^{III} oxidation by δ-MnO_2 followed by desorption by $CaCl_2$. As^{III} oxidation was carried out for the first 24 hours, and desorption by $CaCl_2$ was carried out from 24 to 48 hours.

within the reactor). These 'dilution curves' are necessary to account for affects of dilution when a reactant is added (e.g. at the beginning of As^{III} oxidation) or removed from the influent solution (e.g. at the beginning of desorption). For example, prior to As^{III} oxidation, As concentration in the reactor is zero, and under the conditions used in these experiments, approximately 3 hours of pumping influent solution into the reactor are required for the concentration of total As in the reactor to equal the concentration of As in the influent solution. By subtracting the total As measured in the reactor effluent during initial As^{III} oxidation from the predicted amount of As in the reactor (from the dilution curve), the amount of As sorbed at any given time can be determined. Also, by subtracting the amounts of As^{V}, As^{III}, or Mn^{II} predicted to be removed from the reactor during desorption from the measured quantity removed, the amount of each species desorbed from δ-MnO_2 can be determined. Figure 3.2 shows data and calculated dilution curves of As^{III} oxidation as well as As^{III}, As^{V}, and Mn^{II} desorption plotted together. To quantify the total amount sorbed and desorbed of As^{V}, As^{III}, and Mn^{II}, data were integrated using the 'area below curves' tool in SigmaPlot 8 (Systat Software Inc., San Jose, California).

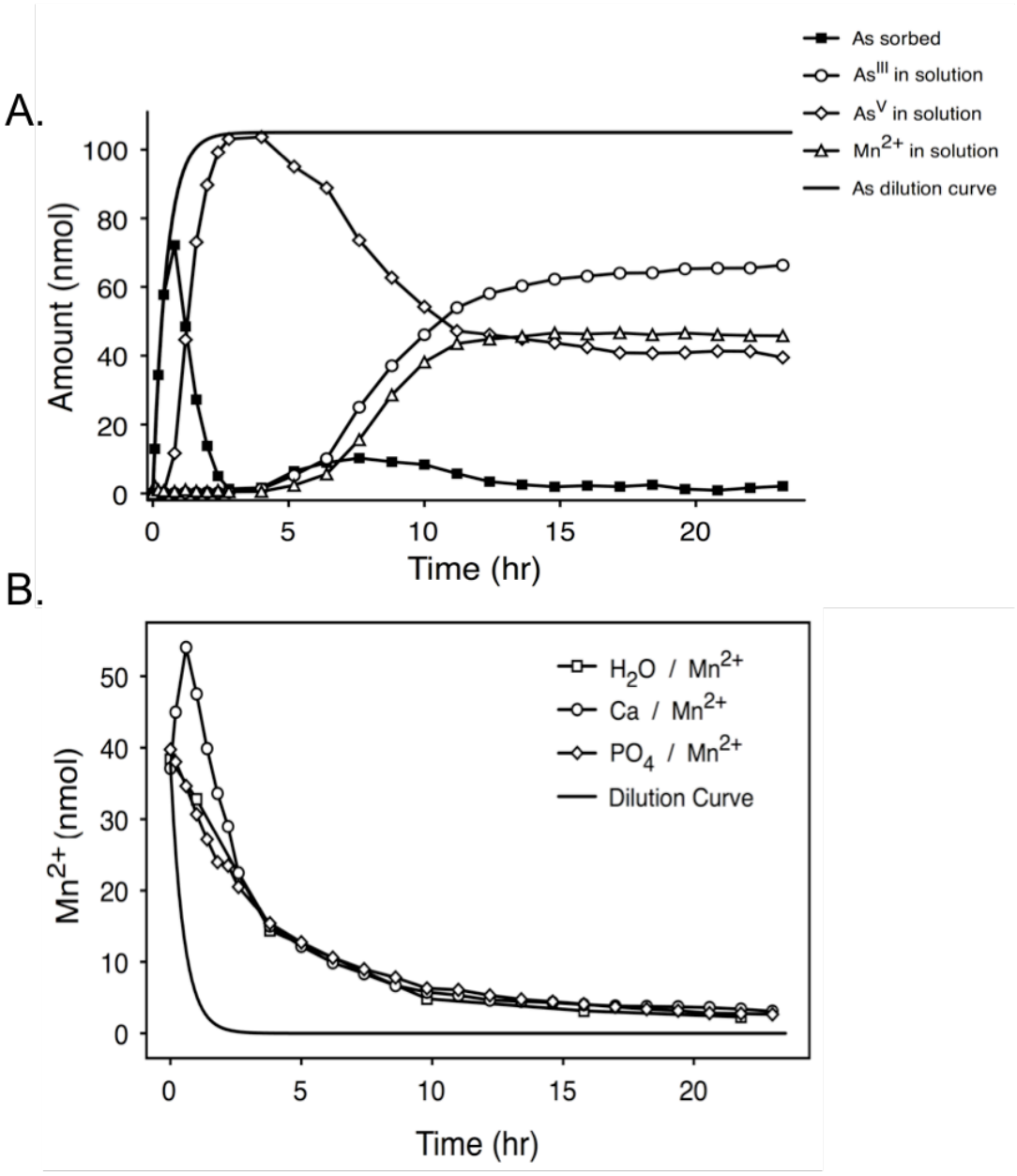

Figure 3.2. Amount of As^{III}, As^{V}, and Mn^{II} in solution as well as amount of As sorbed, all during As^{III} oxidation by δ-MnO_2 (A.) and desorption by $CaCl_2$ (B.). Also plotted is the calculated dilution curve of predicted As in stirred-flow effluent under ideal conditions (i.e. no sorption) in each case.

Results and Discussion

δ-MnO_2 Structure

It is important to understand the structure of δ-MnO_2 in order to interpret desorption data as accurately as possible. The δ-MnO_2 used in this study is a poorly ordered form of hexagonal birnessite (Chapter 2). Hexagonal birnessite (and thus δ-MnO_2) has reactive sites at vacancies within Mn^{IV} octahedral sheets (vacancy sites) and at the edges of Mn^{IV} octahedral sheets (edge sites) (Drits et al., 1997; Silvester et al., 1997). It has been shown that As reacts primarily with edge sites, rather than vacancy sites of birnessite (Manning et al., 2002; Tournassat et al., 2002; Villalobos et al., 2005), therefore, in this study, As adsorption and desorption is expected to occur at δ-MnO_2 edge sites. On the other hand, heavy metals sorb strongly at phyllomanganate vacancy sites (Drits et al., 1997; Manceau et al., 2002; Manceau et al., 2007; Manceau et al., 2005; Marcus et al., 2004; Peacock and Sherman, 2007; Pena et al., 2010; Silvester et al., 1997; Toner et al., 2006), and can also react with edge sites of phyllomanganates (Manceau et al., 2007; Villalobos et al., 2005). In this study, it is likely that vacancy sites are the primary location of Mn^{II} sorption on δ-MnO_2 until all are occupied (Chapters 1 and 2). Once δ-MnO_2 vacancy sites are fully occupied, Mn^{II} is expected to begin to sorb on edge sites. Therefore, desorption of Mn^{II} could potentially occur at both edge and vacancy sites of δ-MnO_2.

As^{III} Oxidation and Sorption

All desorption experiments discussed in this study are preceded by reaction of As^{III} with δ-MnO_2 for 4, 10, or 24 hours. The initial reaction between As^{III} and δ-MnO_2 results in As^{III} oxidation and produces As^{V} and Mn^{II} (Equation 3.1). Subsequently, As^{V} and Mn^{II} produced during As^{III} oxidation are sorbed on δ-MnO_2.

$$>Mn^{IV}\text{-}OH + H_3As^{III}O_3(aq) \rightarrow Mn^{II}(aq) + HAs^{V}O_4^{2-}(aq) + 3H^{+} \qquad [3.1]$$

To briefly summarize, the reaction between As^{III} and δ-MnO_2 in a stirred-flow reactor proceeds in two distinct phases. First, an initial reaction phase occurs from 0 – 6.4 hours, including the period of fastest As^{III} oxidation, highest As^{V} sorption, and no Mn^{II} release into solution (Figure 3.3). A second phase characterized by lower δ-MnO_2 reactivity occurs beyond 6.4 hours of reaction, which includes a second period of (decreased) As sorption, a decrease in As^{III} oxidation rate, and the presence of Mn^{II} in solution (Figure 3.3). Decreased δ-MnO_2 reactivity in the second phase of this reaction has been attributed to Mn^{II} sorption and subsequent production of Mn^{III} via $Mn^{II\,/\,IV}$ conproportionation at the δ-MnO_2 surface (Chapter 2).

In this study, desorption experiments are conducted by stopping the initial reaction between As^{III} and δ-MnO_2 after 4, 10, or 24 hours, and simultaneously beginning desorption by PO_4, Ca^{2+}, or background electrolyte. The first time point for beginning desorption is after 4 hours of reaction between As^{III} and δ-MnO_2, which

coincides with maximum As^{V} concentration in the stirred-flow reactor effluent, and the end of an initial period of As^{V} sorption (Figure 3.3). Before the first time point for beginning desorption (4 hours), Mn^{II} is expected to react primarily with vacancy sites and not edge sites. The second time point for beginning desorption is after 10 hours of As^{III} oxidation by δ-MnO_2, which is near the end of a second period of lesser As sorption, and occurs early in the second, less reactive phase of As^{III} oxidation (Figure 3.3). Between 4 and 10 hours, Mn^{II} is expected to begin reacting with edge sites, and Mn^{III} formation begins (Chapter 2). A change in the sorption complexes between As^{V} and δ-MnO_2 also occurs between 4 and 10 hours of As^{III} oxidation (Chapter 2). The last time point for desorption is after 24 hours of reaction, within the less reactive phase of the reaction (Figure 3.3).

Mn Desorption

Some cations could potentially desorb Mn^{II} more readily than Ca^{2+} (Murray, 1975; Toner et al., 2006; Tonkin et al., 2004), however Ca^{2+} is present in many environments and thus has a high probability of interacting with Mn-oxides in nature. It is expected that Ca^{2+} will desorb Mn^{II} from δ-MnO_2 more effectively than will PO_4 or background electrolyte. As a divalent cation, Ca^{2+} is expected to react with δ-MnO_2 vacancy sites (Drits et al., 2007) and edge sites as does Mn^{II}, while PO_4, which is structurally analogous to As^{V}, is expected to react only with edge sites similar to

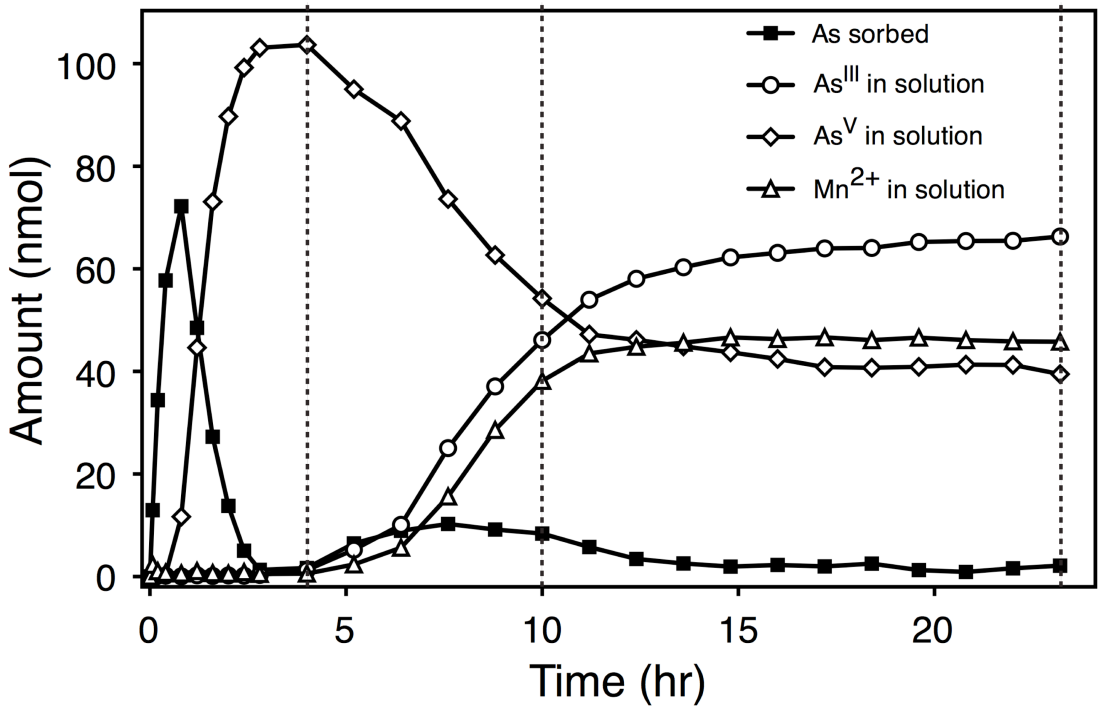

Figure 3.3. The amount (nmol) of As^{III}, As^{V}, and Mn^{II} in stirred flow reactor effluent as well as the amount (nmol) of As sorbed during As^{III} oxidation by δ-MnO_2, prior to desorption by Ca^{2+}, PO_4, or background electrolyte. Vertical dashed lines indicate times at which desorption was initiated.

As^{V}. The primary desorbing agent in background electrolyte is expected to be Na^{+} because it is the only cation in background electrolyte solutions, and because δ-$MnO_2$is negatively charged under the conditions used in this study. However, Na^{+} is expected to react with δ-MnO_2 interlayers differently than Ca^{2+} or Mn^{II}. Na^{+} is not expected to bind in triple corner sharing complexes at vacancy sites as is the case with Mn^{II} and Ca^{2+} (Drits et al., 2007).

When As^{III} is reacted with δ-MnO_2, the amount of Mn^{II} desorbed increases as the reaction proceeds (Figure 3.4). The largest increase in Mn^{II} desorption occurs between 4 and 10 hours in all treatments (Table 3.1). Also, as expected, Ca^{2+} is the most efficient Mn^{II} desorptive of those studied. Similar desorption of Mn^{II} by PO_4 and background electrolyte indicates that Na^{+} is capable of desorbing Mn^{II} (at edge sites) since the PO_4 desorbing solution also contains Na^{+} in the background electrolyte (Figure 3.4). Thus, we conclude that PO_4 has a negligible desorbing effect on Mn^{II}.

Previous data show that Mn^{II} sorbs at vacancy sites on δ-MnO_2 during the initial rapid phase of As^{III} oxidation under the conditions used in this study (Chapter 2). No Mn^{II} desorption is observed by any desorptive after 4 hours of As^{III} oxidation (Table 3.1), which is during the initial rapid phase of As^{III} oxidation. Therefore, any desorption of Mn^{II} after the 4 hour sample is expected to occur at vacancy sites. The lack of Mn^{II} desorption from vacancy sites by PO_4 and background electrolyte is expected because PO_4 is only expected to react at edge sites and Na^{+} is not expected to react with vacancy sites as strongly as Mn^{II}. However, the lack of Mn^{II} desorption by

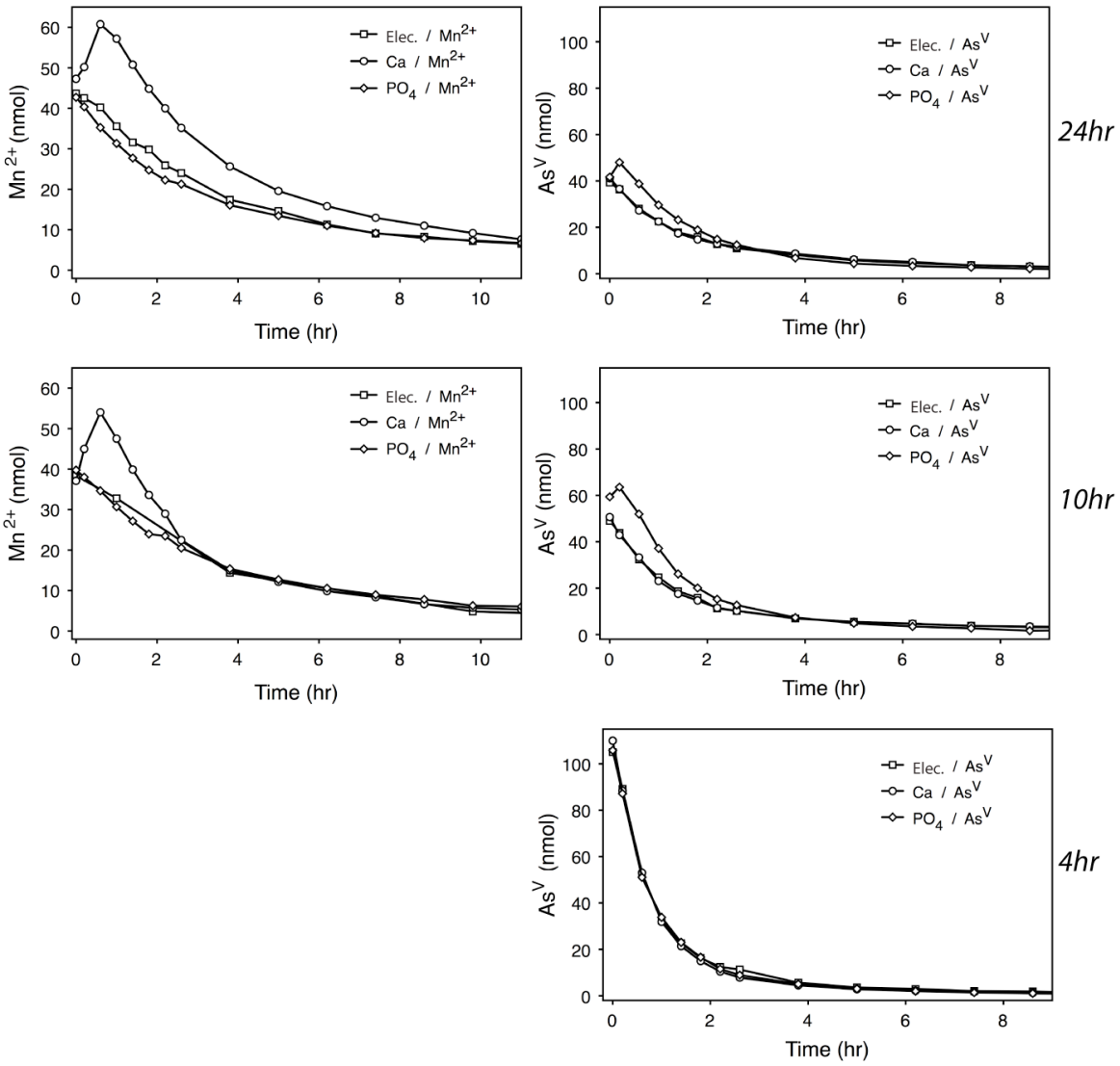

Figure 3.4. Amount (nmol) of Mn^{II} (left) and As^{V} (right) desorbed by Ca^{2+}, PO_4, and background electrolyte (10 mM NaCl, 5 mM MOPS) after 4, 10, and 24 hours of As^{III} oxidation by δ-MnO_2. The initial data points on each graph (time = 0 hours) correspond to the beginning of desorption (initial As^{III} oxidation data not shown). Data shown are first ~10 hours of 24 hour desorption experiments.

Table 3.1. Amounts (nmol) and percentages of As^{V}, As^{III}, and Mn^{II} desorbed by PO_4, Ca^{2+}, and background electrolyte (10 mM NaCl, 5mM MOPS) after 4, 10, and 24 hours of As^{III} oxidation by δ-MnO_2.

	As^{V} Desorbed by:			As^{III} Desorbed by:			Mn^{2+} Desorbed by:		
	Elec.	*Ca*	*PO_4*	*Elec.*	*Ca*	*PO_4*	*Elec.*	*Ca*	*PO_4*
					4 HOUR				
nmol Desorbed	64.4	61.6	62.4	0.0	0.0	0.0	0.0	0.0	0.0
nmol Sorbed	93.6	93.6	93.6	93.6	93.6	93.6			
% Desorbed	68.8	65.8	66.7						
					10 HOUR				
nmol Desorbed	94.4	93.0	102.0	-1.9	-1.3	-2.2	188.5	218.0	191.0
nmol Sorbed	140.4	140.4	140.4	140.4	140.4	140.4			
% Desorbed	67.2	66.2	72.7						
					24 HOUR				
nmol Desorbed	93.0	92.1	94.8	-1.8	0.1	0.4	206.6	297.3	207.5
nmol Sorbed	174.8	174.8	174.8	174.8	174.8	174.8			
% Desorbed	53.2	52.7	54.3						

* Amount of Mn sorbed could not be determined.

Ca^{2+} during this period suggests that Mn^{II} sorbed at vacancy sites is somewhat tightly bound and is not readily released into solution.

When As^{III} oxidation proceeds beyond 4 hours, Mn^{II} is thought to fill any remaining vacancy sites and begin sorbing at edge sites (Chapters 1 and 2). Mn^{II} sorption at edge sites is expected to be complete once Mn^{II} appears in reactor effluent, which occurs at ~ 6 hours (Figure 3.3). The first observed Mn^{II} desorption occurs in the 10 hour samples (Table 3.1, Figure 3.3), indicating that Mn^{II} sorbed at edge sites is more labile than Mn^{II} sorbed at vacancy sites. Interestingly, Mn^{II} desorption increases slightly from 10 to 24 hours of As^{III} oxidation by δ-MnO_2. This could indicate that

Mn^{II} sorption at edge sites continues beyond 10 hours, resulting in a larger amount of Mn^{II} at edge sites susceptible to desorption.

It has been previously observed that Mn^{III} begins to appear within δ-MnO_2 layers between 4 and 10 hours of As^{III} oxidation and remains present until 24 hours, under the conditions used in this study (Chapter 2). However, it is not clear where Mn^{III} occurs within the δ-MnO_2 structure. There is evidence that some Mn^{III} in δ-MnO_2 is being formed at edge sites through conproportionation of Mn^{II} sorbed on Mn^{IV} (Chapter 2). If Mn^{III} is formed at δ-MnO_2 edge sites, it would be expected to affect both Mn^{II} and As^{V} sorption at these sites. The increased desorption of Mn^{II} by Na^{+} and Ca^{2+} after 10 and 24 hours provides some evidence for this. Specifically, increased Mn^{II} desorption after 10 and 24 hours compared to 10 hours could be due to weaker Mn^{II} complexes with edge sites composed of Mn^{III} rather than Mn^{IV}. It is also possible that Mn^{III} content at edge sites increases slightly from 10 to 24 hours, which could also account for the slight increase in Mn^{II} desorption at 24 hours.

As^{III} Desorption

No As^{III} is desorbed under any conditions in this study (Table 3.1). This observation agrees with previous results indicating that As present on phyllomanganate surfaces only occurs as As^{V} (Chapter 2) (Manning et al., 2002; Parikh et al., 2008; Tournassat et al., 2002). In fact, As^{III} flushed from the reactor during desorption experiments, in some cases, is less than the predicted value,

resulting in an apparent negative desorption (Table 3.1). Negative As^{III} desorption indicates that As^{III} is either retained in the reactor (e.g. sorption by δ-MnO_2) or oxidized to As^{V} more rapidly than it can be flushed out of the reactor. Because there is no evidence of As^{III} sorption on phyllomanganates without being oxidized, we must assume that negative As^{III} desorption is due to rapid oxidation of As^{III}. Overall, the amount of As^{III} affected by this process appears to be less than 2% of total As desorbed, and thus can be considered a negligible amount.

As^{V} Desorption

Previous studies have shown that As reacts primarily with edge sites of phyllomanganates (Chapter 2) (Manning et al., 2002; Tournassat et al., 2002). Therefore, in the current study, it is expected for As^{V} desorption to occur at edge sites of δ-MnO_2 rather than vacancy sites. PO_4 is expected to desorb more As^{V} than background electrolyte or Ca^{2+} because of its similarity to As^{V}, and due to its known ability to compete with As^{V} for sorption sites on metal oxides (Jackson and Miller, 2000; Lafferty and Loeppert, 2005; Liu et al., 2001; Parikh et al., 2010). As discussed previously, Ca^{2+} is expected to react with δ-MnO_2 vacancy sites as well as edge sites, thus Ca^{2+} also has the potential to desorb As^{V}, while background electrolyte is expected to react weakly with δ-MnO_2 edge sites.

An interesting trend can be observed by comparing desorption curves in Figure 3.4 with total As^{V} desorbed in Table 3.1. It appears, from Figure 2, that PO_4 desorbs

more As^V than Ca^{2+} or background electrolyte after 10 and 24 hours of As^{III} oxidation, while after 4 hours all three desorptives are equally effective. However, when comparing the total amount desorbed by each desorptive, at 4, 10 and 24 hours there is little difference observed between the desorptives at each time (Table 3.1). The initial spike in As^V desorption by PO_4 after 10 and 24 hours of reaction is apparently due to a more rapid desorption by PO_4 compared to Ca^{2+} and background electrolyte. This initial more rapid desorption indicates that, as expected, PO_4 preferentially desorbs As^V. However, the similar amount of total As^V desorbed by all three desorptives over 24 hours (of desorption) implies that labile As^V can be desorbed by a variety of competing ions.

All three desorptives are equally effective at desorbing As^V after 4 hours of reaction between As^{III} and δ-MnO_2, resulting in only ~30% of sorbed As remaining on δ-MnO_2 in stable complexes. This could be due to As^V sorption at different surface sites on δ-MnO_2, and As^V sorption complexes at some sites being more stable than others. As^V is bound in mononuclear-monodentate as well as binuclear-bidentate complexes on the δ-MnO_2 surface during the first 4 hours of As^{III} oxidation by δ-MnO_2 (Chapter 2). One could hypothesize that the more labile (desorbed) As^v is bound in monodentate-mononuclear complexes while the more stable (remaining) As^V is bound in binuclear-binuclear complexes. However, it is tenuous to ascribe different affinities for desorption to specific sorption complexes based on only these desorption data. Further spectroscopic evidence is required to verify this hypothesis

An overall increase in As^{V} desorption occurs after 10 hours of As^{III} oxidation by δ-MnO_2 (Table 3.1). Also, a similar amount of As^{V} desorption occurs at 10 and 24 hours, with one exception. The amount of As^{V} desorbed at 10 hours is more than by other treatments at 10 or 24 hours (Table 3.1, Figure 3.4). In this case, PO_4 desorbs only ~ 8 – 9 nmol more As^{V} than the other desorptives, however, this increase accounts for ~ 10 % more desorption by PO_4 than by Ca^{2+} or background electrolyte and must be assumed to be significant. Although, it is expected that PO_4 can desorb more As^{V} than the other desorptives, it is not clear as to why this is only observed after 10 hours of As^{III} oxidation by δ-MnO_2, and not after 4 or 24 hours.

After 10 and 24 hours of As^{III} oxidation by δ-MnO_2, two significant changes occur for δ-MnO_2. First, Mn^{II} begins sorbing at edge sites after the vacancy sites are saturated from Mn^{II} sorption (at ~6.4 hours) (Chapters 1 and 2). Also, Mn^{III} appears in the Mn octahedral layers between 4 and 10 hours of As^{III} oxidation, and increases again between 10 and 24 hours (Chapter 2). The increase in the amount of As^{V} desorbed by all desorptives after 10 and 24 hours (compared to 4 hours) happens concurrently with increased competition from Mn^{II} for edge sites, and an increase in Mn^{III} content within the δ-MnO_2 structure (possibly at edge sites). Thus, increased As^{V} desorption after 4 hours could be a result of direct competition between As^{V} and Mn^{II} for sorption sites or weaker bonds between As^{V} and Mn^{III} (Zhu et al., 2009). It is difficult to distinguish between the effects of increased Mn^{II} sorption and increased Mn^{III} content at δ-MnO_2 edge sites as they seem to occur simultaneously.

Previous studies have also proposed the possibility that As can be bound to phyllomanganates via a bridging complex through sorbed Mn (Parikh et al., 2010; Tani et al., 2004). In this study, desorption of As^{V} by Ca^{2+}, PO_4, and background electrolyte are very similar, and thus we see no evidence for the presence of As^{V}-Mn^{II} bridging complexes. In previous studies that have observed As^{V}-Mn^{II} bridging complexes, traditional batch experiments were used. Thus, it is possible that by using a stirred-flow reactor in this study, bridging complexes were prevented from forming.

Implications for As Mobility

Phyllomanganates are capable sorbents of As^{V}, especially during As^{III} oxidation. However, in this study, As^{V} is desorbed to some extent under all conditions studied. Even Na^{+} (present in background electrolyte) is able to desorb significant amounts of As^{V}, indicating that a portion of As sorbed by Mn-oxides can be potentially quite mobile in the environment. Although a large fraction of sorbed As^{V} can be desorbed from δ-MnO_2, there is a certain amount of As that not desorbed under any of the conditions studied. Thus, if As comes in contact with Mn-oxides in nature, these minerals could potentially decrease As availability and mobility both by oxidation of As^{III} and sorption of As^{V}. It appears that the potential for As^{V} and Mn^{II} to be desorbed from δ-MnO_2 is intricately linked to the type of reaction site on the δ-MnO_2 surface to which each is bound, as well as Mn speciation within the δ-MnO_2 structure. Also, this study emphasizes the importance of understanding mineral

structures when interpreting sorption and desorption data, as well as studying these processes over time.

References

Anderson, M.A., J.F. Ferguson, and J. Gavis. 1976. Arsenate adsorption on amorphous aluminum hydroxide. J. Colloid Interface Sci. 54:391-399.

Arai, Y., E.J. Elzinga, and D.L. Sparks. 2001. X-ray absorption spectroscopic investigation of arsenite and arsenate adsorption at the aluminum oxide-water interface. J. Colloid Interface Sci. 235:80-88.

Dixit, S., and J.G. Hering. 2003. Comparison of arsenic(V) and arsenic(III) sorption onto iron oxide minerals: Implications for arsenic mobility. Environ. Sci. Technol. 37:4182-4189.

Driehaus, W., R. Seith, and M. Jekel. 1995. Oxidation of arsenate(III) with manganese oxides in water treatment. Water Res. 29:297-305.

Drits, V.A., B. Lanson, and A.C. Gaillot. 2007. Birnessite polytype systematics and identification by powder X-ray diffraction. Am. Mineral. 92:771-788.

Drits, V.A., E. Silvester, A.I. Gorshkov, and A. Manceau. 1997. Structure of synthetic monoclinic Na-rich birnessite and hexagonal birnessite. 1. Results from X-ray diffraction and selected-area electron diffraction. Am. Mineral. 82:946-961.

Foster, A.L., G.E. Brown, and G.A. Parks. 2003. X-ray absorption fine structure study of As(V) and Se(IV) sorption complexes on hydrous Mn oxides. Geochim. Cosmochim. Ac. 67:1937-1953.

Ginder-Vogel, M., G. Landrot, J.S. Fischel, and D.L. Sparks. 2009. Quantification of rapid environmental redox processes with quick-scanning x-ray absorption spectroscopy (Q-XAS). Proc. Natl. Acad. Sci. 106:16124-16128.

Gupta, S.K., and K.Y. Chen. 1978. Arsenic removal by adsorption. J. Water Pollut. Control 50:493-506.

Hingston, F.J., A.M. Posner, and J.P. Quirk. 1971. Competitive adsorption of negatively charged ligands on oxide surfaces. Faraday Discussions 52:334-342.

Jackson, B.P., and W.P. Miller. 2000. Effectiveness of phosphate and hydroxide for desorption of arsenic and selenium species from iron oxides. Soil Sci. Soc. Am. J. 64:1616-1622.

Lafferty, B.J., and R.H. Loeppert. 2005. Methyl arsenic adsorption and desorption behavior on iron oxides. Environ. Sci. Technol. 39:2120-2127.

Liu, F., A. De Cristofaro, and A. Violante. 2001. Effect of pH, phosphate and oxalate on the adsorption/desorption of arsenate on/from goethite. Soil Sci. 166:197-208.

Manceau, A., B. Lanson, and V.A. Drits. 2002. Structure of heavy metal sorbed birnessite. Part III: Results from powder and polarized extended X-ray absorption fine structure spectroscopy. Geochim. Cosmochim. Acta 66:2639-2663.

Manceau, A., M. Lanson, and N. Geoffroy. 2007. Natural speciation of Ni, Zn, Ba, and As in ferromanganese coatings on quartz using X-ray fluorescence, absorption, and diffraction. Geochim. Cosmochim. Acta 71:95-128.

Manceau, A., C. Tommaseo, S. Rihs, N. Geoffroy, D. Chateigner, M. Schlegel, D. Tisserand, M.A. Marcus, N. Tamura, and Z.-S. Chen. 2005. Natural speciation of Mn, Ni, and Zn at the micrometer scale in a clayey paddy soil using X-ray fluorescence, absorption, and diffraction. Geochim. Cosmochim. Acta 69:4007-4034.

Manning, B.A., S.E. Fendorf, B. Bostick, and D.L. Suarez. 2002. Arsenic(III) oxidation and arsenic(V) adsorption reactions on synthetic birnessite. Environ. Sci. Technol. 36:976-981.

Marcus, M.A., A. Manceau, and M. Kersten. 2004. Mn, Fe, Zn and As speciation in a fast-growing ferromanganese marine nodule. Geochim. Cosmochim. Acta 68:3125-3136.

Moore, J.N., J.R. Walker, and T.H. Hayes. 1990. Reaction scheme for the oxidation of As(III) to As(V) by birnessite. Clay. Clay Miner. 38:549-555.

Murray, J.W. 1975. Interaction of metal-ions at manganese dioxide solution interface. Geochim. Cosmochim. Ac. 39:505-519.

Nesbitt, H.W., G.W. Canning, and G.M. Bancroft. 1998. XPS study of reductive dissolution of 7 angstrom-birnessite by H_3AsO_3, with constraints on reaction mechanism. Geochim. Cosmochim. Ac. 62:2097-2110.

Oscarson, D.W., P.M. Huang, and W.K. Liaw. 1981a. Role of manganese in the oxidation of arsenite by freshwater sediments. Clay. Clay Miner. 29:219-225.

Oscarson, D.W., P.M. Huang, C. Defosse, and A. Herbillon. 1981b. Oxidative power of Mn(IV) and Fe(III) oxides with respect to As(III) in terrestrial and aquatic environments. Nature 291:50-51.

Oscarson, D.W., P.M. Huang, W.K. Liaw, and U.T. Hammer. 1983. Kinetics of oxidation of arsenite by various manganese dioxides. Soil Sci. Soc. Am. J. 47:644-648.

Parikh, S.J., B.J. Lafferty, and D.L. Sparks. 2008. An ATR-FTIR spectroscopic approach for measuring rapid kinetics at the mineral/water interface. J. Colloid Interface Sci. 320:177.

Parikh, S.J., B.J. Lafferty, T.G. Meade, and D.L. Sparks. 2010. Evaluating environmental influences on AsIII oxidation kinetics by a poorly crystalline Mn-oxide. Environ. Sci. Technol.

Peacock, C.L., and D.M. Sherman. 2007. Sorption of Ni by birnessite: Equilibrium controls on Ni in seawater. Chemical Geology 238:94-106.

Pena, J., K.D. Kwon, K. Refson, J.R. Bargar, and G. Sposito. 2010. Mechanisms of nickel sorption by a bacteriogenic birnessite. Geochim. Cosmochim. Acta 74:3076-3089.

Petrick, J.S., F. Ayala-Fierro, W.R. Cullen, D.E. Carter, and H.V. Aposhian. 2000. Monomethylarsonous acid (MMA(III)) is more toxic than arsenite in Chang human hepatocytes. Toxicol. Appl. Pharmacol. 163:203-207.

Raven, K.P., A. Jain, and R.H. Loeppert. 1998. Arsenite and arsenate adsorption on ferrihydrite: kinetics, equilibrium, and adsorption envelopes. Environ. Sci. Technol. 32:344-349.

Sadiq, M. 1997. Arsenic chemistry in soils: An overview of thermodynamic predictions and field observations. Water Air Soil Poll. 93:117-136.

Scott, M.J., and J.J. Morgan. 1995. Reactions at oxide surfaces. 1. Oxidation of As(III) by synthetic birnessite. Environ. Sci. Technol. 29:1898-1905.

Silvester, E., A. Manceau, and V.A. Drits. 1997. Structure of synthetic monoclinic Na-rich birnessite and hexagonal birnessite. 2. Results from chemical studies and EXAFS spectroscopy. Am. Mineral. 82:962-978.

Tani, Y., N. Miyata, M. Ohashi, T. Ohnuki, H. Seyama, K. Iwahori, and M. Soma. 2004. Interaction of inorganic arsenic with biogenic manganese oxide produced by a Mn-oxidizing fungus, strain KR21-2. Environ. Sci. Technol. 38:6618-6624.

Toner, B., A. Manceau, S.M. Webb, and G. Sposito. 2006. Zinc sorption to biogenic hexagonal-birnessite particles within a hydrated bacterial biofilm. Geochim. Cosmochim. Acta 70:27-43.

Tonkin, J.W., L.S. Balistrieri, and J.W. Murray. 2004. Modeling sorption of divalent metal cations on hydrous manganese oxide using the diffuse double layer model. Appl. Geochem. 19:29-53.

Tournassat, C., L. Charlet, D. Bosbach, and A. Manceau. 2002. Arsenic(III) oxidation by birnessite and precipitation of manganese(II) arsenate. Environ. Sci. Technol. 36:493-500.

Villalobos, M., J. Bargar, and G. Sposito. 2005. Mechanisms of Pb(II) sorption on a biogenic manganese oxide. Environ. Sci. Technol. 39:569-576.

Zhu, M., K.W. Paul, J.D. Kubicki, and D.L. Sparks. 2009. Quantum chemical study of arsenic (III, V) adsorption on Mn-oxides: Implications for arsenic(III) oxidation. Environ. Sci. Technol. 43:6655-6661.

CONCLUSIONS

The presence of As in soil and water around the world currently poses a significant risk to human health and environmental sustainability. Thus, understanding the processes that control As mobility and bioavailability in the environment is crucial in developing strategies for limiting human exposure to As contamination as well as mitigating contaminated sites. Mineral surfaces greatly influence the mobility and speciation of As in the environment. Specifically, poorly crystalline phyllomanganates capable of oxidizing and sorbing As have the potential to dramatically affect the behavior of As in the environment.

The reactions involved in As^{III} oxidation by poorly-crystalline phyllomanganates (e.g. δ-MnO_2) are quite complex and can change with time. As^{III} oxidation by pristine δ-MnO_2 initially favors the formation of Mn^{II} rather than Mn^{III} which suggests that the oxidation of As^{III} to As^{V} by δ-MnO_2 occurs via a single two-electron transfer rather than two, one-electron transfers. However, Mn^{III} is present in the δ-MnO_2 structure during As^{III} oxidation, especially at later times during the reaction. Thus it appears that Mn^{III} forms through conproportionation of Mn^{II} sorbed on δ-MnO_2, and Mn^{IV} in the mineral structure. This change in Mn speciation in the δ-MnO_2 structure, and on its surface, greatly affects all other reactions that occur during As^{III} oxidation by δ-MnO_2.

Passivation is commonly observed during As^{III} oxidation by phyllomanganates. The primary factor in passivation of δ-MnO_2 during As^{III} oxidation is Mn speciation. Passivation of the mineral surface is initiated by sorption of Mn^{II} at δ-MnO_2 edge sites, and can potentially be influenced by formation of Mn^{III} sites on the δ-MnO_2 surface as As^{III} oxidation proceeds. Mn^{III} reactive sites on the δ-MnO_2 surface are expected to oxidize As^{III} to a lesser degree and at a slower rate than Mn^{IV} sites, while Mn^{II} sorbed on δ-MnO_2 is expected to block As^{III} from reacting with the surface. However, some Mn^{II} remains on the δ-MnO_2 surface after 24 hours of As^{III} oxidation, indicating that not all Mn^{II} sorbed on the δ-MnO_2 surface is oxidized to Mn^{III}. Thus, both Mn^{II} sorption and Mn^{III} production seem to play a role in δ-MnO_2 surface passivation.

δ-MnO_2 is capable of sorbing As^{V}, especially during As^{III} oxidation. However, a large portion of As^{V} sorbed on δ-MnO_2 remains quite mobile. Although some As^{V} sorbed on δ-MnO_2 is mobile, a considerable fraction is persistently bound to the mineral surface. It does not appear that As^{V} sorbed on δ-MnO_2 plays a role in passivation of the mineral surface during As^{III} oxidation. However, the presence of Mn^{III} in the δ-MnO_2 structure does alter As sorption complexes on the δ-MnO_2 surface.

Reactions between As and Mn-oxides in the environment have the potential to decrease As availability and mobility both by oxidation of As^{III} and sorption of As^{V}. However, the mineral structure of Mn-oxides, and especially the oxidation state of Mn

within the mineral structure have a dramatic effect on the extent and rates of these reactions. Also, As reactions with δ-MnO_2 can be quite complex, and the reactions involved vary in their importance over time. This study clearly demonstrates the value of investigating environmentally important sorption and redox reactions over time, and the results of this study the underscore the value of understanding mineral structures when interpreting sorption and desorption data.

FUTURE RESEARCH

Passivation of Mn-oxides is expected be an important process in the environment because of its potential to decrease the reactivity of some of the most reactive minerals in nature. Mn speciation in the δ-MnO_2 structure as well as on the δ-MnO_2 surface plays a crucial, determining role in both As^V sorption and As^{III} oxidation. However, a better understanding of the reactions controlling Mn speciation at the δ-MnO_2 surface is needed. Specifically, the extent and location of $Mn^{II\ /\ IV}$ conproportionation on the δ-MnO_2 surface after Mn^{II} sorption is not clear. Also, new methods are greatly needed to more accurately determine the proportion of $Mn^{II\ /\ III\ /\ IV}$ within Mn-oxide structures.

As^V sorbed on δ-MnO_2, during As^{III} oxidation, forms a variety of sorption complexes with the mineral surface. The sorption complexes formed between As^V and δ-MnO_2 change as Mn oxidation state changes within the Mn-oxide structure. Although As can be sorbed by δ-MnO_2, a portion of the As which is sorbed remains mobile. Further study is needed to elucidate the mobility of As^V associated with the various As-Mn sorption complexes. Spectroscopic techniques would be extremely beneficial in the investigation of As desorption from Mn-oxides. Understanding the stability of sorption complexes of As on Mn-oxide surfaces would be useful in predicting As mobility in the environment. Also, experiments are needed to determine

the distribution coefficients (K_d) for As sorption by δ-MnO_2 so that the ability of this mineral to sorb As can be evaluated in relation to other relevant mineral phases, such as iron oxides.

It is clear that pristine Mn-oxides can have a dramatic effect on As speciation. However, the ability of Mn-oxides to oxidize and sorb As seems to decrease as the mineral surface becomes passivated. In the environment, it possible that a limiting factor in As^{III} oxidation is the availability of pristine Mn-oxide surfaces. Therefore, it is important to develop a better understanding of the rate of biogenic Mn-oxide production in the environment as well as the factors limiting production of these minerals, such that predictions can be made regarding potential biogenic Mn-oxide contents in specific environments.

It is likely that biogenic Mn-oxides are the dominant Mn-oxide minerals in many soils and sediments. Biogenic Mn-oxides are formed in the exo-cellular polymeric substances surrounding microbial cells, and thus regularly interact with organic compounds in natural settings. Therefore, it is important to understand how organic compounds in the environment affect the reactivity of Mn-oxides. Further research is needed to determine how organic compounds on Mn-oxide surfaces affect the rates and mechanisms of As^{III} oxidation by Mn-oxides.